REDUCED ORDER MODELLING FOR MULTIPHYSICS PROBLEMS

A THESIS SUBMITTED TO
THE GRADUATE SCHOOL OF NATURAL AND APPLIED SCIENCES
OF
MIDDLE EAST TECHNICAL UNIVERSITY

BY

FATMA GÜLER EROĞLU

IN PARTIAL FULFILLMENT OF THE REQUIREMENTS
FOR
THE DEGREE OF DOCTOR OF PHILOSOPHY
IN
MATHEMATICS

DECEMBER 2018

Approval of the thesis:

REDUCED ORDER MODELLING FOR MULTIPHYSICS PROBLEMS

submitted by **FATMA GÜLER EROĞLU** in partial fulfillment of the requirements for the degree of **Doctor of Philosophy in Mathematics Department, Middle East Technical University** by,

Prof. Dr. Halil Kalıpçılar
Dean, Graduate School of **Natural and Applied Sciences** _____

Prof. Dr. Yıldıray Ozan
Head of Department, **Mathematics** _____

Prof. Dr. Songul Kaya Merdan
Supervisor, **Mathematics Department, METU** _____

Examining Committee Members:

Prof. Dr. Mustafa Türkyılmazoğlu
Mathematics Department, Hacettepe University _____

Prof. Dr. Songul Kaya Merdan
Mathematics Department, METU _____

Prof. Dr. Bülent Karasözen
Mathematics Department, METU _____

Assoc. Prof. Dr. Canan Bozkaya
Mathematics Department, METU _____

Assoc. Prof. Dr. Murat Uzunca
Mathematics Department, Sinop University _____

Date:

I hereby declare that all information in this document has been obtained and presented in accordance with academic rules and ethical conduct. I also declare that, as required by these rules and conduct, I have fully cited and referenced all material and results that are not original to this work.

Name, Surname: Fatma Güler Eroğlu

Signature :

ABSTRACT

REDUCED ORDER MODELLING FOR MULTIPHYSICS PROBLEMS

Güler Eroğlu, Fatma
Ph.D., Department of Mathematics
Supervisor: Prof. Dr. Songul Kaya Merdan

December 2018, 117 pages

Proper orthogonal decomposition (POD), as one of the most commonly used tools to generate reduced order models, has been utilized in many engineering and scientific applications. The idea of POD consists of extracting the dominant features of a data set, which are naturally assumed to represent Galerkin finite element solution of a partial differential equation. In this way, POD reduces the complexity of systems. Despite the widespread use of POD, it can perform quite poorly for turbulence flows. Projection-based variational multiscale (VMS) method is one of the best approaches that increase the numerical stability. The basic idea in VMS is adding artificial viscosity only to smallest resolved scales instead of all resolved scales to eliminate small scale oscillations. The usual finite element discretization sorting of scales is complicated, but in POD, basis functions are sorted in descending order with respect to their kinetic energy. Thus, the POD is suitable to the VMS methodology. First, we propose, analyze and test a post-processing implementation of a projectionbased VMS method with POD for the incompressible Navier–Stokes equations. We present a theoretical analysis of the method, and give results for several numerical tests on benchmark problems which both illustrate the theory and show the proposed method's effective-

ness. Second, we extend POD reduced order modeling to flows governed by double diffusive convection, which models flow driven by two potentials with different rates of diffusion. We present a stability and convergence analysis for it, and give results for numerical tests. In the last part of the thesis, we present a VMS reduced order model based on POD for the Darcy Brinkman equations. The proposed scheme uses VMS type stabilization in POD. For the temporal discretization of the system, Crank Nicholson is utilized. The numerical analysis for the VMS-POD is carried out and numerical studies are performed to verify the theoretical findings.

Keywords: Proper orthogonal decomposition, reduced order models, projection-based variational multiscale, post-processing, double-diffusive.

ÖZ

ÇOKLU FİZİK PROBLEMLERİ İÇİN MERTEBE DÜŞÜREN MODELLEMELER

Güler Eroğlu, Fatma
Doktora, Matematik Bölümü
Tez Yöneticisi: Prof. Dr. Songul Kaya Merdan

Aralık 2018 , 117 sayfa

En yaygın kullanılan mertebe düşüren modellemelerden biri olan uygun dik ayrıştırma metodu (POD), birçok mühendislik ve bilimsel uygulamada kullanılmaktadır. POD metodunun temeli bir kısmi diferansiyel denkleminin Galerkin sonlu eleman çözümünü temsil eden veri kümesinden en çok kinetik enerjiye sahip olanlarını ortaya çıkarmaktır. Bu şekilde POD, sistemlerin karmaşıklığını azaltır. POD metodu yaygın olarak kullanılmasına rağmen, sayısal stabilizasyon olmaksızın oldukça zayıf bir şekilde davranır. Projeksiyon tabanlı varyasyonel çoklu ölçek (VMS) yöntemi, verilen sistemin sayısal kararlılığını artıran en iyi yaklaşımlardan biridir. VMS'deki temel fikir, küçük ölçekli salınımları ortadan kaldırmak için tüm çözülmüş ölçekler yerine yapay viskoziteyi sadece en küçük çözümlenmiş ölçeklere eklemektir. Sonlu elemanlar discretizasyonunun ölçeklendirilmesi karmaşıktır, fakat POD'da, temel fonksiyonlar kinetik enerjilerine göre azalan düzende sıralanmıştır. Bu yüzden POD metodu VMS metodolojisi ile uyumludur.

Bu tezde ilk olarak, sıkıştırılamaz Navier-Stokes denklemleri için POD ile projeksiyon tabanlı VMS yönteminin bir işlem-sonrası uygulaması önerilmiş, analiz edilmiş

ve test edilmiştir. İkinci olarak, uygun dik ayrıştırmalı metodu farklı çözünme oranlarına sahip iki potansiyel tarafından modellenen çifte çözünümlü konveksiyon denklemleri için genişletilmiştir. İndirgenmiş model için kararlılık ve yakınsaklık analizleri sunulmuştur. Teorik sonuçları sayısal testlerle doğrulamak için bir ölçüt problemi kullanılmıştır. Tezin son bölümünde, Darcy Brinkman denklemleri için POD'a dayalı bir VMS indirgenmiş modeli sunulmuştur. Sistemin tamamen ayrıştırılmasında, zaman değişkenleri için Crank Nicholson zaman ayrımı ve uzay değişkenleri için sonlu elemanlar yöntemi kullanılmıştır. VMS-POD metodunun sayısal analizi gerçekleştirilmiştir ve en uygun hata tahminleri kanıtlanmıştır. Son olarak, teorik bulguları doğrulamak için sayısal çalışmalar yapılmıştır.

Anahtar Kelimeler: Uygun dik ayrıştırma, mertebe düşürme modellemeleri, projeksiyona dayalı çok ölçekli varyasyonel metot, işlem sonrası, çift difüzyon

To GÜLER family

ACKNOWLEDGMENTS

First of all, I would like to express my deepest gratitude to my supervisor Prof. Dr. Songül Kaya Merdan for his encouragement, patience and constant guidance during my thesis. It was a great honor to work with her and our cooperation influenced my academical and world view highly.

A lot of people influenced and supported this work scientifically and their contribution were most valuable for me. I would like to thank Prof. Dr. Bülent Karasözen for his helpful suggestions and constitutive criticisms. I also would like to thank Prof. Dr. Mustafa Türkyılmazoğlu for his helpful comments and advice. In particular, I wish to express my appreciation to Assoc. Prof. Dr. Canan Bozkaya and Assoc. Prof. Dr. Murat Uzunca for their participation and advice. Above all, my special thanks go to Prof. Dr. Leo G. Rebholz for his valuable guidance, encouragement and support.

Last, I would like to thank all my friends and my family for supporting me spiritually throughout writing this thesis and my life in general. I am grateful to my husband Hasan Hüseyin Eroğlu for his unfailing support and continuous encouragement. I would like to thank my colleagues in the math department especially Özlem Erşen and Elçin Çalışkan for their support and help. I special thank to my mother Hatice GÜLER, my sister Ümran SİVAS, my brother in law Murat SİVAS and my little niece Azra SİVAS for their continuous support, endless love and believing in my success. Finally, special thanks to my precious uncles Mehmet GÜLER, Emin GÜLER, and to GÜLER family for their support and patience through all my educational life.

This research has been supported by a grant from TÜBİTAK, the Scientific and Technical Research Council of Turkey.

TABLE OF CONTENTS

LIST OF TABLES

TABLES

LIST OF FIGURES

FIGURES

CHAPTER 1

INTRODUCTION

Nowadays, the capacities of computers used for numerical simulations of many engineering and physics problems increase, as a consequence the amount of data produced also increases. Therefore, millions of degrees of freedom are needed to analyse this large amount of data. This causes a burden on the computational resources. Thus, efficient methods are required to approximate solutions. Utilizing reduced order models (ROMs) is an efficient method for lowering the computational complexity in such settings. The proper orthogonal decomposition (POD) approach has proven to be quite successful for generating reduced order models that capture many dominant flow features. POD reduces the complexity of systems, often by orders of magnitude, by representing it with only its most energetic structures. Some examples for the application of the POD consist of image processing in [80], optimization and control theory in [52], inverse problem in [95], signal analysis in [1], data compression in [2], random variables in [72], oceanography and meteorology in [76, 61, 25].

The soul of POD can be found equivalently in statistics, matrix theory, and signal analysis. The equivalent names in these areas are Karhunen-Loéve decomposition, singular systems analysis, principal component analysis, and singular value decomposition, respectively. Although these methods were presented by Kosambi [49], Loéve [59], Karhunen [46], Pougachev [75] and Obukhov [70], POD method was firstly introduced by Lumley [60] in the context of turbulence. Recent studies show that it is an efficient approach for Boussinesq equations [8, 83, 84], convection dominant convection diffusion reaction equations [36], Navier Stokes equations [37], neutron diffusion equations [85], and also for magnetohydrodynamics flow [78].

This thesis is concerned with the utilization of the POD-based reduced order modeling

for the multiphysics problems. There are two major contributions of the thesis. The first consists of developing a modular POD-based reduced order modeling along with projection based stabilization for the Navier Stokes equations (NSE), (1.3.1). The second includes studying POD for the Darcy-Brinkman equations, (1.3.15).

The NSE are one of the common multiphysics problem and derived from conservation of mass and conservation of momentum. These equations are used to model many important phenomena, such as airflow around the airfoil [6, 43, 90], weather forecasts [71, 88], flows in pipe [17, 81, 82], pollution analysis [15, 19], and blood flow [58, 67, 74]. NSE is obtained by applying the laws of conservation to fluid motion. These equations can be considered as generalizations of the famous Euler's equations that define the frictionless fluids and incompressible flows. In the 19^{th} century, Claude-Louis Navier introduced NSE by adding a Newton viscous term to the motion equation, [68]. George Gabriel Stokes made the equation more credible by developing the analysis of the NSE with a different description of the internal friction in the fluids, [92].

Although NSE were introduced a century ago, their estimates and results have not been fully understood. The difficulty comes from the nature of NSE. It is known that due to the wide range of scales in many complex fluid flows, simulating these flows by a direct numerical simulation (DNS) can be very expensive, and sometimes is even infeasible from the Kolmogorov 1941 theory, it is known that a resolved DNS requires $O(Re^{9/4})$ mesh points [9], where Re is the Reynolds number in NSE. To make the situation even more difficult, in the engineering design process, flow simulations must be run many times, e.g. to perform parameter studies or for system control purposes, which multiplies the DNS cost by at least several times.
NSE includes an important control parameter Re. It is given as a ratio of inertial forces to viscous forces as

$$Re = \frac{\mathcal{U}L}{\nu}, \tag{1.0.1}$$

where $\nu = \mu/\rho$ is the kinematic viscosity, μ is the dynamic viscosity, ρ is the density, L is the characteristic length scale, and $\mathcal{U}$ is the characteristic velocity of the flow. Viscous terms dominate inertial terms for low Re, in which laminar flow occurs. For high Re, the convective term become dominant and flow behaviour becomes

turbulent. One of the difficulties in solving the NSE is the instability caused by these large changes in Re. When NSE is solved by the standard finite element method, stabilization methods are used to obtain physically correct numerical approximations.

In the literature, there are different stabilization methods as residual based and projection based. In recent years, utilizing projections to make the system stable is getting more common. One of the popular projection based stabilization method is variational multiscale (VMS) method. VMS was introduced in [35] in a variational setting. Guermond [31] developed this idea by adding artificial diffusion which only affects small scales. To recover the inconsistency caused by extra terms, Layton [55] expanded the Guermode's method by adding and then subtracting artificial viscosity term. It (and its variants) has been studied extensively in the finite element frameworks for NSE [40, 41] and convection-diffusion equations [42]. However, the separation of scales is the challenge in this method. The combining of VMS with the POD method has been successful to solve this challenge. In POD, the hierarchy of small and large scales is presented naturally. That is, basis functions are ordered with respect to their kinetic energy content. Thus, the POD is particularly suitable to the VMS methodology. Using VMS in POD was pioneered in [36, 37, 79, 21], and their studies showed this could increase numerical accuracy for convection-dominated convection–diffusion equations [36] and for NSE [37, 79, 21]. Furthermore, in [36, 37], analyses were performed to show optimal error bounds (in terms of mesh width, time step size, and eigenvalues and eigenvectors removed from the system)

Another multiphysics problem of interest is Darcy-Brinkman equations with double diffusive convection. In this system the flow is driven by two potentials with different diffusion rates. The detailed derivation of the system (1.3.15) can be found in [69]. The physical model uses the momentum forced by heat and mass transfer. In this model, a Darcy term accounts for the porous boundary.

Double diffusive is of great important in many applications such as oceanography, geology, biology and chemical processes. In particular, when the oceanography sample was examined, temperature and salt concentration gradients and diffusivity drive the flow of salt water. It was seen that the temperature is distributed faster than the concentration (salinity). In fact, double diffusion convection in oceanography is a vertical

operation, and there are two modes as salt fingers and diffusive. The salt fingers mode of double diffusive were first noticed with pumping cold, less salty and dense water with a tube from the deep of ocean to the its surface [93]. The cold water moved upwards and continued to rise, the opposite direction being similarly expressed. On the other hand, diffusive convection has been observed that occurs when cold and fresh water is above from saline and warmer water.

The physical mechanism of double diffusive effects was studied in several works, e.g., [45, 91]. Due to the coupling between fluid flow, the heat and mass transfer equations, different boundary layers are formed. As a result, Darcy-Brinkman equations are solved numerically by varying a variety of numerical techniques. Many researchers were interested in solving numerically the scheme (1.3.15) by using the finite volume method (FVM) [64, 4, 63] and the boundary element method (BEM) [51, 50]. This model was also studied with finite element method (FEM) in different flow configurations in a cavity [26] and in a porous medium [47, 48, 66].

Although tremendous development of computing power is available, solving Darcy Brinkman equations accurately and efficiently remains a challenge for the computational fluid dynamics community. Furthermore, the use of full order methods lead to large algebraic systems and high computational time. Hence the extension POD methodology to Darcy-Brinkman equations with double diffusive convection is significant.

In this system, heat transfer is expressed with Rayleigh number (Ra) which is defined as

$$Ra = \frac{\mathbf{g}\beta_T(T_{bottom} - T_{top})L^3}{\nu\gamma} \tag{1.0.2}$$

where g denotes gravitational acceleration vector, β_T denotes thermal expansion coefficient, L denotes the vertical length, ν denotes kinematic viscosity, γ denotes thermal diffusivity, T_{bottom} and T_{top} denote the temperature in the bottom and in the top, respectively. The magnitude of the Ra indicates whether the flow is laminar or turbulent. For high Ra, the instability occurs due to the emergence of convection cells. Thus, the behaviour of the flow becomes turbulent. In such a case, the VMS method can be used to eliminate the oscillation and stabilize the convective terms.

This thesis has three main objectives. As recent work with POD has shown that the approach can work well on multiphysics flow problems, the first objective is to extend the novel ideas of [56] to the POD setting for NSE. In particular, to create a VMS-POD, stabilization is added as a completely decoupled second step in a time stepping scheme for incompressible flow simulation. That is, at each step there is a two step procedure at each time step: the first step evolves with a standard POD (i.e. unstabilized Galerkin POD), and then the second step is a weighted POD projection that adds (in a sense) extra viscosity to the lower POD modes. The method can thus be easily incorporated into a standard (or legacy) Galerkin POD code, since the approach adds an uncoupled and a separate postprocessing step. The second objective is to introduce POD methodology for Darcy-Brinkman equations with double diffusive convection and apply the post-processing VMS-POD idea only for the momentum equation in this system. As the Ra number increases, the convection cells emerge and the instability occurs in the system. Thus, the third objection is to develop the POD method by adding a coupled projection-based VMS method for Darcy-Brinkman system. In addition, to obtain a fully linear system at each time level, the nonlinear terms are treated with the extrapolated Crank Nicholson method.

1.1 Outline

To achieve these objectives, mathematical preliminaries and continuous variational formulation of the NSE and the double diffusive Darcy-Brinkman system are presented in the next section. The remaining chapters are organized as follows.

Chapter 2 is devoted to a review of POD-based reduced-order modelling. First, the essentials of the continuous and discrete POD are described in details. Then, the POD spaces and POD Galerkin formulation of the incompressible NSE are introduced. Note that, to derive a priori error estimation, an optimal approach of the true solutions on the POD spaces are needed. In this thesis, for this purpose, the L^2 projection of each variable is utilized. Some error estimations of L^2 projection to be used in the error analysis are stated. Afterwards, the VMS method used to increase the effect of the POD method is introduced. At the end of the section, POD preliminaries, POD spaces and POD formulations of the double diffusion system are given similar to the

NSE case.

Chapter 3 focuses on proposing, analyzing, and testing a post-processing implementation of VMS method with POD for the incompressible NSE. The projection-based VMS stabilization is added as a separate post-processing step to the standard POD approximation, and since the stabilization step is completely decoupled, the method can easily be incorporated into existing codes, and stabilization parameters can be tuned independent from the time evolution step. A theoretical analysis of the method is presented with the backward Euler and BDF2 temporal discretization. Several numerical experiments are performed on benchmark problems.

Chapter 4 extends the POD methodology to flows governed by the double-diffusive convection, which models the flow driven by two potentials with different diffusion rates. The stability and convergence analyses of the POD Galerkin formulation which is given in Chapter 1 are performed with backward Euler temporal discretization. Then, for high Rayleigh number, the POD method is combined with decoupled VMS method similar to Chapter 3. Especially, artificial diffusion viscosity gets added to the smaller R velocity modes in a post-processing step. The numerical analysis of the VMS-POD formulation are given. The numerical tests on a benchmark problem are illustrated to test the efficiency of the reduction model in this setting.

Chapter 5 presents stabilized POD formulation which is defined in Chapter 4 with coupled VMS method for the Darcy Brinkman equations with double diffusive convection. The system is equipped with a Crank Nicholson temporal discretization and a finite element method for spacial discretization. The nonlinear terms are treated with the extrapolated Crank Nicholson method, to get a fully linear system at each time level. Numerical analysis of the VMS-POD formulation is presented. The analytical results are verified with numerical experiments.

Finally, the thesis ends with conclusions of this dissertation and the discussion for future research directions in Chapter 6.

1.2 Mathematical Preliminaries and Notations

In this section, some mathematical notations and preliminaries which will be used throughout this thesis are introduced.

1.2.1 Sobolev Spaces

We assume that $\Omega \subset \mathbb{R}^d$, $d = \{2, 3\}$ is a polygonal or polyhedral domain, with boundary $\partial\Omega$. Let $g : \Omega \to \mathbb{R}^d$ be a function. Partial derivative of order $|\alpha|$ is defined by

$$D^{\alpha} g = \frac{\partial^{|\alpha|} g}{\partial {x_1}^{\alpha_1} \partial {x_2}^{\alpha_2} \cdots \partial {x_n}^{\alpha_d}} \tag{1.2.1}$$

where $\alpha = (\alpha_1, \alpha_2, \cdots, \alpha_d)$ is a multi-index of non-negative integer numbers and its length is defined by $|\alpha| = \alpha_1 + \alpha_2 + \cdots + \alpha_d$.

Definition 1.2.1 *Let $g \in C(\Omega)$, Then*

$$supp(g) = \overline{\{x : g(x) \neq 0\}} \tag{1.2.2}$$

is the support of g. If $supp(g) \subset \Omega$ compact in $\mathbb{R}^d$, g has compact support in Ω.

Definition 1.2.2 *The space $C_0^{\infty}(\Omega)$ is defined by*

$$C_0^{\infty}(\Omega) = \{g \in C^{\infty}(\Omega) : g \text{ has a compact support in } \Omega\}. \tag{1.2.3}$$

Definition 1.2.3 *The Lebesgue spaces consists of functions that p^{th} powers are integrable and they are denoted by*

$$L^p(\Omega) = \{g : g \text{ is Lebesgue measurable function and } \int_{\Omega} |g(x)|^p \mathrm{d}x < \infty\}. \tag{1.2.4}$$

for all $1 \leq p \leq \infty$.

The $L^p(\Omega)$-norm is defined by

$$\|g\|_{L^p} = \Big(\int_{\Omega} |g(x)|^p \mathrm{d}x \Big)^{1/p}, \quad 1 \leq p < \infty \tag{1.2.5}$$

$$\|g\|_{L^{\infty}} = ess \sup_{x \in \Omega} |g(x)|, \qquad p = \infty. \tag{1.2.6}$$

Specially, for $p = 2$, we get $L^2(\Omega)$ which is a Hilbert space equipped with the following inner product

$$(g, h) = \int_\Omega g(x)h(x)\mathrm{d}x, \quad \|g\| = \sqrt{(g, g)}. \tag{1.2.7}$$

The zero-mean subspace of $L^2(\Omega)$ is given by

$$L_0^2(\Omega) = \{g \in L^2(\Omega) : \int_\Omega g\,\mathrm{d}x = 0\}. \tag{1.2.8}$$

Definition 1.2.4 *Sobolev spaces are defined as*

$$W^{m,p}(\Omega) = \{g \in L^p(\Omega) : D^\alpha g \in L^p(\Omega),\ \forall |\alpha| \le m\} \tag{1.2.9}$$

for any $m \in \mathbb{N}$, $1 \le p \le \infty$.

The norms in Sobolev spaces are given as:

$$\|g\|_{W^{m,p}(\Omega)} = \Big(\sum_{|\alpha|\le k}\int_\Omega \|D^\alpha g\|_{L^p}^p\Big)^{1/p}, \quad 1 \le p < \infty \tag{1.2.10}$$

$$\|g\|_{W^{m,\infty}(\Omega)} = \sum_{|\alpha|\le k}\int_\Omega ess\sup_{x\in\Omega}|D^\alpha g|, \quad p = \infty. \tag{1.2.11}$$

Sobolev spaces are Banach spaces with these norms, e.g., see [23]. The interested Sobolev spaces in this thesis are

- *for* $m = 0$, $W^{0,p}(\Omega) = L^p(\Omega)$
- *for* $p = 2$, $W^{m,2}(\Omega) = H^m(\Omega)$ *is Hilbert space equipped with the norm* $\|\cdot\|_m$.
- *The closed subspace of* $H^1(\Omega)$ *is our special interest,*

$$H_0^1(\Omega) := \{v \in L^2(\Omega) : \nabla v \in L^2(\Omega),\ v = 0\, on\, \partial\Omega\}. \tag{1.2.12}$$

We denote the dual space of $H_0^1(\Omega)$ by H^{-1} with norm

$$\|f\|_{-1} = \sup_{v\in X}\frac{|(f, v)|}{\|\nabla v\|}.$$

Definition 1.2.5 *For all (scalar or vector valued) function $v(x,t) \in \Omega \times (0,T]$, the following norms are used*

$$\|v\|_{\infty,p} := ess \sup_{0\le t\le T} \|v(\cdot,t)\|_p, \quad \|v\|_{m,p} := \left(\int_0^T \|v(\cdot,t)\|_p^m \, \mathrm{d}t \right)^{1/m},$$

where T represents to end point. The following notations are utilized for discrete norms

$$|||v|||_{\infty,p} := \max_{0\le n\le M} \|v^n\|_p, \quad |||v|||_{m,p} := \left(\Delta t \sum_{n=0}^{M} \|v^n\|_p^m \right)^{1/m}.$$

where Δt is the time step, we denote variables at time $t^n = n\Delta t$, $\forall n = 0,1,2,...,M$ using superscripts, e.g. $v(t^n) = v^n$.

Definition 1.2.6 *Let $A \in \mathbb{R}^{m\times n}$ be a matrix. Then matrix $2-$norm of A and A^{-1} is given by*

$$\|A\|_2 := \max_{\mathbf{x}\neq 0} \frac{\|A\mathbf{x}\|_2}{\|\mathbf{x}\|_2} = \rho_{max}, \tag{1.2.13}$$

where ρ_{max} is largest singular value of A.

Definition 1.2.7 *(see [73]) Let $\mathcal{F}$ be a functional defined as $\mathcal{F} : D \to \mathbb{R}$, for any manifold D representing functions f. Then for any function $\theta(x)$, the functional derivative $\frac{\delta \mathcal{F}}{\delta f}$ is defined as*

$$\lim_{\alpha\to 0} \frac{\mathcal{F}[f+\alpha\theta] - \mathcal{F}[f]}{\alpha} = \left\{ \frac{d}{d\alpha} \mathcal{F}[f+\alpha\theta] \right\}_{\alpha=0} = \int \frac{\delta \mathcal{F}}{\delta f(x)} \theta(x) dx. \tag{1.2.14}$$

1.2.2 Important Inequalities

Some useful mathematical inequalities and lemmas that are used in the numerical analysis are given below.

Young's inequality: Let α, β be non-negative finite numbers, then the following inequality holds

$$\alpha\beta \le \frac{\xi}{p}\alpha^p + \frac{\xi^{-\frac{q}{p}}}{q}\beta^q, \tag{1.2.15}$$

for any $\xi > 0$, $1 < p, q < \infty$ and $\dfrac{1}{p} + \dfrac{1}{q} = 1$.

Ladyzhenskaya inequality [54] $(2d)$: For any $\nabla f \in L^2(\Omega)$ and $f \in L^4(\Omega)$ with compact support, there is a constant C satisfying for $\Omega \subseteq \mathbb{R}^2$

$$\|f\|_{L^4} \leq C\sqrt{\|f\|\|\nabla f\|}. \tag{1.2.16}$$

Proof It is enough to prove the inequality (1.2.16) only for $\Omega = \mathbb{R}^2$. From (1.2.5), we get

$$\|f\|^4_{L^4(\mathbb{R}^2)} = \int_{\Omega} f^4 \,\mathrm{d}\mathbf{x} \leq \int_{-\infty}^{\infty} \max_{x_1} f^2 \,\mathrm{d}x_2 \int_{-\infty}^{\infty} \max_{x_2} f^2 \,\mathrm{d}x_1. \tag{1.2.17}$$

We also have that

$$\max_{x_k} f^2(x_1, x_2) = 2\int_{-\infty}^{\infty} |f f_{x_k}| \,\mathrm{d}x_k. \tag{1.2.18}$$

Using (1.2.18), we get

$$\begin{aligned} \|f\|^4_{L^4(\mathbb{R}^2)} &\leq 4\int_{-\infty}^{\infty}\int_{-\infty}^{\infty} |f f_{x_1}| \,\mathrm{d}x_1 \,\mathrm{d}x_2 \int_{-\infty}^{\infty}\int_{-\infty}^{\infty} |f f_{x_2}| \,\mathrm{d}x_1 \,\mathrm{d}x_2 \\ &\leq 4\int_{\Omega} f^2 \,\mathrm{d}\mathbf{x} \int_{\Omega} f_{x_1} f_{x_2} \,\mathrm{d}\mathbf{x}. \end{aligned} \tag{1.2.19}$$

Applying Young's inequality (1.2.15) to second factor of the right hand side of (1.2.19), we get

$$\begin{aligned} \|f\|^4_{L^4(\mathbb{R}^2)} &\leq 2\int_{\Omega} f^2 \,\mathrm{d}\mathbf{x} \int_{\Omega} (f_{x_1}^2 + f_{x_2}^2) \,\mathrm{d}\mathbf{x} \\ &\leq 2\int_{\Omega} f^2 \,\mathrm{d}\mathbf{x} \int_{\Omega} (\nabla f)^2 \,\mathrm{d}\mathbf{x}. \end{aligned} \tag{1.2.20}$$

Taking the fourth root both of sides in (1.2.20) results in (1.2.16).

Sylvester's determinant identity: Let $A \in \mathbb{R}^{m\times n}$ and $B \in \mathbb{R}^{n\times m}$ be matrices. Then

$$\det(\mathbb{I}_m + AB) = \det(\mathbb{I}_n + BA), \tag{1.2.21}$$

where $\mathbb{I}_m$, $\mathbb{I}_n$ are identity matrices with order m and n, respectively.

Proof Let C be a matrix as

$$C = \begin{pmatrix} \mathbb{I}_m & -A \\ B & \mathbb{I}_n \end{pmatrix}. \tag{1.2.22}$$

Since $\mathbb{I}_m$, $\mathbb{I}_n$ be invertible matrices, then $\det C$ can be expressed as

$$\det\begin{pmatrix} \mathbb{I}_m & -A \\ B & \mathbb{I}_n \end{pmatrix} = \det(\mathbb{I}_n)\det(\mathbb{I}_m - (-A)\mathbb{I}_n^{-1}B) = \det(\mathbb{I}_m + AB). \tag{1.2.23}$$

Also, $\det C$ can be written as

$$\det\begin{pmatrix} \mathbb{I}_m & -A \\ B & \mathbb{I}_n \end{pmatrix} = \det(\mathbb{I}_m)\det(\mathbb{I}_n - B\mathbb{I}_m^{-1}(-A)) = \det(\mathbb{I}_n + BA). \tag{1.2.24}$$

This gives us the stated result (1.2.21).

Lemma 1.2.8 *(Discrete Gronwall) If $\alpha_n, \beta_n, \gamma_n, \delta_n, K$ and c are nonnegative numbers for $n \geq 0$ and*

$$\alpha_n + K\sum_{n=0}^{M}\beta_n \leq K\sum_{n=0}^{M}\delta_n\alpha_n + K\sum_{n=0}^{M}\gamma_n + c \qquad for\ M \geq 1 \tag{1.2.25}$$

then if $\Delta t d_n < 1$ for every $n = 1, 2, ..., M$,

$$\alpha_n + K\sum_{n=0}^{M}\beta_n \leq \exp\left(K\sum_{n=0}^{M}\frac{\delta_n}{1-\Delta t\delta_n}\right)(K\sum_{n=0}^{M}\gamma_n + c), \qquad for\ M \geq 1. \tag{1.2.26}$$

Proof For the proof, see reference [34].

Lemma 1.2.9 *(Hölder inequality) For any $f \in L^p(\Omega)$ and $g \in L^q(\Omega)$*

$$\|fg\|_{L^1} \leq \|f\|_{L^p}\|g\|_{L^q}, \tag{1.2.27}$$

for all finite $p, q \geq 1$ with $\dfrac{1}{p} + \dfrac{1}{q} = 1$.

Proof For either $\|f\|_{L^p} = 0$ or $\|g\|_{L^q} = 0$, (1.2.27) is satisfied trivially. Otherwise, letting $\xi = 1$, $\alpha = \frac{|f(x)|}{\|f\|_p}$ and $b = \frac{|g(x)|}{\|g\|_q}$ in (1.2.15) gives

$$\frac{|f(x)g(x)|}{\|f\|_{L^p}\|g\|_{L^q}} < \frac{|f(x)|^p}{p\|f\|_{L^p}^p} + \frac{|g(x)|^q}{q\|g\|_{L^q}^q}. \tag{1.2.28}$$

Integrating (1.2.28) over the domain Ω, we get

$$\frac{1}{\|f\|_{L^p}\|g\|_{L^q}}\int_\Omega |f(x)g(x)|\,\mathrm{d}\mathbf{x} < \frac{1}{p\|f\|_{L^p}^p}\int_\Omega |f(x)|^p\,\mathrm{d}\mathbf{x} + \frac{1}{q\|g\|_{L^q}^q}\int_\Omega |g(x)|^q\,\mathrm{d}\mathbf{x}. \tag{1.2.29}$$

From the definition of Lebesgue integral (1.2.5), we have

$$\frac{1}{\|f\|_{L^p}\|g\|_{L^q}} \int_{\Omega} |f(x)g(x)| \, \mathrm{d}\mathbf{x} < \frac{1}{p} + \frac{1}{q}. \tag{1.2.30}$$

Using $\frac{1}{p} + \frac{1}{q} = 1$ and multiplying $\|f\|_{L^p}\|g\|_{L^q}$ results in (1.2.27).

Lemma 1.2.10 *(Cauchy-Schwarz inequality) Let $f, g \in L^2(\Omega)$, then*

$$|(f, g)| \leq \|f\|\|g\| \tag{1.2.31}$$

holds.

Proof Substituting $p = q = 2$ in (1.2.27) gives the stated result (1.2.31).

Lemma 1.2.11 *(Poincaré-Friedrichs' Inequality [11]) Suppose $\Omega \subset F = \{(x_1, x_2, \cdots, x_n) : 0 < x_i < C_p\}$. Then*

$$\|f\| \leq C_p \|\nabla f\| \tag{1.2.32}$$

holds for any $f \in H_0^1$.

Proof To prove (1.2.32), it is sufficient to show $f \in C_0^\infty(\Omega)$ since $C_0^\infty(\Omega)$ is dense in $H_0^1(\Omega)$. One can write

$$f(x_1, x_2, \cdots, x_n) = f(x_1, x_2, \cdots, 0) + \int_0^{x_n} \frac{\partial f(x_1, x_2, \cdots, \alpha)}{\partial \alpha} \, \mathrm{d}\alpha \tag{1.2.33}$$

$f \in H_0^1$ and we set $f = 0$ on $F \setminus \Omega$. Applying (1.2.31) for (1.2.33), we get

$$\begin{aligned} |f(x)| &\leq \Big(\int_0^{x_n} 1^2 \, \mathrm{d}\alpha\Big)^{1/2} \cdot \Big(\int_0^{x_n} |\nabla f(x_1, x_2, \cdots, \alpha)|^2 \, \mathrm{d}\alpha\Big)^{1/2} \\ &\leq \Big(C_p \int_0^{C_p} |\nabla f(x_1, x_2, \cdots, \alpha)|^2 \, \mathrm{d}\alpha\Big)^{1/2} \end{aligned} \tag{1.2.34}$$

Integrating over the x_n coordinates gives

$$\int_0^{x_n} |f(x)| \, \mathrm{d}x_n \leq C_p \Big(\int_0^{C_p} |\nabla f(x)|^2 \, \mathrm{d}x_n \Big)^{1/2} \tag{1.2.35}$$

Integrating over the other coordinates gives

$$\int_F |f| \, \mathrm{d}\mathbf{x} \leq C_p \Big(\int_F |\nabla f|^2 \, \mathrm{d}\mathbf{x} \Big)^{1/2} \tag{1.2.36}$$

Lemma 1.2.12 *The following inequalities satisfies,*

$$\int_\Omega fgh \leq \|f\|_{L^p} \|g\|_{L^q} \|h\|_{L^r}, \tag{1.2.37}$$

where $1 \leq p, q, r \leq \infty$ *with* $\dfrac{1}{p} + \dfrac{1}{q} + \dfrac{1}{r} = 1$.

Proof Applying (1.2.27) gives

$$\int_\Omega fgh \leq \Big(\int_\Omega f^p \Big)^{\frac{1}{p}} \Big(\int_\Omega (gh)^m \Big)^{\frac{1}{m}}, \tag{1.2.38}$$

where $\dfrac{1}{p} + \dfrac{1}{m} = 1$. Applying the (1.2.27) again for the second term of the right hand side of (1.2.38), we have

$$\int_\Omega fgh \leq \Big(\int_\Omega f^p \Big)^{\frac{1}{p}} \Big(\int_\Omega g^{mn} \Big)^{\frac{1}{mn}} \Big(\int_\Omega h^{mr} \Big)^{\frac{1}{mr}}. \tag{1.2.39}$$

Substituting $mn = q$ and $mr = r$ in (1.2.39) results in (1.2.37) with $\dfrac{1}{p} + \dfrac{1}{q} + \dfrac{1}{r} = 1$.

Lemma 1.2.13 *Let* $w(t, \mathbf{x})$ *be a function and* $t^{n/2} = \frac{t^{n+1}+t^n}{2}$. *Then for* $w, w_t, w_{tt}, w_{ttt} \in C^0(0, \tau, L^2(\Omega))$ *and* $\forall t^* \in (t_0, \tau)$ *following inequalies holds*

$$\Big\| \frac{w(t^{n+1}) + w(t^n)}{\Delta t} \Big\| \leq K \|w_t(t^*)\| \tag{1.2.40}$$

$$\Big\| \frac{w(t^{n+1}) + w(t^n)}{2} - w(t^{n/2}) \Big\| \leq K \Delta t^2 \|w_{tt}(t^*)\| \tag{1.2.41}$$

$$\Big\| \frac{3w(t^n)}{2} - \frac{w(t^{n-1})}{2} - w(t^{n/2}) \Big\| \leq K \Delta t^2 \|w_{tt}(t^*)\| \tag{1.2.42}$$

$$\Big\| \frac{w(t^{n+1}) + w(t^n)}{\Delta t} - w_t(t^{n/2}) \Big\| \leq K \Delta t^2 \|w_{ttt}(t^*)\| \tag{1.2.43}$$

for simplicity we use $w(t^n)$ *instead of* $w(\mathbf{x}, t^n)$.

Proof This can be proved by using Taylor series expansion of $w(\mathbf{x}, t)$.

1.3 Full Order Models of Navier Stokes and Darcy-Brinkman Equations

Finite element method (FEM) is successful in analyzing and solving differential equations. Complex geometries can be easily modelled in FEM. Also, the incorporation of boundary conditions is easy. FEM can be applied in many fields such as chemical engineering, acoustic wave, heat transfer, electromagnetic, electrostatics, magnetostatics, multiphysics, CFD, etc. In this section, we focus on the Galerkin FEM discretization of two multiphysics equations:

- the incompressible Navier-Stokes equations (NSE)
- the Darcy-Brinkman equations with double diffusive convection

1.3.1 Galerkin FEM for the Navier Stokes Equations

First of all, we deal with the discretization of the time dependent incompressible Navier-Stokes equations by the standard Galerkin FEM. The incompressible NSE on a polyhedral domain $\Omega \subset \mathbb{R}^d, d \in \{2,3\}$ with boundary $\partial\Omega$ is given as

$$\begin{aligned} \mathbf{u}_t - \nu\Delta\mathbf{u} + (\mathbf{u}\cdot\nabla)\mathbf{u} + \nabla p &= \mathbf{f} \quad \text{in } \Omega\times(0,T], \\ \nabla\cdot\mathbf{u} &= 0 \quad \text{in } \Omega\times[0,T], \\ \mathbf{u} &= \mathbf{0} \quad \text{in } \partial\Omega\times[0,T], \\ \mathbf{u}(\mathbf{x},0) &= \mathbf{u}_0 \quad \text{in } \Omega, \\ \int_\Omega p\, d\mathbf{x} &= 0 \quad \text{in } (0,T], \end{aligned} \tag{1.3.1}$$

where $\mathbf{u}(\mathbf{x},t)$ is the fluid velocity and $p(\mathbf{x},t)$ the fluid pressure. The parameters in (1.3.1) are the kinematic viscosity $\nu > 0$, inversely proportional to Reynolds number $Re = O(\nu^{-1})$, the prescribed body forces $\mathbf{f}(\mathbf{x},t)$ and the initial velocity field $\mathbf{u}_0(\mathbf{x})$. The term, $(\mathbf{u}\cdot\nabla)\mathbf{u}$ is called the convection term, which describes the heat energy transmitted by the bulk motion of particles in a fluid. The term, $Re^{-1}\Delta\mathbf{u}$ is called diffusion term that describes the random movement of particles in a fluid from a highly concentrated region to a lowly concentrated region.

The continuous velocity and pressure spaces are denoted by $\mathbf{X} := (\mathbf{H}_0^1(\Omega))^d$, and

$Q := L_0^2(\Omega)$, respectively, and the divergence free space

$$\mathbf{V} \quad := \quad \{\mathbf{v} \in \mathbf{X} : (\nabla \cdot \mathbf{v}, q) = 0, \ \forall q \in Q\}.$$

Multiplying (1.3.1) with test functions $(\mathbf{v}, q) \in (\mathbf{X}, Q)$ and integrating over the domain Ω results in variational formulation as: Find $\mathbf{u} : (0,T] \to \mathbf{X}$, $p : (0,T] \to Q$

$$\begin{aligned} (\mathbf{u}_t, \mathbf{v}) + (\nu \nabla \mathbf{u}, \nabla \mathbf{v}) + ((\mathbf{u} \cdot \nabla)\mathbf{u}, \mathbf{v}) - (p, \nabla \cdot \mathbf{v}) &= (\mathbf{f}, \mathbf{v}), \\ (q, \nabla \cdot \mathbf{u}) &= 0, \end{aligned} \tag{1.3.2}$$

for all $(\mathbf{v}, q) \in (\mathbf{X}, Q)$. For the nonlinear term in (1.3.2), we use the following vector identity: For any $\mathbf{u}, \mathbf{v}, \mathbf{w} \in \mathbf{V}$

$$\mathbf{u} \cdot \nabla \mathbf{v} \cdot \mathbf{w} = \frac{1}{2} \nabla \cdot (\mathbf{u}|\mathbf{v}||\mathbf{w}|) - \frac{1}{2} |\mathbf{u}||\mathbf{v}| \nabla \cdot \mathbf{w} \tag{1.3.3}$$

It is clear that $(\mathbf{u} \cdot \nabla \mathbf{v}, \mathbf{v}) = 0$ from the (1.3.3), as $\mathbf{u}, \mathbf{v} \in \mathbf{V}$ i.e., then $\mathbf{u} \cdot \mathbf{n} = 0$ on $\partial\Omega$ and $\nabla \cdot \mathbf{v} = 0$. The convective term is defined as

$$b(\mathbf{u}, \mathbf{v}, \mathbf{w}) = \frac{1}{2}((\mathbf{u} \cdot \nabla)\mathbf{v}, \mathbf{w}) - \frac{1}{2}((\mathbf{u} \cdot \nabla)\mathbf{w}, \mathbf{v}). \tag{1.3.4}$$

The form of convective term (1.3.4) is the skew-symmetric and satisfies the following properties.

Lemma 1.3.1 *Let the trilinear form be defined by (1.3.4). Then it satisfies the following properties for constant $C = C(\Omega)$:*

$$b(\mathbf{u}, \mathbf{v}, \mathbf{w}) \quad \leq \quad C\sqrt{\|\mathbf{u}\|\|\nabla \mathbf{u}\|}\|\nabla \mathbf{v}\|\|\nabla \mathbf{w}\|, \tag{1.3.5}$$

$$b(\mathbf{u}, \mathbf{v}, \mathbf{w}) \quad \leq \quad C\|\nabla \mathbf{u}\|\|\nabla \mathbf{v}\|\|\nabla \mathbf{w}\|, \tag{1.3.6}$$

for all $\mathbf{u}, \mathbf{v}, \mathbf{w} \in \mathbf{X}$.

Proof Substituting $p = r = 4$ and $q = 2$ in (1.2.37) results in

$$(\mathbf{u} \cdot \nabla \mathbf{v}, \mathbf{w}) \quad \leq \quad C\|\mathbf{u}\|_{L^4}\|\nabla \mathbf{v}\|_{L^2}\|\mathbf{w}\|_{L^4}. \tag{1.3.7}$$

Using (1.2.16) gives (1.3.5) and applying (1.2.32) gives (1.3.6).

Let Π_h be an admissible triangulations of the domain Ω. For the discretization, a conforming FEM is used for both velocity and pressure spaces $(\mathbf{X}^h, Q^h) \subset (\mathbf{X}, Q)$

satisfying the inf-sup condition (see [28, 32]): There is a constant β such that independent of the mesh size h such that

$$\inf_{q_h \in Q^h} \sup_{\mathbf{v}_h \in \mathbf{X}^h} \frac{(q_h, \nabla \cdot \mathbf{v}_h)}{\| \nabla \mathbf{v}_h \| \| q_h \|} \geq \beta > 0. \tag{1.3.8}$$

In this thesis, we use the Taylor-Hood element pair $(\mathbf{X}^h, Q^h) = (P_m^d, P_{m-1})$ which are defined as

$$\mathbf{X}^h = \{\mathbf{u}_h \in \mathbf{X} : u_h|_K \in P_m^d(K)\}, \tag{1.3.9}$$

$$Q^h = \{q_h \in Q : q_h|_K \in P_{m-1}(K)\}, \tag{1.3.10}$$

for all $K \in \Pi_h$. As noted in [29], for $k \geq 2$, the element pair (1.3.9)-(1.3.10) satisfies the inf-sup condition (1.3.8).

The finite element spaces have the same inner product and norm with $(\mathbf{X}, Q)$ and generally, they are chosen as piecewise polynomials of degrees at most m and $m-1$, respectively. Additionally, we suppose that the spaces satisfy the following interpolation estimates given in [39, 12]: For any $\mathbf{u} \in \mathbf{X} \cap \mathbf{H}^{m+1}(\Omega)$ and $p \in Q \cap H^m(\Omega)$

$$\inf_{\mathbf{v}_h \in X^h} (\|(\mathbf{u} - \mathbf{v}_h)\| + h\|\nabla(\mathbf{u} - \mathbf{v}_h)\|) \leq Ch^{m+1}\|\mathbf{u}\|_{m+1}, \tag{1.3.11}$$

$$\inf_{q_h \in Q^h} \|p - q_h\| \leq Ch^m \|p\|_m. \tag{1.3.12}$$

We denote the discretely divergence free space by

$$\mathbf{V}^h = \{\mathbf{v}_h \in \mathbf{X}^h : (\nabla \cdot \mathbf{v}_h, q_h) = 0, \forall q_h \in Q^h\}. \tag{1.3.13}$$

The inf-sup condition (1.3.8) implies that the space $\mathbf{V}^h$ is a closed subspace of $\mathbf{X}^h$ and the formulation in $\mathbf{X}^h$ is equivalent to $\mathbf{V}^h$, [39].

Thus, the Galerkin FEM approximation of (1.3.2) in $\mathbf{V}^h$ has the following form: Find $\mathbf{u}_h \in \mathbf{V}^h$ satisfying

$$(\mathbf{u}_{h,t}, \mathbf{v}_h) + (\nu \nabla \mathbf{u}_h, \nabla \mathbf{v}_h) + b(\mathbf{u}_h, \mathbf{u}_h, \mathbf{v}_h) = (\mathbf{f}, \mathbf{v}_h), \tag{1.3.14}$$

for all $\mathbf{v}_h \in \mathbf{V}_h$.

Picking a basis in $\mathbf{V}^h$ and expressed $\mathbf{u}_h$ in terms of the basis, the equation (1.3.14) turn into a nonlinear ordinary differential equation that depends on the time. Thus, to obtain an approximate solution, the temporal discretization is required. We use the backward Euler and the backward differentiation (BDF) formula to discretize the equation (1.3.14) in time.

1.3.2 Galerkin FEM for the Darcy-Brinkman Equations with Double Diffusive Convection

Secondly, we now consider the Darcy-Brinkman equations with double diffusive convection, in a confined porous enclosure $\Omega \subset \mathbb{R}^d, d \in \{2,3\}$ with polygonal boundary $\partial\Omega$. In dimensionless form, the system reads as:

$$\begin{aligned}
\mathbf{u}_t - 2\nu\nabla\cdot\mathbb{D}u + (\mathbf{u}\cdot\nabla)\mathbf{u} + Da^{-1}\mathbf{u} + \nabla p &= (\beta_T T + \beta_C C)\mathbf{g} && \text{in } \Omega\times(0,\tau],\\
\nabla\cdot\mathbf{u} &= 0 && \text{in } \Omega\times(0,\tau],\\
\mathbf{u} &= \mathbf{0} && \text{in } \partial\Omega\times(0,\tau],\\
T_t + \mathbf{u}\cdot\nabla T &= \gamma\Delta T && \text{in } \Omega\times(0,\tau],\\
C_t + \mathbf{u}\cdot\nabla C &= D_c\Delta C && \text{in } \Omega\times(0,\tau],\\
T, C &= 0 && \text{on } \Gamma_D,\\
\nabla T\cdot\mathbf{n} = \nabla C\cdot\mathbf{n} &= 0 && \text{on } \Gamma_N,\\
\mathbf{u}(\mathbf{x},0) &= \mathbf{u}_0, && \text{in } \Omega,\\
T(\mathbf{x},0) = T_0,\ C(\mathbf{x},0) &= C_0 && \text{in } \Omega.
\end{aligned} \tag{1.3.15}$$

Let Γ_N be a regular open subset of the boundary and $\Gamma_D = \partial\Omega \setminus \Gamma_N$. The functions $\mathbf{u}(\mathbf{x},t)$, $p(\mathbf{x},t)$, $T(\mathbf{x},t)$, $C(\mathbf{x},t)$ denote the fluid velocity, the pressure, the temperature, and the concentration fields, respectively, and the initial velocity, temperature and concentration fields are given by $\mathbf{u}_0,\ T_0,\ C_0$. The dimensionless parameters are the Schmidt number $Sc = \nu/D_c$, the Lewis number $Le = Sc/Pr$, the Darcy number $Da = k/H^2$, the buoyancy ratio $N = (\beta_C\Delta C)/(\beta_T\Delta T)$, Prandtl number $Pr = \nu/\gamma$, and the thermal and solutal Grashof numbers $Gr_T = (\mathbf{g}\beta_T\Delta T H^3)/\nu^3$ and $Gr_C = (\mathbf{g}\beta_C\Delta C H^3)/\nu^3$, respectively. The parameters in (1.3.15) are the kinematic viscosity $\nu > 0$, the velocity deformation tensor $\mathbb{D}\mathbf{u} = (\nabla\mathbf{u} + \nabla\mathbf{u}^T)/2$, the Darcy number Da, the thermal diffusivity $\gamma > 0$, the mass diffusivity $D_c > 0$, and the gravitational acceleration vector $\mathbf{g}$. The thermal and the solutal expansion coefficients are β_T and β_C, respectively. Here H is the cavity height, k is the permeability, τ is the end time interval and ΔT and ΔC are the temperature and the concentration differences, respectively.

As in the NSE case, the continuous velocity and pressure spaces are given by

$$\mathbf{X} := (\mathbf{H}_0^1(\Omega))^d, \quad Q := L_0^2(\Omega).$$

Similarly temperature and concentration spaces are given by

$$\begin{aligned} W &:= \{S \in H^1(\Omega) : S = 0 \text{ on } \Gamma_D\}, \\ \Psi &:= \{\Phi \in H^1(\Omega) : \Phi = 0 \text{ on } \Gamma_D\}. \end{aligned}$$

The variational formulation of (1.3.15) reads as follows: Find $\mathbf{u} : (0,\tau] \to \mathbf{X}$, $p : (0,\tau] \to Q$, $T : [0,\tau] \to W$ and $C : [0,\tau] \to \Psi$ satisfying

$$\begin{aligned} &(\mathbf{u}_t, \mathbf{v}) + 2\nu(\mathbb{D}\mathbf{u}, \mathbb{D}\mathbf{v}) + b_1(\mathbf{u}, \mathbf{u}, \mathbf{v}) - (p, \nabla \cdot \mathbf{v}) \\ &\quad + (Da^{-1}\mathbf{u}, \mathbf{v}) = \beta_T(\mathbf{g}T, \mathbf{v}) + \beta_C(\mathbf{g}C, \mathbf{v}), \qquad (1.3.16) \\ &(\nabla \cdot \mathbf{u}, q) = 0, \qquad (1.3.17) \\ &(T_t, S) + b_2(\mathbf{u}, T, S) + \gamma(\nabla T, \nabla S) = 0, \qquad (1.3.18) \\ &(C_t, \Phi) + b_3(\mathbf{u}, C, \Phi) + D_c(\nabla C, \nabla \Phi) = 0, \qquad (1.3.19) \end{aligned}$$

for all $(\mathbf{v}, q, S, \Phi) \in (\mathbf{X}, Q, W, \Psi)$, where

$$\begin{aligned} b_1(\mathbf{u}, \mathbf{v}, \mathbf{w}) &:= \frac{1}{2}\left(((\mathbf{u} \cdot \nabla)\mathbf{v}, \mathbf{w}) - ((\mathbf{u} \cdot \nabla)\mathbf{w}, \mathbf{v})\right), \qquad (1.3.20) \\ b_2(\mathbf{u}, T, S) &:= \frac{1}{2}\left(((\mathbf{u} \cdot \nabla)T, S) - ((\mathbf{u} \cdot \nabla)S, T)\right), \qquad (1.3.21) \\ b_3(\mathbf{u}, C, \Phi) &:= \frac{1}{2}\left(((\mathbf{u} \cdot \nabla)C, \Phi) - ((\mathbf{u} \cdot \nabla)\Phi, C)\right) \qquad (1.3.22) \end{aligned}$$

represent the skew-symmetric forms of the convective terms. These forms satisfy the properties in Lemma 1.3.1.

In this part, we consider a conforming FEM for (1.3.16)-(1.3.19), with spaces $\mathbf{X}^h \subset \mathbf{X}$, $Q^h \subset Q$, $W^h \subset W$ and $\Psi^h \subset \Psi$ such that Π_h is an admissible triangulations of the domain Ω. We also assume that the pair $(\mathbf{X}^h, Q^h)$ satisfies the discrete inf-sup condition (1.3.8). It will also be assumed for simplicity that the finite element spaces $\mathbf{X}^h$, W^h, Ψ^h are composed of piecewise polynomials of degree at most m and Q^h is composed of piecewise polynomials of degree at most $m-1$. In addition, we assume that the velocity and the pressure spaces satisfy the interpolation approximation properties (1.3.11)-(1.3.12). Similarly, the temperature and the concentration spaces satisfy the following interpolation estimates:

$$\begin{aligned} \inf_{S_h \in W^h} \|T - S_h\| &\leq Kh^{m+1}\|T\|_{m+1}, \qquad (1.3.23) \\ \inf_{\Phi_h \in \Psi_h} \|C - \Phi_h\| &\leq Kh^{m+1}\|C\|_{m+1}, \qquad (1.3.24) \end{aligned}$$

for $T \in W \cap H^{m+1}(\Omega)$ and $C \in \Psi \cap H^{m+1}(\Omega)$. The finite element formulation of (1.3.16)-(1.3.19) is given as: Find $(\mathbf{u}_h, T_h, C_h) \in (\mathbf{V}^h, W^h, \Psi^h)$ satisfying

$$(\mathbf{u}_{h,t}, \mathbf{v}_h) + 2\nu(\mathbb{D}\mathbf{u}_h, \mathbb{D}\mathbf{v}_h) + b_1(\mathbf{u}_h, \mathbf{u}_h, \mathbf{v}_h) + (Da^{-1}\mathbf{u}_h, \mathbf{v}_h) = \beta_T(\mathbf{g}T_h, \mathbf{v}_h) + \beta_C(\mathbf{g}C_h, \mathbf{v}_h), \tag{1.3.25}$$

$$(T_{h,t}, S_h) + b_2(\mathbf{u}_h, T_h, S_h) + \gamma(\nabla T_h, \nabla S_h) = 0, \tag{1.3.26}$$

$$(C_{h,t}, \Phi_h) + b_3(\mathbf{u}_h, C_h, \Phi_h) + D_c(\nabla C_h, \nabla \Phi_h) = 0, \tag{1.3.27}$$

for all $(\mathbf{v}_h, S_h, \Phi_h) \in (\mathbf{V}^h, W^h, \Psi^h)$.

Choosing a basis in $(\mathbf{V}^h, W^h, \Psi^h)$ and expressed $(\mathbf{u}_h, T_h, C_h)$ in terms of the basis, the equations (1.3.25)-(1.3.27) turn into a nonlinear ordinary differential equation that depends on the time. Hence, to obtain an approximate solution, the temporal discretization is required. We use the backward Euler and the backward differentiation (BDF) formula to discretize the equation (1.3.25)-(1.3.27) in time.

It is well known that if problems (1.3.1) and (1.3.15) are solved by using finite element methods (1.3.14) and (1.3.25)-(1.3.27) respectively, due to the complex behaviour of the fluid flow, the finite element solution may exhibit nonphysical oscillations [30, 65]. This causes a poor and inaccurate approach. The use of stabilization techniques prevents the problems resulting from the dominance of the convection term. Thus, to get an efficient, robust and accurate numerical approximation in this thesis, a projection-based VMS method is implemented to the systems.

CHAPTER 2

REDUCED ORDER MODELLING WITH POD

Simulating complex fluid flows by a direct numerical simulation (DNS) can be very expensive, and sometimes is even infeasible due to the wide range of scales. In particular, in the engineering design process, flow simulations must be run many times, e.g. to perform parameter studies or for system control purposes; this multiplies the DNS cost by at least several times. In addition, using full order models such as finite volume method (FVM), finite difference method (FDM), finite element method (FEM) cause to large algebraic systems and high computational times. The concept of reduced order models was introduced as a way of lowering the computational complexity in such settings. With the emergence of the ROM method, such as Krylov subspace based methods, moment matching methods, proper orthogonal decomposition, balanced truncation, the computing time is reduced and more reliable solutions are obtained.

The POD method is the most efficient technique in complex flows for lowering the computational complexity. The basic idea of the POD is to get new basis functions such that these basis functions cover the space and has lower dimension than the finite element. The method aims to seek good representation of the snapshots and project each one onto POD basis functions which are belong to an inner product space. In this thesis, the POD basis is defined in the Hilbert space.

In the process of obtaining POD basis, we need an ensemble of data. As the exact solution cannot be obtained in NSE type flows, the discrete solution is acquired by recording hundreds of snapshots at a constant time interval. Then to derive optimal POD basis, the obtained experimental data are analysed by revealing dominant structures and snapshots correlation data matrix is constructed. To decompose this matrix,

the singular value decomposition is utilized and the POD method is established as a constrained error minimization problem. Hence solving the minimization problem by using Lagrange multiplier method yields the low dimensional POD basis. Using this new optimal basis, the full order model is projected with the Galerkin projection onto the low-dimensional subspace.

The performance of the POD method can be improved with the optimal choice of the snapshot set. Since the POD basis contains as much information as the snapshots contains, the success of the POD method depends on the selection of the snapshot set. There are many successful methods that provide better selection of snapshots such as the sequential proper orthogonal decomposition (SPOD), trust-region proper orthogonal decomposition (TRPOD), the centroidal Voronoi tessellation (CVT), etc. In SPOD, snapshots are selected in equally distributed in the space [44]. However, TRPOD gives better results by using the trust region philosophy to select the snapshot set [3, 24]. Another better choice of the snapshot set is developed by creating a special Voronoi cluster of snapshots in CVT [13].

The POD performance also depends on POD modes number. As the number of POD modes increases, more information is retained, but the computational cost increases. To find optimal basis, one of the approaches is the principal interval decomposition (PID) method. In PID, the dominant POD modes are extracted over the time subinterval [10]. Another method used for same purpose is the principal interaction patterns (PIP) method in which the optimal POD modes are obtained by a nonlinear minimization procedure [33]. However, in nonlinear problems, the optimality of POD modes might not reduce the computational time of the approach sufficiently. For such problem, the efficiency of POD method is increased by using the empirical interpolation method (EIM) [7] and discrete empirical interpolation method (DEIM) ([16, 52, 96]).

In this dissertation, the efficiency of POD method is increased by variational multiscale (VMS) method of [36, 37] which is based on locality of energy transfer. The idea of the VMS method is to improve the approach by adding an artificial viscosity term to only resolved small-scales.

2.1 POD-ROM Preliminaries for NSE

In this section the essentials of POD are described in continuous and discrete setting.

2.1.1 POD in Continuous Setting

The aim of the POD is to find a low-dimensional ordered, orthonormal basis functions $\{\boldsymbol{\psi}_1, \boldsymbol{\psi}_2, \ldots, \boldsymbol{\psi}_r\}$ by solving the minimization problem of

$$\begin{aligned} \underset{\boldsymbol{\psi}_1,\ldots,\boldsymbol{\psi}_r}{\arg\min} \int_0^T \|\mathbf{u}(\cdot,t) - \sum_{i=1}^{r} a_i(t)\boldsymbol{\psi}_i(\cdot)\|^2 \,\mathrm{d}t, \\ \text{subject to } (\boldsymbol{\psi}_i, \boldsymbol{\psi}_j) = \delta_{ij}, \end{aligned} \tag{2.1.1}$$

where δ_{ij} denote Kronecker delta function, $a_i(t)$ denote time varying coefficients, $1 \le i, j \le r$ and $r << d$. The best approximation for $\mathbf{u}$ is given by

$$\sum_{i=1}^{r} \Big(\mathbf{u}(\cdot,t), \boldsymbol{\psi}_i(\cdot)\Big)\boldsymbol{\psi}_i(\cdot) \tag{2.1.2}$$

in Hilbert space theory. Hence the time varying coefficients are represented by

$$a_i(t) = (\mathbf{u}(\cdot,t), \boldsymbol{\psi}_i(\cdot)) \tag{2.1.3}$$

Inserting (2.1.2) in (2.1.1), the optimization problem becomes

$$\begin{aligned} \underset{\boldsymbol{\psi}_1,\ldots,\boldsymbol{\psi}_r}{\arg\min} \int_0^T \|\mathbf{u}(\cdot,t) - \sum_{i=1}^{r} (\mathbf{u}(\cdot,t), \boldsymbol{\psi}_i(\cdot))\boldsymbol{\psi}_i(\cdot)\|^2 \,\mathrm{d}t, \\ \text{subject to } (\boldsymbol{\psi}_i, \boldsymbol{\psi}_j) = \delta_{ij}, \end{aligned} \tag{2.1.4}$$

Rearranging (2.1.4) by using properties of inner product gives

$$\begin{aligned} &\underset{\boldsymbol{\psi}_1,\ldots,\boldsymbol{\psi}_r}{\arg\min} \int_0^T \Big(\mathbf{u}(\cdot,t) - \sum_{i=1}^{r} (\mathbf{u}(\cdot,t), \boldsymbol{\psi}_i(\cdot))\boldsymbol{\psi}_i(\cdot), \mathbf{u}(\cdot,t) - \sum_{j=1}^{r} (\mathbf{u}(\cdot,t), \boldsymbol{\psi}_j(\cdot))\boldsymbol{\psi}_j(\cdot)\Big) \,\mathrm{d}t \\ = \; &\underset{\boldsymbol{\psi}_1,\ldots,\boldsymbol{\psi}_r}{\arg\min} \int_0^T \Bigg((\mathbf{u}(\cdot,t), \mathbf{u}(\cdot,t)) - \Big(\mathbf{u}(\cdot,t), \sum_{j=1}^{r} (\mathbf{u}(\cdot,t), \boldsymbol{\psi}_j(\cdot))\boldsymbol{\psi}_j(\cdot)\Big) \\ &- \Big(\sum_{i=1}^{r} (\mathbf{u}(\cdot,t), \boldsymbol{\psi}_i(\cdot))\boldsymbol{\psi}_i(\cdot), \mathbf{u}(\cdot,t)\Big) \\ &+ \Big(\sum_{i=1}^{r} (\mathbf{u}(\cdot,t), \boldsymbol{\psi}_i(\cdot))\boldsymbol{\psi}_i(\cdot), \sum_{j=1}^{r} (\mathbf{u}(\cdot,t), \boldsymbol{\psi}_j(\cdot))\boldsymbol{\psi}_j(\cdot)\Big)\Bigg) \,\mathrm{d}t \end{aligned} \tag{2.1.5}$$

Using $(\boldsymbol{\psi}_i, \boldsymbol{\psi}_j) = \delta_{ij}, 1 \le i, j \le r$ gives

$$\underset{\boldsymbol{\psi}_1,\ldots,\boldsymbol{\psi}_r}{\arg\min} \int_0^T \Big(\|\mathbf{u}(\cdot,t)\|^2 - \sum_{i=1}^{r} |(\mathbf{u}(\cdot,t), \boldsymbol{\psi}_i(\cdot))|^2\Big) \,\mathrm{d}t \tag{2.1.6}$$

Since the first term is independent of POD basis functions, the problem (2.1.6) is simplified as

$$\begin{aligned} &\underset{\boldsymbol{\psi}_1,\ldots,\boldsymbol{\psi}_r}{\arg\max} \int_0^T \sum_{i=1}^{r} |(\mathbf{u}(\cdot,t),\boldsymbol{\psi}_i(\cdot))|^2 \,\mathrm{d}t \\ &\text{subject to } (\boldsymbol{\psi}_i,\boldsymbol{\psi}_j) = \delta_{ij}, 1 \le i,j \le r. \end{aligned} \tag{2.1.7}$$

To solve this optimization problem, Lagrange multiplier functional can be written as

$$\mathcal{F}(\boldsymbol{\psi}_1,\boldsymbol{\psi}_2,\ldots,\boldsymbol{\psi}_r;\boldsymbol{\Theta}) = \int_0^T \sum_{i=1}^{r} |(\mathbf{u}(\cdot,t),\boldsymbol{\psi}_i(\cdot))|^2 - \sum_{i=1}^{r}\sum_{j=1}^{r} \lambda_{ij}((\boldsymbol{\psi}_i,\boldsymbol{\psi}_j) - \delta_{ij}),$$

where $(\boldsymbol{\Theta})_{ij} = \lambda_{ij}$ and $\boldsymbol{\Theta} \in \mathbb{R}^{r\times r}$, $1 \le i,j \le r$,. The constraint problem is solved by finding the values that make zero the derivative of $\mathcal{F}$ with respect to $\boldsymbol{\psi}_i$ and Λ_i i.e.,

$$\frac{\partial \mathcal{F}}{\partial \boldsymbol{\psi}_i} = 0, \frac{\partial \mathcal{F}}{\partial \Lambda_{ij}} = 0, \quad i,j = 1,\ldots,r. \tag{2.1.8}$$

Using the Gâteaux Derivative, the solution of the system (2.1.8) for any $i = 1,\ldots,r$ becomes

$$\begin{aligned} \frac{\partial \mathcal{F}}{\partial \boldsymbol{\psi}_i} &= \lim_{\alpha\to 0} \frac{\int_0^T (\mathbf{u},\boldsymbol{\psi}_i+\alpha\boldsymbol{\phi})(\boldsymbol{\psi}_i+\alpha\boldsymbol{\phi},\mathbf{u}) - (\mathbf{u},\boldsymbol{\psi}_i)(\boldsymbol{\psi}_i,\mathbf{u})\,\mathrm{d}t}{\alpha} \\ &\quad - \lim_{\alpha\to 0} \frac{\sum_{j=1}^{r} \lambda_{ij}\Big((\boldsymbol{\psi}_i+\alpha\boldsymbol{\phi},\boldsymbol{\psi}_j) - (\boldsymbol{\psi}_i,\boldsymbol{\psi}_j)\Big)}{\alpha} \\ &\quad - \lim_{\alpha\to 0} \frac{\sum_{j=1}^{r} \lambda_{ji}\Big((\boldsymbol{\psi}_j,\boldsymbol{\psi}_i+\alpha\boldsymbol{\phi}) - (\boldsymbol{\psi}_j,\boldsymbol{\psi}_i)\Big)}{\alpha}. \end{aligned} \tag{2.1.9}$$

Reorganizing (2.1.9), we get

$$\begin{aligned} \frac{\partial \mathcal{F}}{\partial \boldsymbol{\psi}_i} &= \lim_{\alpha\to 0} \frac{\int_0^T (\mathbf{u},\boldsymbol{\psi}_i)(\alpha\boldsymbol{\phi},\mathbf{u}) + (\mathbf{u},\alpha\boldsymbol{\phi})(\boldsymbol{\psi}_i,\mathbf{u}) + (\mathbf{u},\alpha\boldsymbol{\phi})(\alpha\boldsymbol{\phi},\mathbf{u})\,\mathrm{d}t}{\alpha} \\ &\quad - \lim_{\alpha\to 0} \frac{\sum_{j=1}^{r} \lambda_{ij}(\alpha\boldsymbol{\phi},\boldsymbol{\psi}_j) + \lambda_{ji}(\boldsymbol{\psi}_j,\alpha\boldsymbol{\phi})}{\alpha}. \end{aligned} \tag{2.1.10}$$

Taking the limit gives

$$\begin{aligned} \frac{\partial \mathcal{F}}{\partial \boldsymbol{\psi}_i} &= 2\int_0^T (\mathbf{u},\boldsymbol{\psi}_i)(\mathbf{u},\boldsymbol{\phi})\,\mathrm{d}t - \sum_{j=1}^{r}(\lambda_{ij}+\lambda_{ji})(\boldsymbol{\psi}_j,\boldsymbol{\phi}) \\ &= \left(2\int_0^T (\mathbf{u},\boldsymbol{\psi}_i)\mathbf{u}\,\mathrm{d}t - \sum_{j=1}^{r}(\lambda_{ij}+\lambda_{ji})\boldsymbol{\psi}_j,\boldsymbol{\phi}\right) = 0. \end{aligned} \tag{2.1.11}$$

Hence we get

$$\int_0^T (\mathbf{u},\boldsymbol{\psi}_i)\mathbf{u}\,\mathrm{d}t = \frac{1}{2}\sum_{j=1}^{r}(\lambda_{ij}+\lambda_{ji})\boldsymbol{\psi}_j \;\forall i = 1,\ldots,r. \tag{2.1.12}$$

Note that the problem

$$\int_0^T (\mathbf{u}, \boldsymbol{\psi}_i)\mathbf{u}\,\mathrm{d}t = \sum_{j=1}^{r} \lambda_i \boldsymbol{\psi}_j \;\forall i = 1, \ldots, r. \tag{2.1.13}$$

is equivalent to (2.1.12) where $\lambda_i = \lambda_{ii}$, [27].

As the formulation $\int_0^T (\mathbf{u}, \mathbf{u})$ is proportional to kinetic energy, in the literature it is thought to represent kinetic energy. Hence to obtain energy, we use the properties of inner product as follows.

$$\begin{aligned}
\int_0^T (\mathbf{u}, \mathbf{u})\,\mathrm{d}t &= \int_0^T \Big(\sum_{i=1}^{r} (\mathbf{u}, \boldsymbol{\psi}_i)\boldsymbol{\psi}_i, \sum_{j=1}^{r} (\mathbf{u}, \boldsymbol{\psi}_j)\boldsymbol{\psi}_j \Big)\,\mathrm{d}t \\
&= \sum_{i=1}^{r}\sum_{j=1}^{r} \int_0^T (\mathbf{u}, \boldsymbol{\psi}_i)(\mathbf{u}, \boldsymbol{\psi}_j)(\boldsymbol{\psi}_i, \boldsymbol{\psi}_j)\,\mathrm{d}t \\
&= \sum_{i=1}^{r} \int_0^T (\mathbf{u}, \boldsymbol{\psi}_i)(\mathbf{u}, \boldsymbol{\psi}_i)\,\mathrm{d}t \\
&= \sum_{i=1}^{r} \Big(\int_0^T (\mathbf{u}, \boldsymbol{\psi}_i)\mathbf{u}\,\mathrm{d}t, \boldsymbol{\psi}_i \Big).
\end{aligned} \tag{2.1.14}$$

Inserting (2.1.13) in the (2.1.14) produce the energy as

$$\int_0^T (\mathbf{u}, \mathbf{u})\,\mathrm{d}t = \sum_{i=1}^{r} \lambda_i. \tag{2.1.15}$$

Then the captured energy by POD modes is defined as

$$E_u = \frac{\sum_{j=1}^{r} \lambda_j}{\sum_{j=1}^{M} \lambda_j} \tag{2.1.16}$$

Thus the basis functions $\{\boldsymbol{\psi}_i\}_{i=1}^{r}$ correspond to the first r largest eigenvalues, i.e., the most energetic structures in the system.

2.1.2 POD in Discrete Setting

Consider the finite number of the discrete solutions,

$$\mathcal{R}_1 = span\{\mathbf{u}(\cdot, t_1), \ldots, \mathbf{u}(\cdot, t_M)\}$$

at time $t_i = i\Delta t$, $i = 1, \ldots, M$ and let $\Delta t = \frac{T}{M}$, where $rank(\mathcal{R}_1) = d$. In what follows, these discrete solutions will be assumed to come from a DNS computed with a finite element spatial discretization. For simplicity, we assume snapshots are calculated using equidistant time steps.

Let $\{\boldsymbol{\psi}_1, \boldsymbol{\psi}_2, \ldots, \boldsymbol{\psi}_r\}$ be the low-dimensional ordered POD basis functions to approximate these time instances. Since snapshots are calculated as finite element solutions of the system, the velocity and POD basis terms can be expressed in terms of nodal basis $\{\alpha_s(\mathbf{x})\}_{s=1}^N$ with $\alpha_n(\mathbf{x}_m) = \delta_{nm}$ as

$$\mathbf{u}(\cdot, t_k) = \sum_{s=1}^{N} \mathbf{u}(\mathbf{x}_s, t_k)\alpha_s,\ \boldsymbol{\psi}_i(\cdot) = \sum_{s=1}^{N} \boldsymbol{\psi}_i(\mathbf{x}_s)\alpha_s \tag{2.1.17}$$

Then (2.1.13) becomes

$$\begin{aligned} \sum_{k=1}^{M}\sum_{s=1}^{N}(\mathbf{u}_{s,k}\alpha_s, \boldsymbol{\psi}_i(\mathbf{x}_s)\alpha_s)\mathbf{u}_{s,k}\alpha_s &= \mathcal{U}\mathcal{U}^T B\underline{\boldsymbol{\psi}_{i,s}}\,\vec{\alpha} \\ &= \lambda_i\underline{\boldsymbol{\psi}_{i,s}}\,\vec{\alpha} \end{aligned} \tag{2.1.18}$$

where $\mathbf{u}_{s,k} = \mathbf{u}(\mathbf{x}_s, t_k)$, $\vec{\alpha} = \{\alpha_1, \ldots, \alpha_N\}$, $\underline{\boldsymbol{\psi}_{i,s}} = (\boldsymbol{\psi}_i(\mathbf{x}_s))_{s=1}^N$ denotes the coefficients vector of the POD basis with respect to the nodal basis $\{\alpha_s\}_{s=1}^N$, the matrix $B = [\alpha_{ij}]_{N\times N}$ with $\alpha_{ij} = (\alpha_i, \alpha_j)$ and the snapshots matrix $\mathcal{U} \in \mathbb{R}^{N\times M}$ denotes

$$\mathcal{U} = \begin{pmatrix} \mathbf{u}_1^1 & \mathbf{u}_1^2 & \ldots & \mathbf{u}_1^M \\ \mathbf{u}_2^1 & \mathbf{u}_2^2 & \ldots & \mathbf{u}_2^M \\ \vdots & \vdots & \vdots & \vdots \\ \mathbf{u}_N^1 & \mathbf{u}_N^2 & \ldots & \mathbf{u}_N^M \end{pmatrix} \tag{2.1.19}$$

where $\mathcal{U}_{ij} = \mathbf{u}(\mathbf{x}_i, t_j) = \mathbf{u}_i^j$. Hence, (2.1.18) turn into an eigenvalue problem as

$$\mathcal{U}\mathcal{U}^T B\underline{\boldsymbol{\psi}_{i,s}} = \lambda_i\underline{\boldsymbol{\psi}_{i,s}}. \tag{2.1.20}$$

Multiplying by $B^{1/2}$, and using the symmetry property of B produces

$$\begin{aligned} B^{1/2}\mathcal{U}\mathcal{U}^T\underline{\boldsymbol{\psi}_{i,s}} &= B^{1/2}\mathcal{U}\mathcal{U}^T B^{T/2}B^{1/2}\underline{\boldsymbol{\psi}_{i,s}} \\ &= \lambda_i B^{1/2}\underline{\boldsymbol{\psi}_{i,s}}. \end{aligned} \tag{2.1.21}$$

Notice that

$$B^{1/2}\mathcal{U}\mathcal{U}^T B^{T/2} = B^{1/2}\mathcal{U}(B^{1/2}\mathcal{U})^T \tag{2.1.22}$$

is symmetric and positive semi-definite matrix. Hence all eigenvalues are nonnegative real numbers and descending order, i.e. $\lambda_1 \geq \lambda_2 \geq \ldots \lambda_r$.

Applying Sylvester's determinant identity (1.2.21) gives characteristic of $\mathcal{U}\mathcal{U}^T B \in \mathbb{R}^{M\times M}$ is same with $\mathcal{U}^T B\mathcal{U} \in \mathbb{R}^{\mathbb{N}\times\mathbb{N}}$ (see [57]). Solving the eigenvalue problem with

the matrix $\mathcal{U}^T B\mathcal{U}$ is cheaper than the eigenvalue problem with the matrix $\mathcal{U}\mathcal{U}^T B$, as $N << M$. Hence the matrix $\mathcal{U}^T B\mathcal{U}$ is used instead of $\mathcal{U}\mathcal{U}^T B$ in this method.

The matrix $\mathcal{U}^T B\mathcal{U}$ can be written as

$$\mathcal{U}^T B\mathcal{U} = (B^{1/2}\mathcal{U})^T (B^{1/2}\mathcal{U}). \tag{2.1.23}$$

Applying singular value decomposition method (SVD) for $B^{1/2}\mathcal{U}$ gives

$$B^{1/2}\mathcal{U} = Y \begin{pmatrix} \Sigma & 0 \\ 0 & 0 \end{pmatrix} W^T. \tag{2.1.24}$$

Thus, applying SVD for the matrix $\mathcal{U}^T B\mathcal{U}$ produces

$$\mathcal{U}^T B\mathcal{U} = (B^{1/2}\mathcal{U})^T (B^{1/2}\mathcal{U}) = W \begin{pmatrix} T & 0 \\ 0 & 0 \end{pmatrix} W^T, \tag{2.1.25}$$

where $diag(T) = \{\lambda_1, \lambda_2, \ldots, \lambda_r\}$. Thus, one gets

$$B^{1/2}\mathcal{U}\mathcal{U}^T B^{T/2} W = W \begin{pmatrix} T & 0 \\ 0 & 0 \end{pmatrix}. \tag{2.1.26}$$

The eigenvalues of the matrix $\mathcal{U}^T B\mathcal{U}$ denote energy [57], corresponding POD basis functions

$$\boldsymbol{\psi}_l(\cdot) = \frac{1}{\sqrt{\lambda_l}} \sum_{i=1}^{M} (\phi_l)_i \mathbf{u}(\cdot, t_i), \quad 1 \le l \le r, \tag{2.1.27}$$

become most energetic structures in the system. Here $(\phi_l)_i$ is the i^{th} component of the eigenvector ϕ_l of the snapshots correlation matrix.

Remark Since the energy is defined as $\frac{1}{T} \int_{t_0}^{t_0+T} \|\mathbf{u}(\cdot, t)\|^2 \, \mathrm{d}t = \sum_{m=1}^{d} \lambda_m$, (see [94]), the relative error is given as

$$E_r = \frac{\frac{1}{T} \int_{t_0}^{t_0+T} \|\mathbf{u}(\cdot, t) - \sum_{m=1}^{r} (\mathbf{u}(\cdot, t), \boldsymbol{\psi}_m(\cdot)) \boldsymbol{\psi}_m(\cdot)\|^2}{\frac{1}{T} \int_{t_0}^{t_0+T} \|\mathbf{u}(\cdot, t)\|^2 \, \mathrm{d}t} = \frac{\sum_{m=r+1}^{d} \lambda_m}{\sum_{m=1}^{d} \lambda_m}. \tag{2.1.28}$$

By the definition, the relative error is decreasing, i.e., $0 \le E_{r+1} \le E_r \le 1$.

The results of the following lemmas will be applied to bound the POD projection error.

Lemma 2.1.1 *[53] The error estimation satisfies*

$$\frac{1}{M}\sum_{s=1}^{N}\|\mathbf{u}(\cdot,t_k)-\sum_{m=1}^{r}(\mathbf{u}(\cdot,t_k),\boldsymbol{\psi}_m(\cdot))\boldsymbol{\psi}_m(\cdot)\|^2=\sum_{m=r+1}^{d}\lambda_m. \tag{2.1.29}$$

Proof Let $A=\{\mathbf{u}(\cdot,t_1),\ldots,\mathbf{u}(\cdot,t_M)\}$ be a snapshot matrix and A satisfies

$$\frac{1}{M}AA^T\psi_m=\lambda_m\psi_m. \tag{2.1.30}$$

Then the error in POD projection with L^2 norm can be obtained utilizing properties of inner product, the definition of A and (2.1.30) as

$$\begin{aligned}
&\frac{1}{M}\sum_{k=1}^{M}\|\mathbf{u}(\cdot,t_k)-\sum_{m=1}^{r}(\mathbf{u}(\cdot,t_k),\boldsymbol{\psi}_m(\cdot))\boldsymbol{\psi}_m(\cdot)\|^2\\
&=\frac{1}{M}\sum_{k=1}^{M}\|\sum_{m=r+1}^{d}(\mathbf{u}(\cdot,t_k),\boldsymbol{\psi}_m(\cdot))\boldsymbol{\psi}_m(\cdot)\|^2\\
&=\frac{1}{M}\sum_{k=1}^{M}\left(\sum_{m=r+1}^{d}(\mathbf{u}(\cdot,t_k),\boldsymbol{\psi}_m(\cdot))\boldsymbol{\psi}_m(\cdot),\sum_{n=r+1}^{d}(\mathbf{u}(\cdot,t_k),\boldsymbol{\psi}_n(\cdot))\boldsymbol{\psi}_n(\cdot)\right)\\
&=\frac{1}{M}\sum_{k=1}^{M}\sum_{m=r+1}^{d}\sum_{n=r+1}^{d}(\mathbf{u}(\cdot,t_k),\boldsymbol{\psi}_m(\cdot))(\mathbf{u}(\cdot,t_k),\boldsymbol{\psi}_n(\cdot))(\boldsymbol{\psi}_m(\cdot),\boldsymbol{\psi}_n(\cdot))\\
&=\sum_{m=r+1}^{d}\sum_{n=r+1}^{d}\left(\frac{1}{M}\sum_{k=1}^{M}(\mathbf{u}(\cdot,t_k),\boldsymbol{\psi}_m(\cdot))\mathbf{u}(\cdot,t_k),\boldsymbol{\psi}_n(\cdot)\right)(\boldsymbol{\psi}_m(\cdot),\boldsymbol{\psi}_n(\cdot))\\
&=\sum_{m=r+1}^{d}\sum_{n=r+1}^{d}\left(\frac{1}{M}AA^T\boldsymbol{\psi}_m(\cdot),\boldsymbol{\psi}_n(\cdot)\right)(\boldsymbol{\psi}_m(\cdot),\boldsymbol{\psi}_n(\cdot))\\
&=\sum_{m=r+1}^{d}\sum_{n=r+1}^{d}(\lambda_m\boldsymbol{\psi}_m,\boldsymbol{\psi}_n(\cdot))(\boldsymbol{\psi}_m(\cdot),\boldsymbol{\psi}_n(\cdot))=\sum_{m=r+1}^{d}\lambda_m.
\end{aligned} \tag{2.1.31}$$

Let

$$\mathbf{X}^r \;=\; span\{\boldsymbol{\psi}_1,\boldsymbol{\psi}_2,\ldots,\boldsymbol{\psi}_r\}, \tag{2.1.32}$$

be the POD-ROM space, then POD-Galerkin (POD-G) formulation of the NSE is : Find $\mathbf{u}_r\in\mathbf{X}^r$ satisfying

$$(\mathbf{u}_{r,t},\boldsymbol{\psi})+(\nu\nabla\mathbf{u}_r,\nabla\boldsymbol{\psi})+b(\mathbf{u}_r,\mathbf{u}_r,\boldsymbol{\psi})=(\mathbf{f},\boldsymbol{\psi}),\quad\forall\;\boldsymbol{\psi}\in\mathbf{X}^r. \tag{2.1.33}$$

Note that the POD-G solution of the NSE is constructed by writing,

$$\mathbf{u}(\mathbf{x},t)\approx\mathbf{u}_r(\mathbf{x},t):=\sum_{i=1}^{r}a_j(t)\boldsymbol{\psi}_j(\mathbf{x}),$$

where $a_j(t)$ are just point values of approximate solutions. To carry out the error analysis, we state and prove the following error estimations. Let $M_{u,r}$ and $S_{u,r}$ denote the POD mass matrix and stiffness matrix, respectively, with

$$\begin{aligned}(M_{u,r})_{i,j} &= \int_\Omega \boldsymbol{\psi}_j \boldsymbol{\psi}_i \,\mathrm{d}\mathbf{x} \\ (S_{u,r})_{i,j} &= \int_\Omega \nabla\boldsymbol{\psi}_j \cdot \nabla\boldsymbol{\psi}_j \,\mathrm{d}\mathbf{x}\end{aligned}$$

Note that, since we use $L^2(\Omega)$ to generate snapshots, $M_{u,r} = I_{r\times r}$. Our analysis will utilize the following POD inequality.

Lemma 2.1.2 *[53] For all $\mathbf{u}_r \in \mathbf{X}^r$, we have*

$$\|\nabla \mathbf{u}_r\| \leq \|S_{u,r}\|_2^{\frac{1}{2}} \|\mathbf{u}_r\|, \tag{2.1.34}$$

$$\|\mathbf{u}_r\| \leq \|S_{u,r}^{-1}\|_2^{\frac{1}{2}} \|\nabla \mathbf{u}_r\|, \tag{2.1.35}$$

where $\|\cdot\|_2$ denotes the matrix 2-norm.

Proof Let $\mathbf{u}_r := \sum_{j=1}^r (\mathbf{u}_r, \boldsymbol{\psi}_j)\boldsymbol{\psi}_j$, and $\mathbf{x} = \Big((\mathbf{u}_r, \psi_1), \ldots (\mathbf{u}_r, \psi_r)\Big)^T$ be a column vector. Then, from the definition of 2−norm (1.2.13), we get

$$\begin{aligned}\|\nabla \mathbf{u}_r\|^2 &= \mathbf{x}^T S_{u,r}\mathbf{x} \leq \|S_{u,r}\|_2 \mathbf{x}^T\mathbf{x} \\ &\leq \|S_{u,r}\|_2 \|M_{u,r}^{-1}\|_2 \mathbf{x}^T M_{u,r}\mathbf{x} = \|S_{u,r}\|_2 \|M_{u,r}^{-1}\|_2 \|\mathbf{u}_r\|^2\end{aligned}$$

The second inequality (2.1.35) is obtained analogously as

$$\begin{aligned}\|\mathbf{u}_r\|^2 &= \mathbf{x}^T M_{u,r}\mathbf{x} \leq \|M_{u,r}\|_2 \mathbf{x}^T\mathbf{x} \\ &\leq \|M_{u,r}\|_2 \|S_{u,r}^{-1}\|_2 \mathbf{x}^T S_{u,r}\mathbf{x} = \|M_{u,r}\|_2 \|S_{u,r}^{-1}\|_2 \|\nabla \mathbf{u}_r\|^2\end{aligned}$$

The fact that $M_{u,r} = M_{u,r}^{-1} = I_{r\times r}$, gives stated result (2.1.34) and (2.1.35).

The finite element error estimate consists of the splitting the error into an approximation term and a finite element remainder term.

Lemma 2.1.3 *[37] The error in POD projection for the snapshots $\mathbf{u}_h(\cdot, t_k)$, $k = 1, \ldots, M$ satisfies*

$$\frac{1}{M}\sum_{k=1}^{M} \|\mathbf{u}_h(\cdot,t_k) - \sum_{m=1}^{r} (\mathbf{u}_h(\cdot,t_k), \boldsymbol{\psi}_m(\cdot))\boldsymbol{\psi}_m(\cdot)\|_1^2 = \sum_{m=r+1}^{d} \|\boldsymbol{\psi}_m\|_1^2 \lambda_m. \tag{2.1.36}$$

Proof Let $A = \{\mathbf{u}_h(\cdot,t_1),\ldots,\mathbf{u}_h(\cdot,t_M)\}$ be a snapshot matrix and the necessary optimality condition (2.1.30) holds for A. Note that, the approximate velocity function $\mathbf{u}_h$ can be expressed in terms of basis function as in (2.1.2). This yields

$$\begin{aligned}&\frac{1}{M}\sum_{k=1}^{M}\|\mathbf{u}_h(\cdot,t_k)-\sum_{m=1}^{r}(\mathbf{u}_h(\cdot,t_k),\boldsymbol{\psi}_m(\cdot))\boldsymbol{\psi}_m(\cdot)\|_1^2\\ &\quad=\quad\frac{1}{M}\sum_{k=1}^{M}\|\sum_{m=r+1}^{d}(\mathbf{u}_h(\cdot,t_k),\boldsymbol{\psi}_m(\cdot))\boldsymbol{\psi}_m(\cdot)\|_1^2\end{aligned}\tag{2.1.37}$$

Applying the properties of H^1 norm and inner product gives

$$\begin{aligned}&\frac{1}{M}\sum_{k=1}^{M}\|\mathbf{u}_h(\cdot,t_k)-\sum_{m=1}^{r}(\mathbf{u}_h(\cdot,t_k),\boldsymbol{\psi}_m(\cdot))\boldsymbol{\psi}_m(\cdot)\|_1^2\\ &\quad=\quad\frac{1}{M}\sum_{k=1}^{M}\left(\sum_{m=r+1}^{d}(\mathbf{u}_h(\cdot,t_k),\boldsymbol{\psi}_m(\cdot))\boldsymbol{\psi}_m(\cdot),\sum_{n=r+1}^{d}(\mathbf{u}_h(\cdot,t_k),\boldsymbol{\psi}_n(\cdot))\boldsymbol{\psi}_n(\cdot)\right)_1\\ &\quad=\quad\frac{1}{M}\sum_{k=1}^{M}\sum_{m=r+1}^{d}\sum_{n=r+1}^{d}(\mathbf{u}_h(\cdot,t_k),\boldsymbol{\psi}_m(\cdot))(\mathbf{u}_h(\cdot,t_k),\boldsymbol{\psi}_n(\cdot))(\boldsymbol{\psi}_m(\cdot),\boldsymbol{\psi}_n(\cdot))_1\\ &\quad=\quad\sum_{m=r+1}^{d}\sum_{n=r+1}^{d}\left(\frac{1}{M}\sum_{k=1}^{M}(\mathbf{u}_h(\cdot,t_k),\boldsymbol{\psi}_m(\cdot))\mathbf{u}_h(\cdot,t_k),\boldsymbol{\psi}_n(\cdot)\right)(\boldsymbol{\psi}_m(\cdot),\boldsymbol{\psi}_n(\cdot))_1\end{aligned}$$

Utilizing the definition of A, (2.1.30) and the fact that $(\boldsymbol{\psi}_m(\cdot),\boldsymbol{\psi}_n(\cdot)) = \delta_{m,n}$, for $1 \le m,n \le d$ produces

$$\begin{aligned}&\frac{1}{M}\sum_{k=1}^{M}\|\mathbf{u}_h(\cdot,t_k)-\sum_{m=1}^{r}(\mathbf{u}_h(\cdot,t_k),\boldsymbol{\psi}_m(\cdot))\boldsymbol{\psi}_m(\cdot)\|_1^2\\ &\quad=\quad\sum_{m=r+1}^{d}\sum_{n=r+1}^{d}\left(\frac{1}{M}AA^T\boldsymbol{\psi}_m(\cdot),\boldsymbol{\psi}_n(\cdot)\right)(\boldsymbol{\psi}_m(\cdot),\boldsymbol{\psi}_n(\cdot))_1\\ &\quad=\quad\sum_{m=r+1}^{d}\sum_{n=r+1}^{d}(\lambda_m\boldsymbol{\psi}_m,\boldsymbol{\psi}_n(\cdot))(\boldsymbol{\psi}_m(\cdot),\boldsymbol{\psi}_n(\cdot))_1\\ &\quad=\quad\sum_{m=r+1}^{d}\|\boldsymbol{\psi}_m\|_1^2\lambda_m.\end{aligned}\tag{2.1.38}$$

To decompose the error term we use the L^2 projection of $\mathbf{u}$, which fulfills certain interpolation estimates. Lemma 2.1.4 estimates the error between the snapshots and their L^2 projection into $\mathbf{X}^r$. Let $P_{u,r}$ denote a projection operator $P_{u,r} : \mathbf{L}^2 \to \mathbf{X}^r$ that satisfies

$$(\mathbf{u}-P_{u,r}\mathbf{u},\boldsymbol{\psi}_r)=0,\quad\forall\boldsymbol{\psi}_r\in\mathbf{X}^r.\tag{2.1.39}$$

Lemma 2.1.4 *For* $\mathbf{u}^n$ *the true NSE solution at time* t^n*, and* $\mathbf{u} \in L^\infty(0,k;H^{m+1}(\Omega))$*, the difference* $\mathbf{u}^n - P_{u,r}\mathbf{u}^n$ *satisfies*

$$\frac{1}{M}\sum_{n=1}^{M}\|\mathbf{u}^n - P_{u,r}\mathbf{u}^n\|^2 \le C\Big(h^{2m+2}|||\mathbf{u}|||_{2,m+1}^2 + \sum_{i=r+1}^{d}\lambda_i\Big), \quad (2.1.40)$$

$$\frac{1}{M}\sum_{n=1}^{M}\|\nabla(\mathbf{u}^n - P_{u,r}\mathbf{u}^n)\|^2 \le C\Big((h^{2m} + \|S_{u,r}\|_2 h^{2m+2})|||\mathbf{u}|||_{2,m+1}^2 + \varepsilon_u^2\Big), \quad (2.1.41)$$

where $\varepsilon_u = \sqrt{\sum_{i=r+1}^{d}\|\boldsymbol{\psi}_i\|_1^2\lambda_i}$.

Proof Using the definition of L^2 projection and (2.1.39), we have

$$\begin{aligned}\|\mathbf{u}^n - P_{u,r}\mathbf{u}^n\|^2 &= (\mathbf{u}^n - P_{u,r}\mathbf{u}^n, \mathbf{u}^n - P_{u,r}\mathbf{u}^n)\\ &= (\mathbf{u}^n - P_{u,r}\mathbf{u}^n, \mathbf{u}^n - \mathbf{v}_r^n), \quad \forall \mathbf{v}_r^n \in X^r.\end{aligned}$$

Applying the Cauchy-Schwarz inequality produces

$$\|\mathbf{u}^n - P_{u,r}\mathbf{u}^n\| \le \|\mathbf{u}^n - \mathbf{v}_r^n\|$$

Decomposing $\mathbf{u}^n - \mathbf{v}_r^n = (\mathbf{u}^n - \mathbf{u}_h^n) + (\mathbf{u}_h^n - \mathbf{v}_r^n)$, we obtain

$$\|\mathbf{u}^n - P_{u,r}\mathbf{u}^n\| \le \|\mathbf{u}^n - \mathbf{u}_h^n\| + \|\mathbf{u}_h^n - \mathbf{v}_r^n\|.$$

Letting $\mathbf{v}_r^n = P_{u,r}\mathbf{u}_h^n$ and summing over the time steps gives

$$\frac{1}{M}\sum_{n=1}^{M}\|\mathbf{u}^n - P_{u,r}\mathbf{u}^n\|^2 \le \frac{1}{M}\sum_{n=1}^{M}(\|\mathbf{u}^n - \mathbf{u}_h^n\| + \|\mathbf{u}_h^n - P_{u,r}\mathbf{u}_h^n\|)^2$$

Note that estimation for $\|\mathbf{u}^n - \mathbf{u}_h^n\|$ is similarly obtained by using interpolation estimate as it is shown in [77]:

$$\frac{1}{M}\sum_{n=1}^{M}\|\mathbf{u}^n - \mathbf{u}_h^n\|^2 \le Ch^{2m+2}\frac{1}{M}\sum_{n=1}^{M}\|\mathbf{u}^n\|_{m+1}^2 \quad (2.1.42)$$

Picking $P_{u,r}\mathbf{u}_h^n = \sum_{i=1}^{r}(\mathbf{u}_h^n, \boldsymbol{\psi}_i)\boldsymbol{\psi}_i$ and using (2.1.29), we get

$$\frac{1}{M}\sum_{n=1}^{M}\|\mathbf{u}_h^n - P_{u,r}\mathbf{u}_h^n\|^2 = \sum_{i=r+1}^{d}\lambda_i. \quad (2.1.43)$$

Finally, using (2.1.42) and (2.1.43), leads to the following estimation:

$$\frac{1}{M}\sum_{n=1}^{M}\|\mathbf{u}^n - P_{u,r}\mathbf{u}^n\|^2 \le C\Big(h^{2m+2}\frac{1}{M}\sum_{n=1}^{M}\|\mathbf{u}^n\|_{m+1}^2 + \sum_{i=r+1}^{d}\lambda_i\Big).$$

Similarly, we get the following bounds by using Lemma 2.1.2, and Lemma 2.1.3,

$$\begin{aligned}
\frac{1}{M}\sum_{n=1}^{M}\|\nabla(\mathbf{u}^n - P_{u,r}\mathbf{u}^n)\|^2 &\leq \frac{1}{M}\sum_{n=1}^{M}\Big(\|\nabla(\mathbf{u}^n - \mathbf{u}_h^n)\| + \|\nabla(\mathbf{u}_h^n - P_{u,r}\mathbf{u}_h^n)\| \\
&\qquad + \|\nabla(P_{u,r}\mathbf{u}_h^n - P_{u,r}\mathbf{u}^n)\|\Big)^2 \\
&\leq C\Big(h^{2m}\frac{1}{M}\sum_{n=1}^{M}\|\mathbf{u}^n\|_{m+1}^2 + \sum_{i=r+1}^{d}\|\boldsymbol{\psi}_i\|_1^2\lambda_i + \|S_{u,r}\|_2\frac{1}{M}\sum_{n=1}^{M}\|P_{u,r}\mathbf{u}_h^n - P_{u,r}\mathbf{u}^n\|^2\Big) \\
&\leq C\Big(h^{2m}\frac{1}{M}\sum_{n=1}^{M}\|\mathbf{u}^n\|_{m+1}^2 + \sum_{i=r+1}^{d}\|\boldsymbol{\psi}_i\|_1^2\lambda_i + \|S_{u,r}\|_2\frac{1}{M}\sum_{n=1}^{M}\|\mathbf{u}_h^n - \mathbf{u}^n\|^2\Big) \\
&\leq C\Big(h^{2m}\frac{1}{M}\sum_{n=1}^{M}\|\mathbf{u}^n\|_{m+1}^2 + \sum_{i=r+1}^{d}\|\boldsymbol{\psi}_i\|_1^2\lambda_i + \|S_{u,r}\|_2 h^{2m+2}\frac{1}{M}\sum_{n=1}^{M}\|\mathbf{u}^n\|_{m+1}^2\Big).
\end{aligned}$$

Assumption 2.1.1 *We also assume that,*

$$\|\mathbf{u}^n - P_{u,r}\mathbf{u}^n\|^2 \leq C\Big(h^{2m+2} + \sum_{i=r+1}^{d}\lambda_i\Big) \quad \textit{and} \tag{2.1.44}$$

$$\|\nabla(\mathbf{u}^n - P_{u,r}\mathbf{u}^n)\|^2 \leq C\Big(h^{2m} + \|S_{u,r}\|_2 h^{2m+2} + \sum_{i=r+1}^{d}\|\boldsymbol{\psi}_i\|_1^2\lambda_i\Big). \tag{2.1.45}$$

are satisfied.

We note that Assumption 2.1.1 is very common in error analysis for POD type methods [37, 97]. Basically, it assumes that the estimations in Lemma 2.1.4 are similarly valid in a single term.

2.1.3 Projection-Based VMS Formulation for POD

In turbulence simulation, the eddy viscosity concept is commonly used. The VMS method is one of the most popular eddy viscosity model. In the VMS method, variational projections are used instead of filters and small scale modelling is performed by preserving consistency. Therefore, many difficulties arising from inhomogeneous, non-commutative, or complex filters are removed. VMS aims to model unresolved scales by adding an artificial viscosity to only resolved small-scales. Hence, the oscillations in small scales can be removed. As this stabilization method is acting only on the small modes they do not pollute the large scale components of the approximations. In this respect, one can formulate the POD setting in the VMS framework by

choosing the appropriate finite element spaces and adding to projection in the POD formulation, (see [37, 36] for details).

The method that we propose in the next chapter adds one uncoupled modular projection step for the VMS eddy viscosity. In the VMS-POD setting, the eddy viscosity model is introduced only to the small resolved POD modes $\{\boldsymbol{\psi}_{R+1}, \boldsymbol{\psi}_{R+2}, \ldots, \boldsymbol{\psi}_r\}$ with $R < r$. R represents the number of POD modes used in the projection operator, which is required for VMS-setting. In the projection-based VMS method, besides the standard finite element spaces representing all resolved scales an additional large resolved scale is needed. For VMS-POD setting, the following spaces are used for $R < r$:

$$\mathbf{X}^r = \mathbf{X}^R \oplus \mathbf{X}^S \tag{2.1.46}$$

$$\mathbf{X}^R = span\{\boldsymbol{\psi}_1, \boldsymbol{\psi}_2, \ldots, \boldsymbol{\psi}_R\}, \tag{2.1.47}$$

$$\mathbf{X}^S = span\{\boldsymbol{\psi}_{R+1}, \boldsymbol{\psi}_{R+2}, \ldots, \boldsymbol{\psi}_r\}, \tag{2.1.48}$$

$$\mathbf{L}^R = \nabla \mathbf{X}^R := span\{\nabla\boldsymbol{\psi}_1, \nabla\boldsymbol{\psi}_2, \ldots, \nabla\boldsymbol{\psi}_R\}. \tag{2.1.49}$$

Note that from the construction, we have $\mathbf{X}^R \subset \mathbf{X}^r \subset \mathbf{X}^h \subset \mathbf{X}$. Since POD basis functions are sorted in descending order with respect to their kinetic energy, we can consider the space $\mathbf{X}^R$ as large resolved scale i.e. basis functions corresponding to low energy and the space $\mathbf{X}^S$ as small resolved scale, with $R < r$. The L^2 orthogonal projection $P_R : \mathbf{L}^2 \to \mathbf{L}^R$ will be needed in the VMS formulation, and is defined by

$$(\mathbf{u} - P_R\mathbf{u}, \mathbf{v}_R) = 0, \quad \forall \mathbf{v}_R \in \mathbf{L}^R. \tag{2.1.50}$$

and the initial condition $\mathbf{u}_r(\cdot, 0)$ is given by orthogonal projection of $\mathbf{u}^0$ on X^r,

$$\mathbf{u}_r(\cdot, 0) = \mathbf{u}_r^0 := \sum_{i=1}^{r} (\mathbf{u}^0, \boldsymbol{\psi}_j)\boldsymbol{\psi}_j(\mathbf{x}). \tag{2.1.51}$$

The projection of $\mathbf{u}_r$ onto $\mathbf{X}^R$ are denoted as $\mathbf{u}_r^R$, it represents large resolved scale and the projection of $\mathbf{u}_r$ onto $\mathbf{X}^S$ are denoted as $\mathbf{u}_r^S$, it represents small resolved scale. They are defined as

$$\mathbf{u}_r^R = \sum_{i=1}^{R} a_i\boldsymbol{\psi}_i, \ \mathbf{u}_r^S = \sum_{i=R+1}^{r} a_i\boldsymbol{\psi}_i. \tag{2.1.52}$$

Note that $\mathbf{u}_r = \mathbf{u}_r^R + \mathbf{u}_r^S$. The coefficient of the artificial viscosity term is denoted by ν_T. It can be chosen element-wise constant or nonconstant even nonlinear. In the

case of nonlinear ν_T, more complex mathematical theory is required due to the strong monotonicity, see [87].

2.2 Double Diffusive POD-ROM Preliminaries

In this section the essentials of POD-ROM are described for double diffusive system. The notations, and the POD-ROM spaces (2.1.32) for velocity equation are the same with NSE case. Similarly, consider a finite number of the instances for the temperature and the concentration, respectively,

$$\mathcal{R}_2 = span\{T(\cdot,t_1),\ldots,T(\cdot,t_M)\}, \tag{2.2.1}$$

$$\mathcal{R}_3 = span\{C(\cdot,t_1),\ldots,C(\cdot,t_M)\}, \tag{2.2.2}$$

at times $t_i = i\Delta t_j$, $i = 1,\ldots,M$ and let $\Delta t_j = \frac{\tau}{M}$, where $rank(\mathcal{R}_j) = d_j$, $j = 1,2,3$. In what follows, these time instances will be assumed to come from a DNS computed with a finite element spatial discretization. The goal of the POD is to find low dimensional bases $\{\phi_1,\phi_2,\ldots,\phi_{r_2}\}$ and $\{\eta_1,\eta_2,\ldots,\eta_{r_3}\}$ approximating the $\mathcal{R}_2$ and $\mathcal{R}_3$, respectively, by solving the minimization problems of the form

$$\min \frac{1}{M}\sum_{k=1}^{M}\|T(\cdot,t_k)-\sum_{i=1}^{r_2}(T(\cdot,t_k),\phi_i(\cdot))\phi_i(\cdot)\|^2, \tag{2.2.3}$$

$$\min \frac{1}{M}\sum_{k=1}^{M}\|C(\cdot,t_k)-\sum_{i=1}^{r_3}(C(\cdot,t_k),\eta_i(\cdot))\eta_i(\cdot)\|^2, \tag{2.2.4}$$

such that $(\phi_i,\phi_j) = (\eta_i,\eta_j) = \delta_{ij}$, $1 \le i,j \le r_j$ and $r_j << d_j$, $\forall j = 2,3$. The solution of the problem (2.2.3)-(2.2.4) is obtained by using the method of snapshots [89]. Then solutions become

$$\phi_l(\cdot) = \frac{1}{\sqrt{\mu_l}}\sum_{i=1}^{M}(S_l)_i T(\cdot,t_i), \quad 1 \le l \le r_2, \tag{2.2.5}$$

$$\eta_l(\cdot) = \frac{1}{\sqrt{\gamma_l}}\sum_{i=1}^{M}(\Phi_l)_i C(\cdot,t_i), \quad 1 \le l \le r_3, \tag{2.2.6}$$

where $(S_l)_i$ and $(\Phi_l)_i$ are the i^{th} components of the eigenvectors S_l, Φ_l corresponding to μ_l, ξ_l, which are the eigenvalues of the snapshots correlation matrices. We note that all eigenvalues are sorted in descending order. Thus, the basis functions $\{\phi_i\}_{i=1}^{r_2}$ and $\{\eta_i\}_{i=1}^{r_3}$ correspond to the first r_2 and r_3 largest eigenvalues, respectively. For simplicity, we will denote POD-ROM spaces using just r instead of r_1, r_2 and r_3.

However, in the analysis, we are careful to distinguish that these parameters can be chosen independently.

Let W^r and Ψ^r be the POD-ROM spaces spanned by POD basis functions:

$$W^r = span\{\phi_1, \phi_2, \ldots, \phi_{r_2}\}, \tag{2.2.7}$$

$$\Psi^r = span\{\eta_1, \eta_2, \ldots, \eta_{r_3}\}. \tag{2.2.8}$$

Note that by construction $W^r \subset W^h \subset W$ and $\Psi^r \subset \Psi^h \subset \Psi$.

Let the POD mass and stiffness matrices for the temperature and the concentration are respectively given by

$$\begin{aligned} (M_{T,r})_{i,j} &= \int_\Omega \phi_j \phi_i, \quad (S_{T,r})_{i,j} = \int_\Omega \nabla\phi_j \cdot \nabla\phi_i, \\ (M_{C,r})_{i,j} &= \int_\Omega \eta_j \eta_i, \quad (S_{C,r})_{i,j} = \int_\Omega \nabla\eta_j \cdot \nabla\eta_i. \end{aligned} \tag{2.2.9}$$

Note that $M_{u,r} = M_{T,r} = M_{C,r} = I_{r\times r}$ since the eigenvectors are created to be L^2 orthogonal, see [37].

After these preliminaries, we can now state the POD-Galerkin (POD-G) formulation of the Darcy-Brinkman double diffusive system. Given

$$\mathbf{g} \in L^2(0,k;H^{-1}(\Omega)) \text{ and } \mathbf{u}_0 \in (L^2(\Omega))^d,\ T_0, C_0 \in L^2(\Omega). \tag{2.2.10}$$

Find $(\mathbf{u}_r, T_r, C_r) \in (\mathbf{X}^r, W^r, \Psi^r)$ satisfying

$$\begin{aligned} &(\mathbf{u}_{r,t}, \mathbf{v}_r) + 2\nu(\mathbb{D}\mathbf{u}_r, \mathbb{D}\mathbf{v}_r) + b_1(\mathbf{u}_r, \mathbf{u}_r, \mathbf{v}_r) \\ &\quad + (Da^{-1}\mathbf{u}_r, \mathbf{v}_r) = \beta_T(\mathbf{g}T_r, \mathbf{v}_r) + \beta_C(\mathbf{g}C_r, \mathbf{v}_r), \end{aligned} \tag{2.2.11}$$

$$(T_{r,t}, S_r) + b_2(\mathbf{u}_r, T_r, S_r) + \gamma(\nabla T_r, \nabla S_r) = 0, \tag{2.2.12}$$

$$(C_{r,t}, \Phi_r) + b_3(\mathbf{u}_r, C_r, \Phi_r) + D_c(\nabla C_r, \nabla \Phi_r) = 0, \tag{2.2.13}$$

for all $(\mathbf{v}_r, S_r, \Phi_r) \in (\mathbf{X}^r, W^r, \Psi^r)$.

In order to prove an error estimate for the error between the true solution and the POD solution of the double diffusive Darcy-Brinkman system, we first recall the main estimates for projections. For the error assessment, we use the L^2 projections of T_r and C_r, respectively. The L^2 projection operators $P_{T,r} : L^2 \to W^r$, $P_{C,r} : L^2 \to \Psi^r$ are

defined by

$$\begin{aligned}(T - P_{T,r}T, \phi_r) &= 0 \quad \forall \phi_r \in W^r,\\ (C - P_{C,r}C, \eta_r) &= 0 \quad \forall \eta_r \in \Psi^r.\end{aligned} \tag{2.2.14}$$

We now state the L^2 projection error estimates. For a detailed derivation of these estimations, the reader is referred to [21, 37].

Lemma 2.2.1 *Let $T \in L^\infty(0,k;H^{m+1}(\Omega))$ and $C \in L^\infty(0,k;H^{m+1}(\Omega))$ be fulfilled. For any $(T^n, C^n) \in (W, \Psi)$ and their L^2 projections $P_{T,r}T^n = \tilde{T}^n$, and $P_{C,r}C^n = \tilde{C}^n$ in (W^r, Ψ^r) at time t^n, the following inequalities are provided*

$$\frac{1}{M}\sum_{n=0}^{M}\|T^n - \tilde{T}^n\|^2 \leq K\Big(h^{2m+2}\frac{1}{M}\sum_{n=0}^{M}\|T^n\|_{m+1}^2 + \sum_{i=r_2+1}^{d}\mu_i\Big), \tag{2.2.15}$$

$$\frac{1}{M}\sum_{n=0}^{M}\|C^n - \tilde{C}^n\|^2 \leq K\Big(h^{2m+2}\frac{1}{M}\sum_{n=0}^{M}\|C^n\|_{m+1}^2 + \sum_{i=r_3+1}^{d}\xi_i\Big), \tag{2.2.16}$$

$$\frac{1}{M}\sum_{n=0}^{M}\|\nabla(T^n - \tilde{T}^n)\|^2 \leq K\Big((h^{2m} + \|S_{T,r}\|_2 h^{2m+2})|||T|||_{2,m+1}^2 + \varepsilon_T^2\Big), \tag{2.2.17}$$

$$\frac{1}{M}\sum_{n=0}^{M}\|\nabla(C^n - \tilde{C}^n)\|^2 \leq K\Big((h^{2m} + \|S_{C,r}\|_2 h^{2m+2})|||C|||_{2,m+1}^2 + \varepsilon_C^2\Big), \tag{2.2.18}$$

where $S_{T,r}, S_{C,r}$ are the POD stiffness matrices and

$$\varepsilon_T = \sqrt{\sum_{i=r_2+1}^{d}\|\phi_i\|_1^2\mu_i},\ \varepsilon_C = \sqrt{\sum_{i=r_3+1}^{d}\|\eta_i\|_1^2\xi_i} \tag{2.2.19}$$

denote POD contributions for the temperature and the concentration, respectively.

Proof It can be proved similar to (2.1.4).

The following assumptions are needed for the analysis to follow.

Assumption 2.2.1 *We assume that the following estimations are also satisfied.*

$$\|T^n - \tilde{T}^n\|^2 \leq K\Big(h^{2m+2}\frac{1}{M}\sum_{n=0}^{M}\|T^n\|_{m+1}^2 + \sum_{i=r_2+1}^{d}\mu_i\Big), \tag{2.2.20}$$

$$\|C^n - \tilde{C}^n\|^2 \leq K\Big(h^{2m+2}\frac{1}{M}\sum_{n=0}^{M}\|C^n\|_{m+1}^2 + \sum_{i=r_3+1}^{d}\xi_i\Big), \tag{2.2.21}$$

$$\|\nabla(T^n - \tilde{T}^n)\|^2 \leq K\Big((h^{2m} + \|S_{T,r}\|_2 h^{2m+2})\frac{1}{M}\sum_{n=0}^{M}\|T^n\|_{m+1}^2 + \varepsilon_T^2\Big), \tag{2.2.22}$$

$$\|\nabla(C^n - \tilde{C}^n)\|^2 \leq K\Big((h^{2m} + \|S_{C,r}\|_2 h^{2m+2})\frac{1}{M}\sum_{n=0}^{M}\|C^n\|_{m+1}^2 + \varepsilon_C^2\Big). \tag{2.2.23}$$

Basically, it assumes that similar estimations as above are valid in Lemma 2.2.1 for the single terms of the temperature and the concentration, respectively. While from experience this is expected to hold in general, it is possible that some diabolical counterexamples could be created. However, even in such a diabolical case worst case, the estimates would hold but with an M^{-1} on the right hand side.

CHAPTER 3

A MODULAR REGULARIZED VARIATIONAL MULTISCALE PROPER ORTHOGONAL DECOMPOSITION FOR NAVIER-STOKES EQUATIONS

This chapter describes a post-processing implementation of a projection based VMS method with POD for the incompressible NSE given by (1.3.1). First, the standard POD solutions of NSE are obtained. Second, the projection-based VMS stabilization is added as a separate post-processing step to the standard POD approximation. The post-processing implementation gives us some advantages. One of these, incorporation of the method into existing codes is getting easier. Another one is stabilization parameters can be set independent from the time step. In the stabilization step, the artificial diffusion terms are added, then subtracted to recover inconsistency similar to [55]. Hence the artificial diffusion terms act only on fluctuations.

This chapter is structed as follows. Section 3.1 presents the post-processing VMS-POD method for the NSE based on backward Euler and BDF2 time discretizations. In this section, the stability and the convergence analyzes of the method for the backward Euler discretization are performed. In addition, the stability analysis of VMS-POD with BDF2 is established. Section 3.2 includes several numerical tests on benchmark problems which show the effectiveness of the proposed method.

3.1 Numerical Analysis of Post-Processed VMS-POD Schemes

In this section, the considered algorithm introduces a projection based VMS method as a post processing step. For simplicity, in Section 3.1.1 and Section 3.1.2, we analyze the backward Euler temporal discretization. In Section 3.1.3, extension to BDF2 time stepping is considered.

In that analysis that follows, we denote variables at time $t^n = n\Delta t, n = 0, 1, 2, \ldots, M, T := M\Delta t$ using superscripts, e.g. $\mathbf{f}^n := \mathbf{f}(t^n)$. The two step VMS-POD scheme equipped with backward Euler time stepping reads as follows:

Algorithm 3.1.1 *Let* $\mathbf{f} \in L^2(0,T;\mathbf{H}^{-1}(\Omega))$ *and* $\mathbf{u}_r^0 = \mathbf{w}_r^0$ *be given with* L^2 *projection of* $\mathbf{u}_0$ *in* $\mathbf{X}^r$. *Given* $\mathbf{u}_r^n \in \mathbf{X}^r$ *compute* $\mathbf{u}_r^{n+1}$ *by applying the following two steps:*

Step 1. *Calculate* $\mathbf{w}_r^{n+1} \in \mathbf{X}^r$ *satisfying* $\forall \boldsymbol{\psi} \in \mathbf{X}^r$,

$$\left(\frac{\mathbf{w}_r^{n+1} - \mathbf{u}_r^n}{\Delta t}, \boldsymbol{\psi}\right) + b(\mathbf{w}_r^{n+1}, \mathbf{w}_r^{n+1}, \boldsymbol{\psi}) + \nu(\nabla \mathbf{w}_r^{n+1}, \nabla \boldsymbol{\psi}) = (\mathbf{f}^{n+1}, \boldsymbol{\psi}). \quad (3.1.1)$$

Step 2. *Post-process* $\mathbf{w}_r^{n+1}$ *by applying projection* P_R *to obtain* $\mathbf{u}_r^{n+1} \in \mathbf{X}^r$, $\forall \boldsymbol{\psi} \in \mathbf{X}^r$:

$$\left(\frac{\mathbf{w}_r^{n+1} - \mathbf{u}_r^{n+1}}{\Delta t}, \boldsymbol{\psi}\right) = (\nu_T (I - P_R)\nabla \frac{(\mathbf{w}_r^{n+1} + \mathbf{u}_r^{n+1})}{2}, (I - P_R)\nabla \boldsymbol{\psi}), \quad (3.1.2)$$

In our analysis, we assume that the eddy viscosity coefficient ν_T is known bounded, positive and element-wise constant. The results can be extended in the case ν_T is non-constant even nonlinear. The consideration of a nonlinear ν_T requires more complex mathematical theory due to the strong monotonicity, see [87].

We note that Step 1 is the standard Galerkin POD method, and Step 2 is completely decoupled VMS stabilization step. The projection in Step 2 is not a filter but constructed to recover VMS eddy viscosity term as in [56].

Note that if we let $\boldsymbol{\psi} = \frac{(\mathbf{w}_r^{n+1} + \mathbf{u}_r^{n+1})}{2}$ in (3.1.2), the numerical dissipation induced from Step 2 is immediately seen to be

$$\|\mathbf{w}_r^{n+1}\|^2 = \|\mathbf{u}_r^{n+1}\|^2 + 2\nu_T \Delta t \left\| (I - P_R)\nabla \frac{(\mathbf{w}_r^{n+1} + \mathbf{u}_r^{n+1})}{2} \right\|^2. \quad (3.1.3)$$

3.1.1 Stability of Algorithm 3.1.1

We now prove stability of Algorithm 3.1.1.

Lemma 3.1.1 *The post-processed-VMS-POD approximation is unconditionally sta-*

ble in the following sense: for any $\Delta t > 0$*,*

$$\|\mathbf{u}_r^M\|^2 + \sum_{n=0}^{M-1}\left[2\nu_T\Delta t\left\|(I-P_R)\nabla\frac{(\mathbf{w}_r^{n+1}+\mathbf{u}_r^{n+1})}{2}\right\|^2 + \|\mathbf{w}_r^{n+1}-\mathbf{u}_r^n\|^2 \right.$$
$$\left. +\nu\Delta t\|\nabla\mathbf{w}_r^{n+1}\|^2\right] \le \|\mathbf{u}_r^0\|^2 + \nu^{-1}|||\mathbf{f}|||_{2,-1}^2.$$

Proof Letting $\psi = \mathbf{w}_r^{n+1}$ in (3.1.1) and using the polarization identity yields

$$\frac{1}{2\Delta t}\|\mathbf{w}_r^{n+1}\|^2 - \frac{1}{2\Delta t}\|\mathbf{u}_r^n\|^2 + \frac{1}{2\Delta t}\|\mathbf{w}_r^{n+1}-\mathbf{u}_r^n\|^2 + \nu\|\nabla\mathbf{w}_r^{n+1}\|^2 = (\mathbf{f}^{n+1},\mathbf{w}_r^{n+1}). \quad (3.1.4)$$

Substitute (3.1.3) in (3.1.4) and multiply both sides by $2\Delta t$, which provides

$$\|\mathbf{u}_r^{n+1}\|^2 - \|\mathbf{u}_r^n\|^2 + 2\nu_T\Delta t\left\|(I-P_R)\nabla\frac{(\mathbf{w}_r^{n+1}+\mathbf{u}_r^{n+1})}{2}\right\|^2 + \|\mathbf{w}_r^{n+1}-\mathbf{u}_r^n\|^2$$
$$+2\nu\Delta t\|\nabla\mathbf{w}_r^{n+1}\|^2 = 2\Delta t(\mathbf{f}^{n+1},\mathbf{w}_r^{n+1}). \quad (3.1.5)$$

Bounding the forcing term in the usual way, and then summing over the time steps gives the stated result.

The result of Lemma 3.1.1 also establishes the stability of $\mathbf{w}_r^M$.

Corollary 3.1.2 *(Stability of* $\mathbf{w}_r^M$*)*

$$\|\mathbf{w}_r^M\|^2 + 2\nu_T\Delta t\sum_{n=0}^{M-2}\left\|(I-P_R)\nabla\frac{(\mathbf{w}_r^{n+1}+\mathbf{u}_r^{n+1})}{2}\right\|^2 + \sum_{n=0}^{M-1}\left[\|\mathbf{w}_r^{n+1}-\mathbf{u}_r^n\|^2\right.$$
$$\left. +\nu\Delta t\|\nabla\mathbf{w}_r^{n+1}\|^2\right] \le \|\mathbf{u}_r^0\|^2 + \nu^{-1}|||\mathbf{f}|||_{2,-1}^2 \quad (3.1.6)$$

Proof Expand the summation in Lemma 3.1.1 for $n = M-1$ and use (3.1.3).

3.1.2 A Priori Error Estimation

In this section, we present the error analysis of the true solution of NSE and VMS-POD approximation (3.1.1)-(3.1.2). The optimal asymptotic error estimation requires the following regularity assumptions for the true solution:

$$\mathbf{u} \in L^\infty(0,T;H^{m+1}(\Omega)) \quad p \in L^\infty(0,T;H^m(\Omega)) \quad \mathbf{u}_{tt} \in L^2(0,T;H^1(\Omega))$$
$$\mathbf{f} \in L^2(0,T;H^{-1}(\Omega)) \quad (3.1.7)$$

Theorem 3.1.3 *Suppose (3.1.7) holds and* $\mathbf{u}_r^n$ *and* $\mathbf{w}_r^n$ *given by Algorithm 3.1.1. For sufficiently small* Δt*, i.e.* $\Delta t \le [C\nu^{-3}\|\nabla \mathbf{u}\|_{\infty,0}^4]^{-1}$ *we have the following estimation:*

$$\begin{aligned}
&\|\mathbf{u}^M - \mathbf{u}_r^M\|^2 + \sum_{n=0}^{M-1}\left[\frac{1}{4}\Delta t\nu_T\|(I-P_R)\nabla(\mathbf{u}^{n+1} - (\mathbf{u}_r^{n+1}+\mathbf{w}_r^{n+1})/2)\|^2\right.\\
&\left.+\nu\Delta t\|\nabla(\mathbf{u}^{n+1}-\mathbf{w}_r^{n+1})\|^2\right] \le C\Bigg[h^{2m+2}|||\mathbf{u}|||_{2,m+1}^2 + \sum_{j=r+1}^{d}\lambda_j\\
&+\nu\Bigg(\Big(h^{2m}+\|S_r\|_2 h^{2m+2}\Big)|||\mathbf{u}|||_{2,m+1}^2 + \sum_{j=r+1}^{d}\|\boldsymbol{\psi}_j\|_1^2\lambda_j\Bigg)\\
&+\nu^{-1}|||\nabla\mathbf{u}|||_{2,0}^2\Bigg(\Big(h^{2m}+\|S_r\|_2 h^{2m+2}\Big)|||\mathbf{u}|||_{2,m+1}^2 + \sum_{j=r+1}^{d}\|\boldsymbol{\psi}_j\|_1^2\lambda_j\Bigg)\\
&+\nu_T\Bigg(\Big(h^{2m}+(\|S_R\|_2+\|S_r\|_2)h^{2m+2}\Big)|||\mathbf{u}|||_{2,m+1}^2\\
&+\sum_{j=R+1}^{d}\|\boldsymbol{\psi}_j\|_1^2\lambda_j + \sum_{j=r+1}^{d}\|\boldsymbol{\psi}_j\|_1^2\lambda_j\Bigg) + \nu^{-2}(\|\mathbf{u}_r^0\|^2 + \nu^{-1}|||\mathbf{f}|||_{2,-1}^2)\\
&\times\Bigg(\Big(h^{2m}+\|S_r\|_2 h^{2m+2}\Big)|||\mathbf{u}|||_{2,m+1}^2 + \sum_{j=r+1}^{d}\|\boldsymbol{\psi}_j\|_1^2\lambda_j\Bigg)\\
&+\nu^{-1}h^{2m}|||p|||_{2,m}^2 + \nu^{-1}(\Delta t)^2\|\mathbf{u}_{tt}\|_{L^2(0,T;H^1(\Omega))}^2\Bigg]
\end{aligned}$$

where C *is independent from* $\Delta t, h, \nu$ *and* ν_T*.*

Remark Under the assumptions of Theorem 3.1.3 and the finite element spaces $(\mathbf{X}^h, Q^h)$ with piecewise polynomials of degree m and $m-1$, respectively. We obtain the following asymptotic error estimation:

$$\begin{aligned}
&\|\mathbf{u}^M - \mathbf{u}_r^M\|^2 + \sum_{n=0}^{M-1}\left[\frac{1}{4}\Delta t\nu_T\|(I-P_R)\nabla(\mathbf{u}^{n+1} - (\mathbf{u}_r^{n+1}+\mathbf{w}_r^{n+1})/2)\|^2\right.\\
&\left.+\nu\Delta t\|\nabla(\mathbf{u}^{n+1}-\mathbf{w}_r^{n+1})\|^2\right] \le C\Big(h^{2m} + (\Delta t)^2 + (1+\|S_R\|_2+\|S_r\|_2)h^{2m+2}\\
&+\sum_{j=R+1}^{d}\|\boldsymbol{\psi}_j\|_1^2\lambda_j + \sum_{j=r+1}^{d}(1+\|\boldsymbol{\psi}_j\|_1^2)\lambda_j\Big)
\end{aligned}$$

Proof We begin the proof by deriving error equations. From (1.3.2), we have that true solution $(\mathbf{u}, p)$ at time level $t = t^{n+1}$ satisfies, for $\boldsymbol{\psi}_r \in \mathbf{X}^r$,

$$\begin{aligned}
&\left(\frac{\mathbf{u}^{n+1}-\mathbf{u}^n}{\Delta t}, \boldsymbol{\psi}_r\right) + \nu(\nabla\mathbf{u}^{n+1}, \nabla\boldsymbol{\psi}_r) + b(\mathbf{u}^{n+1}, \mathbf{u}^{n+1}, \boldsymbol{\psi}_r)\\
&\qquad -(p^{n+1}, \nabla\cdot\boldsymbol{\psi}_r) + E(\mathbf{u}, \boldsymbol{\psi}_r) = (\mathbf{f}(t^{n+1}), \boldsymbol{\psi}_r), \qquad (3.1.8)
\end{aligned}$$

where

$$E(\mathbf{u},\boldsymbol{\psi}) = \left(\mathbf{u}_t^{n+1} - \frac{\mathbf{u}^{n+1}-\mathbf{u}^n}{\Delta t}, \boldsymbol{\psi}\right).$$

We define the following notations:

$$\boldsymbol{\eta}^n := \mathbf{u}^n - \mathcal{U}^n, \quad \boldsymbol{\phi}_r^n := \mathbf{w}_r^n - \mathcal{U}^n, \quad \boldsymbol{\theta}_r^n := \mathbf{u}_r^n - \mathcal{U}^n, \quad \mathbf{e}_r^n = \mathbf{u}^n - \mathbf{u}_r^n, \quad \boldsymbol{\varepsilon}_r^n := \mathbf{u}^n - \mathbf{w}_r^n,$$

where $\mathcal{U}^{\mathbf{n}}$ is L^2 projection of $\mathbf{u}^n$ in $\mathbf{X}^r$.

Subtracting (3.1.1) from (3.1.8) yields

$$\begin{aligned}\left(\frac{\boldsymbol{\varepsilon}_r^{n+1}-\mathbf{e}_r^n}{\Delta t}, \boldsymbol{\psi}_r\right) + \nu(\nabla\boldsymbol{\varepsilon}_r^{n+1}, \nabla\boldsymbol{\psi}_r) + b(\mathbf{u}^{n+1}, \mathbf{u}^{n+1}, \boldsymbol{\psi}_r)\\ -b(\mathbf{w}_r^{n+1}, \mathbf{w}_r^{n+1}, \boldsymbol{\psi}_r) - (p^{n+1}, \nabla\cdot\boldsymbol{\psi}_r) + E(\mathbf{u}, \boldsymbol{\psi}_r) = 0. \end{aligned} \tag{3.1.9}$$

Substitute $\boldsymbol{\varepsilon}_r^n = \boldsymbol{\eta}^n - \boldsymbol{\phi}_r^n$ and $\mathbf{e}_r^n = \boldsymbol{\eta}^n - \boldsymbol{\theta}_r^n$ with $\boldsymbol{\psi} = \boldsymbol{\phi}_r^{n+1}$ in the last equation we obtain

$$\begin{aligned}\left(\frac{\boldsymbol{\phi}_r^{n+1}-\boldsymbol{\theta}_r^n}{\Delta t}, \boldsymbol{\phi}_r^{n+1}\right) + \nu\|\nabla\boldsymbol{\phi}_r^{n+1}\|^2 = \left(\frac{\boldsymbol{\eta}^{n+1}-\boldsymbol{\eta}^n}{\Delta t}, \boldsymbol{\phi}_r^{n+1}\right) + \nu(\nabla\boldsymbol{\eta}^{n+1}, \nabla\boldsymbol{\phi}_r^{n+1})\\ +\left[b(\mathbf{u}^{n+1}, \mathbf{u}^{n+1}, \boldsymbol{\phi}_r^{n+1}) - b(\mathbf{w}_r^{n+1}, \mathbf{w}_r^{n+1}, \boldsymbol{\phi}_r^{n+1})\right] - (p^{n+1}, \nabla\cdot\boldsymbol{\phi}_r^{n+1}) + E(\mathbf{u}, \boldsymbol{\phi}_r^{n+1}).\end{aligned}$$

From the definition of L^2 projection (2.1.39), we note that $(\boldsymbol{\eta}^n, \boldsymbol{\phi}_r^{n+1}) = 0$ and $(\boldsymbol{\eta}^{n+1}, \boldsymbol{\phi}_r^{n+1}) = 0$. Using this along with the polarization identity and that $\boldsymbol{\phi}_r^{n+1} \in \mathbf{X}^r \subset \mathbf{V}^h$, we obtain the bound

$$\begin{aligned}\frac{1}{2\Delta t}(\|\boldsymbol{\phi}_r^{n+1}\|^2 - \|\boldsymbol{\theta}_r^n\|^2) + \nu\|\nabla\boldsymbol{\phi}_r^{n+1}\|^2 \le |\nu(\nabla\boldsymbol{\eta}^{n+1}, \nabla\boldsymbol{\phi}_r^{n+1})|\\ +|b(\mathbf{u}^{n+1}, \mathbf{u}^{n+1}, \boldsymbol{\phi}_r^{n+1}) - b(\mathbf{w}_r^{n+1}, \mathbf{w}_r^{n+1}, \boldsymbol{\phi}_r^{n+1})|\\ +|(p^{n+1} - q_h, \nabla\cdot\boldsymbol{\phi}_r^{n+1})| + |E(\mathbf{u}, \boldsymbol{\phi}_r^{n+1})|\end{aligned} \tag{3.1.10}$$

The first term on the right hand side of (3.1.10), and the pressure term, can be bounded using Cauchy-Schwarz and Young's inequalities,

$$|\nu(\nabla\boldsymbol{\eta}^{n+1}, \nabla\boldsymbol{\phi}_r^{n+1})| \le C\nu\|\nabla\boldsymbol{\eta}^{n+1}\|^2 + \frac{\nu}{12}\|\nabla\boldsymbol{\phi}_r^{n+1}\|^2 \tag{3.1.11}$$

$$|(p^{n+1} - q_h, \nabla\cdot\boldsymbol{\phi}_r^{n+1})| \le \frac{C}{\nu}\|p^{n+1} - q_h\|^2 + \frac{\nu}{12}\|\nabla\boldsymbol{\phi}_r^{n+1}\|^2. \tag{3.1.12}$$

For the nonlinear terms, first add and subtract terms to get

$$\begin{aligned}
&b(\mathbf{u}^{n+1},\mathbf{u}^{n+1},\boldsymbol{\phi}_r^{n+1}) - b(\mathbf{w}_r^{n+1},\mathbf{w}_r^{n+1},\boldsymbol{\phi}_r^{n+1}) \\
&= b(\mathbf{u}^{n+1},\mathbf{u}^{n+1},\boldsymbol{\phi}_r^{n+1}) - b(\mathbf{w}_r^{n+1},\mathbf{u}^{n+1},\boldsymbol{\phi}_r^{n+1}) + b(\mathbf{w}_r^{n+1},\mathbf{u}^{n+1},\boldsymbol{\phi}_r^{n+1}) \\
&\quad -b(\mathbf{w}_r^{n+1},\mathbf{w}_r^{n+1},\boldsymbol{\phi}_r^{n+1}) \\
&= b(\boldsymbol{\varepsilon}_r^{n+1},\mathbf{u}^{n+1},\boldsymbol{\phi}_r^{n+1}) + b(\mathbf{w}_r^{n+1},\boldsymbol{\varepsilon}_r^{n+1},\boldsymbol{\phi}_r^{n+1}) \\
&= b(\boldsymbol{\eta}^{n+1},\mathbf{u}^{n+1},\boldsymbol{\phi}_r^{n+1}) - b(\boldsymbol{\phi}_r^{n+1},\mathbf{u}^{n+1},\boldsymbol{\phi}_r^{n+1}) \\
&\quad +b(\mathbf{w}_r^{n+1},\boldsymbol{\eta}^{n+1},\boldsymbol{\phi}_r^{n+1}). \qquad (3.1.13)
\end{aligned}$$

Now using Lemma 1.3.1, Young's and Poincaré's inequalities, the terms in (3.1.13) are estimated as follows:

$$\begin{aligned}
|b(\boldsymbol{\eta}^{n+1},\mathbf{u}^{n+1},\boldsymbol{\phi}_r^{n+1})| &\le C\sqrt{\|\boldsymbol{\eta}^{n+1}\|\|\nabla\boldsymbol{\eta}^{n+1}\|}\|\nabla\mathbf{u}^{n+1}\|\|\nabla\boldsymbol{\phi}_r^{n+1}\| \\
&\le \frac{C}{\nu}\|\boldsymbol{\eta}^{n+1}\|\|\nabla\boldsymbol{\eta}^{n+1}\|\|\nabla\mathbf{u}^{n+1}\|^2 + \frac{\nu}{12}\|\nabla\boldsymbol{\phi}_r^{n+1}\|^2, \\
|b(\boldsymbol{\phi}_r^{n+1},\mathbf{u}^{n+1},\boldsymbol{\phi}_r^{n+1})| &\le C\sqrt{\|\boldsymbol{\phi}_r^{n+1}\|\|\nabla\boldsymbol{\phi}_r^{n+1}\|}\|\nabla\mathbf{u}^{n+1}\|\|\nabla\boldsymbol{\phi}_r^{n+1}\| \\
&\le \frac{C}{\nu^3}\|\boldsymbol{\phi}_r^{n+1}\|^2\|\nabla\mathbf{u}^{n+1}\|^4 + \frac{\nu}{12}\|\nabla\boldsymbol{\phi}_r^{n+1}\|^2, \\
|b(\mathbf{w}_r^{n+1},\boldsymbol{\eta}^{n+1},\boldsymbol{\phi}_r^{n+1})| &\le C\sqrt{\|\mathbf{w}_r^{n+1}\|\|\nabla\mathbf{w}_r^{n+1}\|}\|\nabla\boldsymbol{\eta}^{n+1}\|\|\nabla\boldsymbol{\phi}_r^{n+1}\| \\
&\le \frac{C}{\nu}\|\mathbf{w}_r^{n+1}\|\|\nabla\mathbf{w}_r^{n+1}\|\|\nabla\boldsymbol{\eta}^{n+1}\|^2 + \frac{\nu}{12}\|\nabla\boldsymbol{\phi}_r^{n+1}\|^2.
\end{aligned}$$

The consistency error in (3.1.10) is estimated by

$$|E(\mathbf{u},\boldsymbol{\phi}_r^{n+1})| \le \frac{C}{\nu}\|\mathbf{u}_t^{n+1} - \frac{\mathbf{u}^{n+1}-\mathbf{u}^n}{\Delta t}\|^2 + \frac{\nu}{12}\|\nabla\boldsymbol{\phi}_r^{n+1}\|^2 \qquad (3.1.14)$$

Collecting all bounds for the right hand side terms of (3.1.10) and multiplying both sides by $2\Delta t$ gives

$$\begin{aligned}
(\|\boldsymbol{\phi}_r^{n+1}\|^2 - \|\boldsymbol{\theta}_r^n\|^2) + \nu\Delta t\|\nabla\boldsymbol{\phi}_r^{n+1}\|^2 &\le C\nu\Delta t\|\nabla\boldsymbol{\eta}^{n+1}\|^2 + \frac{C\Delta t}{\nu}\|\boldsymbol{\eta}^{n+1}\|\|\nabla\boldsymbol{\eta}^{n+1}\|\|\nabla\mathbf{u}^{n+1}\|^2 \\
&+\frac{C\Delta t}{\nu^3}\|\boldsymbol{\phi}_r^{n+1}\|^2\|\nabla\mathbf{u}^{n+1}\|^4 + \frac{C\Delta t}{\nu}\|\mathbf{w}_r^{n+1}\|\|\nabla\mathbf{w}_r^{n+1}\|\|\nabla\boldsymbol{\eta}^{n+1}\|^2 + \frac{C\Delta t}{\nu}\|p^{n+1}-q_h\|^2 \\
&+\frac{C\Delta t}{\nu}\|\mathbf{u}_t^{n+1} - \frac{\mathbf{u}^{n+1}-\mathbf{u}^n}{\Delta t}\|^2. \qquad (3.1.15)
\end{aligned}$$

We next get a bound for $\|\boldsymbol{\phi}_r^{n+1}\|^2$. Write (3.1.2) by adding and subtracting the true solution projection $\mathcal{U}^{n+1}$ on both sides to get

$$\left(\frac{\boldsymbol{\phi}_r^{n+1}-\boldsymbol{\theta}_r^{n+1}}{\Delta t},\boldsymbol{\psi}\right) = (\nu_T(I-P_R)\nabla\frac{(\boldsymbol{\phi}_r^{n+1}+\boldsymbol{\theta}_r^{n+1}+2\mathcal{U}^{n+1})}{2},(I-P_R)\nabla\boldsymbol{\psi}), \quad (3.1.16)$$

and then choose $\psi = \frac{(\phi_r^{n+1}+\theta_r^{n+1})}{2}$ in (3.1.16) to obtain

$$\begin{aligned}\|\phi_r^{n+1}\|^2 &= \|\theta_r^{n+1}\|^2 + \frac{1}{2}\Delta t\nu_T\|(I-P_R)\nabla(\phi_r^{n+1}+\theta_r^{n+1})\|^2 \\ &\quad +\Delta t(\nu_T(I-P_R)\nabla\mathcal{U}^{n+1},(I-P_R)\nabla(\phi_r^{n+1}+\theta_r^{n+1})). \quad (3.1.17)\end{aligned}$$

Noting $\mathcal{U}^{n+1} = \mathbf{u}^{n+1} - \boldsymbol{\eta}^{n+1}$ and inserting (3.1.17) into (3.1.15) results into

$$\begin{aligned}&\|\theta_r^{n+1}\|^2 - \|\theta_r^n\|^2 + \frac{1}{2}\Delta t\nu_T\|(I-P_R)\nabla(\phi_r^{n+1}+\theta_r^{n+1})\|^2 + \nu\Delta t\|\nabla\phi_r^{n+1}\|^2 \\ &\leq C\nu\Delta t\|\nabla\boldsymbol{\eta}^{n+1}\|^2 + \frac{C\Delta t}{\nu}\|\boldsymbol{\eta}^{n+1}\|\|\nabla\boldsymbol{\eta}^{n+1}\|\|\nabla\mathbf{u}^{n+1}\|^2 \\ &\quad +\frac{C\Delta t}{\nu^3}\|\nabla\mathbf{u}^{n+1}\|^4\Big[\|\theta_r^{n+1}\|^2 + \frac{1}{2}\Delta t\nu_T\|(I-P_R)\nabla(\phi_r^{n+1}+\theta_r^{n+1})\|^2 \\ &\quad +\Delta t(\nu_T(I-P_R)\nabla(\mathbf{u}^{n+1}-\boldsymbol{\eta}^{n+1}),(I-P_R)\nabla(\phi_r^{n+1}+\theta_r^{n+1}))\Big] \\ &\quad +\Delta t(\nu_T(I-P_R)\nabla(\boldsymbol{\eta}^{n+1}-\mathbf{u}^{n+1}),(I-P_R)\nabla(\phi_r^{n+1}+\theta_r^{n+1})) \\ &\quad +\frac{C\Delta t}{\nu}\|\mathbf{w}_r^{n+1}\|\|\nabla\mathbf{w}_r^{n+1}\|\|\nabla\boldsymbol{\eta}^{n+1}\|^2 + \frac{C\Delta t}{\nu}\|p^{n+1}-q_h\|^2 \\ &\quad +\frac{C\Delta t}{\nu}\|\mathbf{u}_t^{n+1} - \frac{\mathbf{u}^{n+1}-\mathbf{u}^n}{\Delta t}\|^2 \quad (3.1.18)\end{aligned}$$

Assume now $\Delta t \leq \frac{1}{8C}\Big[\frac{\|\nabla\mathbf{u}\|^4}{\nu^3}\Big]^{-1}$. Then, we can bound the remaining right hand terms of (3.1.18) as follows :

$$\frac{C(\Delta t)^2}{\nu^3}\nu_T\|\nabla\mathbf{u}^{n+1}\|^4\|(I-P_R)\nabla(\phi_r^{n+1}+\theta_r^{n+1})\|^2 \leq \frac{1}{8}\Delta t\nu_T\|(I-P_R)\nabla(\phi_r^{n+1}+\theta_r^{n+1})\|^2.$$

Similarly, using the preceding bound and Young's inequality we get

$$\begin{aligned}&\frac{C(\Delta t)^2}{\nu^3}\|\nabla\mathbf{u}^{n+1}\|^4|(\nu_T(I-P_R)\nabla(\mathbf{u}^{n+1}-\boldsymbol{\eta}^{n+1}),(I-P_R)\nabla(\phi_r^{n+1}+\theta_r^{n+1}))| \\ &\leq C\Delta t|(\nu_T(I-P_R)\nabla(\mathbf{u}^{n+1}-\boldsymbol{\eta}^{n+1}),(I-P_R)\nabla(\phi_r^{n+1}+\theta_r^{n+1}))| \\ &\leq C\Delta t\nu_T\|(I-P_R)\nabla(\mathbf{u}^{n+1}-\boldsymbol{\eta}^{n+1})\|^2 \\ &\quad +\frac{1}{8}\Delta t\nu_T\|(I-P_R)\nabla(\phi_r^{n+1}+\theta_r^{n+1})\|^2, \quad (3.1.19)\end{aligned}$$

and

$$\begin{aligned}&\Delta t(\nu_T(I-P_R)\nabla(\boldsymbol{\eta}^{n+1}-\mathbf{u}^{n+1}),(I-P_R)\nabla(\phi_r^{n+1}+\theta_r^{n+1})) \\ &\leq C\Delta t\nu_T\|(I-P_R)\nabla(\boldsymbol{\eta}^{n+1}-\mathbf{u}^{n+1})\|^2 \\ &\quad +\frac{1}{8}\Delta t\nu_T\|(I-P_R)\nabla(\phi_r^{n+1}+\theta_r^{n+1})\|^2. \quad (3.1.20)\end{aligned}$$

Substitute the bounds (3.1.19)-(3.1.20) into (3.1.18) and sum from $n = 0$ to $M - 1$.

This gives

$$\begin{aligned}
&\|\boldsymbol{\theta}_r^M\|^2 + \sum_{n=0}^{M-1}\left[\frac{1}{8}\Delta t\nu_T\|(I-P_R)\nabla(\boldsymbol{\phi}_r^{n+1}+\boldsymbol{\theta}_r^{n+1})\|^2 + \nu\Delta t\|\nabla\boldsymbol{\phi}_r^{n+1}\|^2\right]\\
&\leq \|\boldsymbol{\theta}_r^0\|^2 + C\sum_{n=0}^{M-1}\left[\nu\Delta t\|\nabla\boldsymbol{\eta}^{n+1}\|^2 + \frac{\Delta t}{\nu}\|\nabla\mathbf{u}^{n+1}\|^2\|\nabla\boldsymbol{\eta}^{n+1}\|^2\right.\\
&\quad +\Delta t\nu_T\|(I-P_R)\nabla(\mathbf{u}^{n+1}-\boldsymbol{\eta}^{n+1})\|^2 + \frac{\Delta t}{\nu}\|\mathbf{w}_r^{n+1}\|\|\nabla\mathbf{w}_r^{n+1}\|\|\nabla\boldsymbol{\eta}^{n+1}\|^2\\
&\quad \left.+\frac{\Delta t}{\nu}\|p^{n+1}-q_h\|^2 + \frac{\Delta t}{\nu}\|\mathbf{u}_t^{n+1} - \frac{\mathbf{u}^{n+1}-\mathbf{u}^n}{\Delta t}\|^2\right]\\
&\quad +\frac{C\Delta t}{\nu^3}\sum_{n=0}^{M-1}\|\nabla\mathbf{u}^{n+1}\|^4\|\boldsymbol{\theta}_r^{n+1}\|^2 \qquad (3.1.21)
\end{aligned}$$

Note that since $\mathbf{u}_r^0 = \mathcal{U}^0$, the first right hand side term in (3.1.21) vanishes. The second right hand side term is majorized using Lemma 2.1.4, as

$$\nu\Delta t\sum_{n=0}^{M-1}\|\nabla\boldsymbol{\eta}^{n+1}\|^2 \leq C\nu\Big(\big(h^{2m}+\|S_r\|_2 h^{2m+2}\big)|||\mathbf{u}|||_{2,m+1}^2 + \sum_{j=r+1}^{d}\|\boldsymbol{\psi}_j\|_1^2\lambda_j\Big), \qquad (3.1.22)$$

Third term is bounded by using Assumption (2.1.1) as follows,

$$\begin{aligned}
&\frac{\Delta t}{\nu}\sum_{n=0}^{M-1}\|\nabla\boldsymbol{\eta}^{n+1}\|^2\|\nabla\mathbf{u}^{n+1}\|^2\\
&\leq \frac{\Delta t}{\nu}\sum_{n=0}^{M-1}\|\nabla\mathbf{u}^{n+1}\|^2\Big(\big(h^{2m}+\|S_r\|_2 h^{2m+2}\big)|||\mathbf{u}|||_{2,m+1}^2 + \sum_{j=r+1}^{d}\|\boldsymbol{\psi}_j\|_1^2\lambda_j\Big)\\
&\leq \nu^{-1}|||\nabla\mathbf{u}|||_{2,0}^2\Big(\big(h^{2m}+\|S_r\|_2 h^{2m+2}\big)|||\mathbf{u}|||_{2,m+1}^2 + \sum_{j=r+1}^{d}\|\boldsymbol{\psi}_j\|_1^2\lambda_j\Big) \qquad (3.1.23)
\end{aligned}$$

To bound the fourth term, one can proceed as follows. Using $\|(I-P_R)\nabla\boldsymbol{\eta}^{n+1}\| \leq \|\nabla\boldsymbol{\eta}^{n+1}\|$ along with Lemma 2.1.4 leads to

$$\begin{aligned}
&\Delta t\nu_T\sum_{n=0}^{M-1}\|(I-P_R)\nabla(\mathbf{u}^{n+1}-\boldsymbol{\eta}^{n+1})\|^2\\
&\leq \Delta t\nu_T\sum_{n=0}^{M-1}\|(I-P_R)\nabla\mathbf{u}^{n+1}\|^2 + \Delta t\nu_T\sum_{n=0}^{M-1}\|(I-P_R)\nabla\boldsymbol{\eta}^{n+1}\|^2)\\
&\leq \Delta t\nu_T\sum_{n=0}^{M-1}(\|\nabla\mathbf{u}^{n+1}-P_R\nabla\mathbf{u}^{n+1}\|^2 + \Delta t\nu_T\sum_{n=0}^{M-1}\left\|\nabla\boldsymbol{\eta}^{n+1}\right\|^2 \qquad (3.1.24)
\end{aligned}$$

For the first term on the right-hand side of (3.1.24), we use (2.1.49) to find that

$$\begin{aligned}
\Delta t\nu_T\sum_{n=0}^{M-1}\|\nabla\mathbf{u}^{n+1}-P_R\nabla\mathbf{u}^{n+1}\|^2 &\leq C\nu_T\frac{1}{M}\sum_{n=0}^{M-1}\inf_{\mathbf{v}_R\in\mathbf{X}^r}\|\nabla\mathbf{u}^{n+1}-\nabla\mathbf{v}_R^{n+1}\|^2\\
&\leq C\nu_T\frac{1}{M}\sum_{n=0}^{M-1}\|\nabla\mathbf{u}^{n+1}-\nabla\mathcal{U}_R^{n+1}\|^2 \qquad (3.1.25)
\end{aligned}$$

where $\mathcal{U}_R$ is the large scale representation of the projection. Now using Lemma 2.1.4, the final estimation for (3.1.24) becomes

$$\begin{aligned}
&\Delta t\nu_T \sum_{n=0}^{M-1} \|(I-P_R)\nabla(\mathbf{u}^{n+1}-\boldsymbol{\eta}^{n+1})\|^2 \qquad (3.1.26)\\
&\leq C\nu_T\Bigg(\Big(h^{2m}+(\|S_R\|_2+\|S_r\|_2)h^{2m+2}\Big)|||\mathbf{u}|||^2_{2,m+1}\\
&\quad+\sum_{j=R+1}^{d}\|\boldsymbol{\psi}_j\|_1^2\lambda_j+\sum_{j=r+1}^{d}\|\boldsymbol{\psi}_j\|_1^2\lambda_j\Bigg).
\end{aligned}$$

Corollary 3.1.2, the stability of $\mathbf{w}_r$ and Assumption (2.1.1) provide an estimation for the fifth term in the right-hand side of (3.1.21):

$$\begin{aligned}
&\frac{\Delta t}{\nu}\sum_{n=0}^{M-1}\|\mathbf{w}_r^{n+1}\|\|\nabla\mathbf{w}_r^{n+1}\|\|\nabla\boldsymbol{\eta}^{n+1}\|^2\\
&\leq C\frac{\Delta t}{\nu}\sum_{n=0}^{M-1}\|\nabla\mathbf{w}_r^{n+1}\|^2\|\nabla\boldsymbol{\eta}^{n+1}\|^2\\
&\leq C\nu^{-2}(\|\mathbf{u}_r^0\|^2+\nu^{-1}|||\mathbf{f}|||^2_{2,-1})\Big((h^{2m}+\|S_r\|_2h^{2m+2})|||\mathbf{u}|||^2_{2,m+1}\\
&\quad+\sum_{j=r+1}^{d}\|\boldsymbol{\psi}_j\|_1^2\lambda_j\Big). \qquad (3.1.27)
\end{aligned}$$

The estimation of sixth term in the right hand side of (3.1.21) uses approximation property (1.3.12) to find

$$\frac{\Delta t}{\nu}\sum_{n=0}^{M-1}\|p^{n+1}-q_h\|^2\leq\frac{C}{\nu}h^{2m}|||p|||^2_{2,m}. \qquad (3.1.28)$$

Finally, for the last term in the right hand side of (3.1.21), Taylor series expansion with remainder in integral form is used along with Cauchy Schwarz and the triangle inequality to obtain

$$\frac{\Delta t}{\nu}\sum_{n=0}^{M-1}\|\mathbf{u}_t^{n+1}-\frac{\mathbf{u}^{n+1}-\mathbf{u}^n}{\Delta t}\|^2\leq C\nu^{-1}(\Delta t)^2\|\mathbf{u}_{tt}\|^2_{L^2(0,T;H^1(\Omega))}. \qquad (3.1.29)$$

Collecting all the bounds (3.1.22)-(3.1.29) for (3.1.21) yields

$$
\begin{aligned}
&\|\boldsymbol{\theta}_r^M\|^2 + \sum_{n=0}^{M-1}\left[\frac{1}{8}\Delta t\nu_T\|(I-P_R)\nabla(\boldsymbol{\phi}_r^{n+1}+\boldsymbol{\theta}_r^{n+1})\|^2 + \nu\Delta t\|\nabla\boldsymbol{\phi}_r^{n+1}\|^2\right] \\
&\quad\leq\; C\Bigg[\nu\Bigg(\Big(h^{2m}+\|S_r\|_2 h^{2m+2}\Big)|||\mathbf{u}|||_{2,m+1}^2 + \sum_{j=r+1}^{d}\|\boldsymbol{\psi}_j\|_1^2\lambda_j\Bigg) \\
&\qquad+\nu^{-1}|||\nabla\mathbf{u}|||_{2,0}^2\Bigg(\Big(h^{2m}+\|S_r\|_2 h^{2m+2}\Big)|||\mathbf{u}|||_{2,m+1}^2 + \sum_{j=r+1}^{d}\|\boldsymbol{\psi}_j\|_1^2\lambda_j\Bigg) \\
&\qquad+\nu_T\Bigg(\Big(h^{2m}+(\|S_R\|_2+\|S_r\|_2)h^{2m+2}\Big)|||\mathbf{u}|||_{2,m+1}^2 \\
&\qquad+\sum_{j=R+1}^{d}\|\boldsymbol{\psi}_j\|_1^2\lambda_j + \sum_{j=r+1}^{d}\|\boldsymbol{\psi}_j\|_1^2\lambda_j\Bigg) + \nu^{-2}(\|\mathbf{u}_r^0\|^2+\nu^{-1}|||\mathbf{f}|||_{2,-1}^2) \\
&\qquad\times\Bigg(\Big(h^{2m}+\|S_r\|_2 h^{2m+2}\Big)|||\mathbf{u}|||_{2,m+1}^2 + \sum_{j=r+1}^{d}\|\boldsymbol{\psi}_j\|_1^2\lambda_j\Bigg) \\
&\qquad+\nu^{-1}h^{2m}|||p|||_{2,m}^2 + \nu^{-1}(\Delta t)^2\|\mathbf{u}_{tt}\|_{L^2(0,T;H^1(\Omega))}^2 + \frac{C\Delta t}{\nu^3}\sum_{n=0}^{M-1}|||\nabla\mathbf{u}|||_{\infty,0}^4\|\boldsymbol{\theta}_r^{n+1}\|^2\Bigg]
\end{aligned}
$$

Again using the assumption that $\Delta t \leq \frac{1}{8C}\left[\nu^{-3}|||\nabla\mathbf{u}|||_{\infty,0}^4\right]^{-1}$ allows us to apply the discrete Gronwall inequality, which yields

$$
\begin{aligned}
&\|\boldsymbol{\theta}_r^M\|^2 + \sum_{n=0}^{M-1}\left[\frac{1}{2}\Delta t\nu_T\|(I-P_R)\nabla(\boldsymbol{\phi}_r^{n+1}+\boldsymbol{\theta}_r^{n+1})/2\|^2 + \nu\Delta t\|\nabla\boldsymbol{\phi}_r^{n+1}\|^2\right] \\
&\quad\leq\; C\Bigg[\nu\Bigg(\Big(h^{2m}+\|S_r\|_2 h^{2m+2}\Big)|||\mathbf{u}|||_{2,m+1}^2 + \sum_{j=r+1}^{d}\|\boldsymbol{\psi}_j\|_1^2\lambda_j\Bigg) \\
&\qquad+\nu^{-1}|||\nabla\mathbf{u}|||_{2,0}^2\Bigg(\Big(h^{2m}+\|S_r\|_2 h^{2m+2}\Big)|||\mathbf{u}|||_{2,m+1}^2 + \sum_{j=r+1}^{d}\|\boldsymbol{\psi}_j\|_1^2\lambda_j\Bigg) \\
&\qquad+\nu_T\Bigg(\Big(h^{2m}+(\|S_R\|_2+\|S_r\|_2)h^{2m+2}\Big)|||\mathbf{u}|||_{2,m+1}^2 \\
&\qquad+\sum_{j=R+1}^{d}\|\boldsymbol{\psi}_j\|_1^2\lambda_j + \sum_{j=r+1}^{d}\|\boldsymbol{\psi}_j\|_1^2\lambda_j\Bigg) + \nu^{-2}(\|\mathbf{u}_r^0\|^2+\nu^{-1}|||\mathbf{f}|||_{2,-1}^2) \\
&\qquad\times\Bigg(\Big(h^{2m}+\|S_r\|_2 h^{2m+2}\Big)|||\mathbf{u}|||_{2,m+1}^2 + \sum_{j=r+1}^{d}\|\boldsymbol{\psi}_j\|_1^2\lambda_j\Bigg) \\
&\qquad+\nu^{-1}h^{2m}|||p|||_{2,m}^2 + \nu^{-1}(\Delta t)^2\|\mathbf{u}_{tt}\|_{L^2(0,T;H^1(\Omega))}^2\Bigg].
\end{aligned}
$$

Finally, the triangle inequality is applied to produce the stated result.

3.1.3 Extension to Second Order Time Stepping

We now consider an extension of Algorithm 3.1.1 to BDF2 time stepping.

Algorithm 3.1.2 *Let* $\mathbf{f} \in L^2(0,T;\mathbf{H}^{-1}(\Omega))$ *and initial conditions* $\mathbf{u}_r^0$ *and* $\mathbf{u}_r^{-1}$ *be given in* $\mathbf{X}^r$*. Then for n=0,1,2,...*

Step 1. *Calculate* $\mathbf{w}_r^{n+1} \in \mathbf{X}^r$ *satisfying* $\forall \boldsymbol{\psi} \in \mathbf{X}^r$*,*

$$\left(\frac{3\mathbf{w}_r^{n+1} - 4\mathbf{u}_r^n + \mathbf{u}_r^{n-1}}{2\Delta t}, \boldsymbol{\psi}\right) + b(\mathbf{w}_r^{n+1}, \mathbf{w}_r^{n+1}, \boldsymbol{\psi}) + \nu(\nabla \mathbf{w}_r^{n+1}, \nabla \boldsymbol{\psi}) = (\mathbf{f}^{n+1}, \boldsymbol{\psi}) \quad (3.1.30)$$

Step 2. *Post-process* $\mathbf{w}_r^{n+1}$ *to obtain* $\mathbf{u}_r^{n+1} \in \mathbf{X}^r$ *satisfying* $\forall \boldsymbol{\psi} \in \mathbf{X}^r$*,*

$$\left(\frac{\mathbf{w}_r^{n+1} - \mathbf{u}_r^{n+1}}{\Delta t}, \boldsymbol{\psi}\right) = (\nu_T (I - P_R)\nabla \frac{(\mathbf{w}_r^{n+1} + \mathbf{u}_r^{n+1})}{2}, (I - P_R)\nabla \boldsymbol{\psi}). \quad (3.1.31)$$

We note the post-processing step is exactly the same as in the backward Euler case. Also as in the case of the backward Euler method above, without Step 2, Algorithm 3.1.2 reduces to the classical POD-G formulation for the NSE, although now using BDF2 time stepping.

We now prove stability of Algorithm 3.1.2. A convergence result can be obtained by combining the ideas of Algorithm 3.1.1's convergence proof with the stability proof below. Such a proof is thus long and technical, but produces the expected result (i.e. same convergence as Algorithm 3.1.1, but second order in Δt instead of first order). This expected second order temporal convergence is illustrated in the numerical experiments section below.

Lemma 3.1.4 *The post-processed VMS-POD approximation is stable for the eddy viscosity term* $\nu_T < 4\nu$ *in the following sense:*

$$\begin{aligned}
&\|\mathbf{u}_r^{M+1}\|^2 + \|2\mathbf{u}_r^{M+1} - \mathbf{u}_r^M\|^2 + 2\nu_T \Delta t \left\| (I - P_R)\nabla \frac{(\mathbf{w}_r^{M+1} + \mathbf{u}_r^{M+1})}{2} \right\|^2 \\
&\quad + \frac{\nu_T \Delta t}{2} \|\nabla \mathbf{w}_r^{M+1}\|^2 + \sum_{n=1}^{M} \|\mathbf{w}_r^{n+1} - 2\mathbf{u}_r^n + \mathbf{u}_r^{n-1}\|^2 + (4\nu - \nu_T)\frac{\Delta t}{2} \sum_{n=1}^{M-1} \|\nabla \mathbf{w}_r^{n+1}\|^2 \\
&\quad \leq \|\mathbf{u}_r^1\|^2 + \|2\mathbf{u}_r^1 + \mathbf{u}_r^0\|^2 + \frac{\nu_T \Delta t}{2} \|\nabla \mathbf{u}_r^1\|^2 + 2\nu^{-1} |||\mathbf{f}|||_{2,-1}^2.
\end{aligned}$$

Proof Note that if we let $\boldsymbol{\psi} = \frac{(\mathbf{w}_r^{n+1} + \mathbf{u}_r^{n+1})}{2}$ in Step 2, the numerical dissipation induced from Step 2 is given by

$$\|\mathbf{w}_r^{n+1}\|^2 = \|\mathbf{u}_r^{n+1}\|^2 + 2\nu_T \Delta t \left\| (I - P_R)\nabla \frac{(\mathbf{w}_r^{n+1} + \mathbf{u}_r^{n+1})}{2} \right\|^2. \quad (3.1.32)$$

Letting $\psi = \mathbf{w}_r^{n+1}$ in (3.1.30) and using the identity

$$a(3a-4b+c) = \frac{1}{2}\big((a^2-b^2)+(2a-b)^2-(2b-c)^2+(a-2b+c)^2\big)$$

yields

$$\begin{aligned}
&\frac{1}{4\Delta t}\|\mathbf{w}_r^{n+1}\|^2 - \frac{1}{4\Delta t}\|\mathbf{u}_r^{n}\|^2 + \frac{1}{4\Delta t}(\|2\mathbf{w}_r^{n+1}-\mathbf{u}_r^{n}\|^2 - \|2\mathbf{u}_r^{n}-\mathbf{u}_r^{n-1}\|^2)\\
&+\frac{1}{4\Delta t}\|\mathbf{w}_r^{n+1}-2\mathbf{u}_r^{n}+\mathbf{u}_r^{n-1}\|^2 + \nu\|\nabla\mathbf{w}_r^{n+1}\|^2 = (\mathbf{f}^{n+1},\mathbf{w}_r^{n+1}). \qquad (3.1.33)
\end{aligned}$$

Substitute (3.1.32) in (3.1.33), multiply both sides by $4\Delta t$, add $\|2\mathbf{u}_r^{n+1}-\mathbf{u}_r^{n}\|^2$ to both sides, and then apply the Cauchy-Schwarz inequality to get

$$\begin{aligned}
&\|\mathbf{u}_r^{n+1}\|^2 - \|\mathbf{u}_r^{n}\|^2 + 2\nu_T\Delta t\left\|\|(I-P_R)\nabla\frac{(\mathbf{w}_r^{n+1}+\mathbf{u}_r^{n+1})}{2}\right\|^2\\
&+(\|2\mathbf{w}_r^{n+1}-\mathbf{u}_r^{n+1}\|^2 - \|2\mathbf{u}_r^{n+1}-\mathbf{u}_r^{n}\|^2) + (\|2\mathbf{u}_r^{n+1}-\mathbf{u}_r^{n}\|^2 - \|2\mathbf{u}_r^{n}-\mathbf{u}_r^{n-1}\|^2)\\
&+\|\mathbf{w}_r^{n+1}-2\mathbf{u}_r^{n}+\mathbf{u}_r^{n-1}\|^2 + 2\nu\Delta t\|\nabla\mathbf{w}_r^{n+1}\|^2\\
&\le C\nu^{-1}\Delta t\|\mathbf{f}^{n+1}\|_{-1}^2. \qquad (3.1.34)
\end{aligned}$$

We now consider the term $\|2\mathbf{w}_r^{n+1}-\mathbf{u}_r^{n}\|^2 - \|2\mathbf{u}_r^{n+1}-\mathbf{u}_r^{n}\|^2$ in (3.1.34) . By using the properties of L^2 inner product, the equality (3.1.32) and rearranging terms gives

$$\begin{aligned}
&\|2\mathbf{w}_r^{n+1}-\mathbf{u}_r^{n}\|^2 - \|2\mathbf{u}_r^{n+1}-\mathbf{u}_r^{n}\|^2\\
&= (2\mathbf{w}_r^{n+1}-\mathbf{u}_r^{n}, 2\mathbf{w}_r^{n+1}-\mathbf{u}_r^{n}) - (2\mathbf{u}_r^{n+1}-\mathbf{u}_r^{n}, 2\mathbf{u}_r^{n+1}-\mathbf{u}_r^{n})\\
&= 8(\mathbf{w}_r^{n+1}-\mathbf{u}_r^{n+1}, -\frac{\mathbf{u}_r^{n}}{2}) + 4(\|\mathbf{w}_r^{n+1}\|^2 - \|\mathbf{u}_r^{n+1}\|^2)\\
&= 8\nu_T\Delta t\big((I-P_R)\nabla\frac{(\mathbf{w}_r^{n+1}+\mathbf{u}_r^{n+1})}{2}, (I-P_R)\nabla(-\frac{\mathbf{u}_r^{n}}{2})\big)\\
&\quad +8\nu_T\Delta t\big((I-P_R)\nabla\frac{(\mathbf{w}_r^{n+1}+\mathbf{u}_r^{n+1})}{2}, (I-P_R)\nabla\frac{(\mathbf{w}_r^{n+1}+\mathbf{u}_r^{n+1})}{2}\big)\\
&= 8\nu_T\Delta t((I-P_R)\nabla\frac{(\mathbf{w}_r^{n+1}+\mathbf{u}_r^{n+1})}{2}, (I-P_R)\nabla\frac{(\mathbf{w}_r^{n+1}+\mathbf{u}_r^{n+1}-\mathbf{u}_r^{n})}{2}\\
&= 8\nu_T\Delta t\|(I-P_R)\nabla\frac{(\mathbf{w}_r^{n+1}+\mathbf{u}_r^{n+1}-\mathbf{u}_r^{n})}{2}\|^2\\
&\quad -8\nu_T\Delta t((I-P_R)\nabla(-\frac{\mathbf{u}_r^{n}}{2}), (I-P_R)\nabla\frac{(\mathbf{w}_r^{n+1}+\mathbf{u}_r^{n+1}-\mathbf{u}_r^{n})}{2}). \qquad (3.1.35)
\end{aligned}$$

Inserting (3.1.35) in (3.1.34) and applying Cauchy-Schwarz and Young's inequalities gives

$$\begin{aligned}
&\|\mathbf{u}_r^{n+1}\|^2 - \|\mathbf{u}_r^{n}\|^2 + \|2\mathbf{u}_r^{n+1}-\mathbf{u}_r^{n}\|^2 - \|2\mathbf{u}_r^{n}-\mathbf{u}_r^{n-1}\|^2\\
&\quad +2\nu_T\Delta t\left\|(I-P_R)\nabla\frac{(\mathbf{w}_r^{n+1}+\mathbf{u}_r^{n+1})}{2}\right\|^2 + \|\mathbf{w}_r^{n+1}-2\mathbf{u}_r^{n}+\mathbf{u}_r^{n-1}\|^2 + 2\nu\Delta t\|\nabla\mathbf{w}_r^{n+1}\|^2\\
&\le C\nu^{-1}\Delta t\|\mathbf{f}^{n+1}\|_{-1}^2 + 2\nu_T\Delta t\|(I-P_R)\nabla(\frac{\mathbf{u}_r^{n}}{2})\|^2.
\end{aligned}$$

Adding and subtracting terms for the last term in the previous inequality with the use of $\|I - P_R\| \leq 1$, we get

$$\begin{aligned}
&\|\mathbf{u}_r^{n+1}\|^2 - \|\mathbf{u}_r^n\|^2 + \|2\mathbf{u}_r^{n+1} - \mathbf{u}_r^n\|^2 - \|2\mathbf{u}_r^n - \mathbf{u}_r^{n-1}\|^2 \\
&\quad +2\nu_T\Delta t\left\|(I-P_R)\nabla\frac{(\mathbf{w}_r^{n+1}+\mathbf{u}_r^{n+1})}{2}\right\|^2 + \|\mathbf{w}_r^{n+1} - 2\mathbf{u}_r^n + \mathbf{u}_r^{n-1}\|^2 + 2\nu\Delta t\|\nabla\mathbf{w}_r^{n+1}\|^2 \\
&\leq\ C\nu^{-1}\Delta t\|\mathbf{f}^{n+1}\|_{-1}^2 + 2\nu_T\Delta t\left\|(I-P_R)\nabla(\frac{\mathbf{w}_r^n+\mathbf{u}_r^n}{2})\right\|^2 + \frac{\nu_T\Delta t}{2}\|(I-P_R)\nabla\mathbf{w}_r^n\|^2 \\
&\leq\ C\nu^{-1}\Delta t\|\mathbf{f}^{n+1}\|_{-1}^2 + 2\nu_T\Delta t\left\|(I-P_R)\nabla(\frac{\mathbf{w}_r^n+\mathbf{u}_r^n}{2})\right\|^2 + \frac{\nu_T\Delta t}{2}\|\nabla\mathbf{w}_r^n\|^2.
\end{aligned}$$

Summing over the time step $n = 1, \cdots, M$ gives

$$\begin{aligned}
&\|\mathbf{u}_r^{M+1}\|^2 + \|2\mathbf{u}_r^{M+1} - \mathbf{u}_r^M\|^2 + 2\nu_T\Delta t\left\|(I-P_R)\nabla\frac{(\mathbf{w}_r^{M+1}+\mathbf{u}_r^{M+1})}{2}\right\|^2 \\
&\quad + \sum_{n=1}^{M}\|\mathbf{w}_r^{n+1} - 2\mathbf{u}_r^n + \mathbf{u}_r^{n-1}\|^2 + \frac{\nu_T\Delta t}{2}\|\nabla\mathbf{w}_r^{M+1}\|^2 + (4\nu - \nu_T)\frac{\Delta t}{2}\sum_{n=1}^{M-1}\|\nabla\mathbf{w}_r^{n+1}\|^2 \\
&\leq\ \|\mathbf{u}_r^1\|^2 + \|2\mathbf{u}_r^1 + \mathbf{u}_r^0\|^2 + \frac{\nu_T\Delta t}{2}\|\nabla\mathbf{w}_r^1\|^2 + 2\nu_T\Delta t\left\|(I-P_R)\nabla\frac{(\mathbf{w}_r^1+\mathbf{u}_r^1)}{2}\right\|^2 \\
&\quad +2\nu^{-1}|||\mathbf{f}|||_{2,-1}^2
\end{aligned}$$

With the assumption $\mathbf{w}_r^0 = \mathbf{w}_r^1 = 0$ and $\|I - P_R\| < 1$, we obtain the stated result.

3.2 Numerical Studies

This section gives results for two numerical experiments. In all cases we use Algorithm 3.1.2, i.e. the scheme with second order time stepping. Our first test considers the predicted convergence rates of the previous section, with respect to varying R and Δt. For the second test, we compare accuracy of the proposed VMS-POD scheme compared with the usual Galerkin POD method (i.e. unstabilized POD, computed by eliminating the post-processing step of the VMS-POD) in 2D channel flow past a cylinder.

In this study, we use the test problem of 2D channel flow past a cylinder. Here, the domain is a 2.2×0.41 rectangle with a circle radius = 0.05 centred at $(0.2, 0.2)$ (see figure 3.1). The test problem uses no slip boundary conditions for the walls and

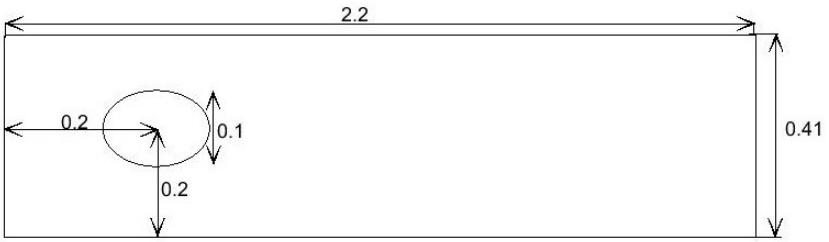

Figure 3.1: The channel flow around a cylinder domain

cylinder, and the time dependent inflow and outflow profiles are given by

$$u_1(0, y, t) = u_1(2.2, y, t) = \frac{6}{0.41^2} y(0.41 - y)\,,$$
$$u_2(0, y, t) = u_2(2.2, y, t) = 0.$$

The kinematic viscosity $\nu = 10^{-3}$, and there is no forcing ($\mathbf{f} = \mathbf{0}$). The POD is created as described in section 2, by taking snapshots from an extrapolated BDF2-finite element DNS simulation using Taylor-Hood elements, after a periodic-in-time solution is reached (a more detailed description of the set up is given in [14]). The tests with the cylinder problem use the projection of the $T = 7$ DNS solution as the initial condition, and run for 10 time units.

3.2.1 Numerical test 1: Convergence in R and Δt

We now test the predicted convergence rates of the previous section. This is a particularly difficult task for this problem, as the parameters are the spatial mesh width h, time step Δt, POD cutoff r, and VMS cutoff R. We assume the spatial mesh width is sufficiently small so that this error source is negligible. Our particular interest here is the scaling of the error with the VMS cutoff R and with time step Δt. In order to see convergence with respect to a particular parameter, it must be part of the dominant error source. Hence, in our tests, different parameter choices are made to see the various scalings.

To test the scaling of the error with R, we fix

$$\Delta t = 0.002,\ \nu_T = 0.0003$$

and perform the computations for varying R and r. The error estimates depend on R by means of

$$\varepsilon = \sqrt{\sum_{j=R+1}^{d} \|\varphi_j\|_1^2 \lambda_j}$$

and $\|S_R\|_2$. We investigate the scaling with ε. For sufficiently large R, $\|S_R\|_2$ become sufficiently large so that it becomes a dominant error source. Results for this test are shown in Table 3.1, and we observe the expected convergence rate of approximately $1/2$ in the $L^2(0,T;H^1(\Omega))$ norm, and seemingly a higher rate in $L^\infty(0,T;L^2(\Omega))$. We see that the velocity error decreases when R increases, which means that stabilizing fewer modes with VMS produces results closer to DNS solutions. However, for larger R, we see a deterioration of the rate, and by $R = 11$ when $r = 12$, the error increases (which is expected, due to increase in $\|S_R\|_2$ with R).

Table 3.1: Convergence of the VMS-POD with BDF2 for varying R

r	R	ε	Δ t	$\|\mathbf{u}-\mathbf{u}_r\|_{L^\infty(L^2(\Omega))}$	rate	$\|\nabla(\mathbf{u}-\mathbf{u}_r)\|_{L^2(H^1(\Omega))}$	rate
20	3	18.1674	0.002	0.0310	-	1.3550	-
20	7	4.7608	0.002	0.0029	1.76	0.4377	0.84
20	11	1.2920	0.002	0.0013	0.61	0.1633	0.75
20	15	0.3703	0.002	2.80e-04	1.22	0.0738	0.63
20	19	0.1183	0.002	2.63e-04	0.06	0.0728	0.01
16	3	18.1674	0.002	0.0280	-	1.3192	-
16	7	4.7608	0.002	0.0041	1.43	0.4502	0.80
16	11	1.2920	0.002	0.0017	0.67	0.2289	0.52
16	15	0.3703	0.002	0.0010	0.42	0.2228	0.02
12	3	18.1674	0.002	0.0294	-	1.4059	-
12	7	4.7608	0.002	0.0075	1.02	0.7039	0.52
12	11	1.2920	0.002	0.0089	-0.13	0.7580	-0.05

To test the scaling with respect to Δt, we evaluate the error in POD solution for $r = 8, 14, 20$ and varying R and Δt. Here, the case $r = R$ means that no mode is

stabilized with VMS. Hence, this situation is described as POD in Table 3.2. In this test, we also aim to compare POD and VMS methods in terms of convergence rates and process time, which are given in Table 3.2.

We observe that the rates are consistent with second order BDF2 in Table 3.2. Furthermore, as seen in Table 3.2, VMS method improves the convergence rates. In particular, when $r = 8$, the convergence rate in POD is not close to 2, whereas VMS method increases the rate to 2 if one chooses $R = 5$.

3.2.2 Numerical test 2: Error Comparison of VMS-POD Versus POD-G for 2D Channel Flow Past a Cylinder

We now consider error comparison of the VMS-POD again the standard POD-G method. The statistics of interest are the maximal drag and the maximal lift coefficients at the cylinder. The reference intervals are given for c_{dmax} and c_{lmax} in [86],

$$c_{dmax}^{ref} \in [3.22, 3.24], \quad c_{lmax}^{ref} \in [0.98, 1.02] \tag{3.2.1}$$

and recent computations of [14], as well as our DNS that created the snapshots, are in agreement with these numbers, as seen in Table 3.3. We compute with $r = 8$ modes, and find that the POD method is not good, and in particular we observe in Figure 3.2 that the energy is growing (seemingly) linearly with time. But at $T = 10$, a significant increase in energy has occurred, leading to very inaccurate lift and drag predictions as well.

Plots of each time evolution of the energy, drag and lift match the DNS results of [38] and [86]. The VMS-POD does a much better job with prediction of energy, lift and drag, however. Shown in Figure 3.2 is the energy, lift and drag with $R = 5$. We first remark that in Algorithm 1 and Algorithm 2, the parameter ν_T is obtained by minimizing the difference between energy of DNS and energy of VMS-POD at final time $T = 10$ by using bisection method. Based on these ideas, we compute the optimal choice of $\nu_T = 0.0003$ to within $\pm\ 0.000005$. We note that with POD, such a parameter optimization is quite cheap. Hence this is an excellent example of how the post-processing step of VMS-POD can remove the nonphysical energy growth that occurs with POD-G, and provide good reduced order solutions.

Table 3.2: Convergence Rates with respect to Δt

r	R	Δt	$\|\mathbf{u} - \mathbf{u}_r\|_{L^\infty(L^2(\Omega))}$	rate
8	5	0.32	0.434386	
8	5	0.16	0.358107	0.279
8	5	0.08	0.126142	1.505
8	5	0.04	0.029191	2.111
8	POD	0.32	0.434369	-
8	POD	0.16	0.360112	0.270
8	POD	0.08	0.153357	1.232
8	POD	0.04	0.053046	1.532
14	9	0.32	0.434345	-
14	9	0.16	0.358689	0.276
14	9	0.08	0.129811	1.466
14	9	0.04	0.023926	2.440
14	POD	0.32	0.434346	-
14	POD	0.16	0.358686	0.276
14	POD	0.08	0.129705	1.468
14	POD	0.04	0.027324	2.247
20	10	0.32	0.483072	-
20	10	0.16	0.379032	0.350
20	10	0.08	0.133079	1.510
20	10	0.04	0.023843	2.480
20	POD	0.32	0.493442	-
20	POD	0.16	0.381596	0.370
20	POD	0.08	0.133928	1.511
20	POD	0.04	0.025196	2.410

Table 3.3: The maximal lift and the maximal drag coefficient for varying R

R	c_{dmax}	c_{lmax}	energy
3	3.2343	1.0162	0.5484
5	3.2249	1.0086	0.5484
7	3.2376	1.0180	0.5490
9	3.2288	1.0072	0.5486
11	3.2298	1.0105	0.5486

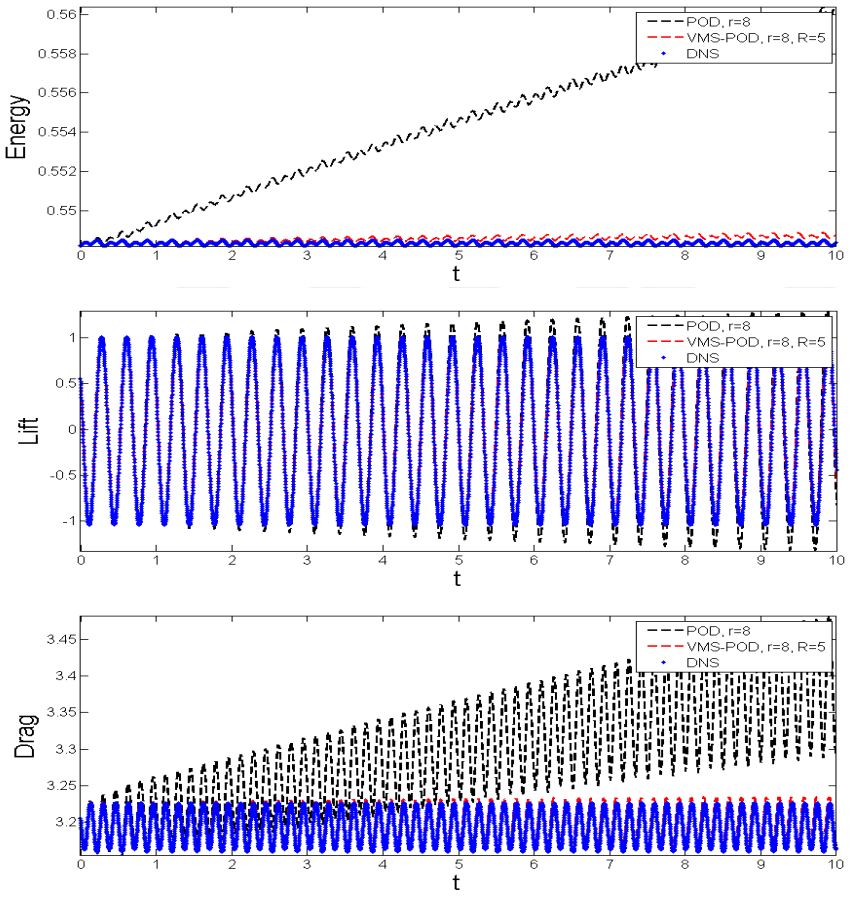

Figure 3.2: Energy, lift and drag for DNS, POD and VMS-POD.

CHAPTER 4

POD-ROM FOR THE DARCY-BRINKMAN EQUATIONS WITH DOUBLE-DIFFUSIVE CONVECTION

This chapter studies reduced order modelling based on POD approach for Darcy-Brinkman with double diffusive convection. As it is described in Chapter 1, the simulation of Navier Stokes type systems leads to large algebraic system and requires high computational time. Therefore, combining heat and mass transport equations to NSE make the situation worse. Hence the numerical studies in double diffusive system become very important. For high Ra numbers, the numerical experiments suggest a stabilization method for POD solution of Darcy-Brinkman equation. Based on our experience in Chapter 3, we support the POD method with post-process VMS method.

This chapter consists of three sections. Section 4.1 presents the discretization of the double diffusive Darcy-Brinkman system (1.3.15) based on POD method. The numerical analysis of the POD-G formulation including stability and a priori error estimation of (4.1.1)-(4.1.3) is also given in Section 4.1. Section 4.2 is devoted to the numerical analysis of VMS-POD extension of the double diffusive system. The analytical results and the comparison of the methods in Section 4.1 and the Section 4.2 are illustrated with several numerical experiments in Section 4.3.

4.1 Numerical Analysis of Double Diffusive Darcy-Brinkman System with POD

This section is devoted to a derivation of the a priori error estimation of (4.1.1)-(4.1.3). The presentation mainly follows an approach developed by Rannacher and Heywood [34]. Recall that in Chapter 2, the POD-G formulation of the Darcy-Brinkman double

diffusive system is given by (2.2.11)-(2.2.13). For simulations, we must equip the system (2.2.11)-(2.2.13) with a temporal discretization and a finite element method for a spatial discretization described in Section 1.3. For simplicity, we consider a backward Euler temporal discretization for our analysis in the next section. The fully discrete backward Euler POD-ROM is given at time $t^n = n\Delta t$, $n = 0, 1, 2, \ldots, M$ and $\tau = M\Delta t$, by

$$\left(\frac{\mathbf{u}_r^{n+1} - \mathbf{u}_r^n}{\Delta t}, \mathbf{v}_r\right) + 2\nu(\mathbb{D}\mathbf{u}_r^{n+1}, \mathbb{D}\mathbf{v}_r) + b_1(\mathbf{u}_r^{n+1}, \mathbf{u}_r^{n+1}, \mathbf{v}_r)$$
$$+(Da^{-1}\mathbf{u}_r^{n+1}, \mathbf{v}_r) = \beta_T(\mathbf{g}T_r^{n+1}, \mathbf{v}_r) + \beta_C(\mathbf{g}C_r^{n+1}, \mathbf{v}_r), \quad (4.1.1)$$

$$\left(\frac{T_r^{n+1} - T_r^n}{\Delta t}, S_r\right) + b_2(\mathbf{u}_r^{n+1}, T_r^{n+1}, S_r) + \gamma(\nabla T_r^{n+1}, \nabla S_r) = 0, \quad (4.1.2)$$

$$\left(\frac{C_r^{n+1} - C_r^n}{\Delta t}, \Phi_r\right) + b_3(\mathbf{u}_r^{n+1}, C_r^{n+1}, \Phi_r) + D_c(\nabla C_r^{n+1}, \nabla \Phi_r) = 0, \quad (4.1.3)$$

for all $(\mathbf{v}_r, S_r, \Phi_r) \in (\mathbf{X}_r, W_r, \Psi_r)$. The goal of the POD is to find low dimensional bases for velocity, temperature, concentration by solving the minimization problems. The solution of the problem is obtained by using the method of snapshots. We note that all eigenvalues are sorted in descending order. Thus, the basis functions $\{\boldsymbol{\psi}_i\}_{i=1}^{r_1}$, $\{\phi_i\}_{i=1}^{r_2}$ and $\{\eta_i\}_{i=1}^{r_3}$ correspond to the first r_1, r_2 and r_3 largest eigenvalues $\{\lambda_i\}_{i=1}^{r_1}$, $\{\mu_i\}_{i=1}^{r_2}$, $\{\xi_i\}_{i=1}^{r_3}$ of the velocity, the temperature, the concentration, respectively. For simplicity, we will denote POD-ROM spaces using just r instead of r_1, r_2 and r_3. However, in the analysis, we are careful to distinguish that these parameters can be chosen independently.

In the numerical experiments, we use second order time discretization, namely BDF2 method as follows.

$$\left(\frac{3\mathbf{u}_r^{n+1} - 4\mathbf{u}_r^n + \mathbf{u}_r^{n-1}}{2\Delta t}, \mathbf{v}_r\right) + 2\nu(\mathbb{D}\mathbf{u}_r^{n+1}, \mathbb{D}\mathbf{v}_r) + b_1(\mathbf{u}_r^{n+1}, \mathbf{u}_r^{n+1}, \mathbf{v}_r)$$
$$+(Da^{-1}\mathbf{u}_r^{n+1}, \mathbf{v}_r) = \beta_T(\mathbf{g}T_r^{n+1}, \mathbf{v}_r) + \beta_C(\mathbf{g}C_r^{n+1}, \mathbf{v}_r), \quad (4.1.4)$$

$$\left(\frac{3T_r^{n+1} - 4T_r^n + T_r^{n-1}}{2\Delta t}, S_r\right) + b_2(\mathbf{u}_r^{n+1}, T_r^{n+1}, S_r) + \gamma(\nabla T_r^{n+1}, \nabla S_r) = 0, \quad (4.1.5)$$

$$\left(\frac{3C_r^{n+1} - 4C_r^n + C_r^{n-1}}{2\Delta t}, \Phi_r\right) + b_3(\mathbf{u}_r^{n+1}, C_r^{n+1}, \Phi_r) + D_c(\nabla C_r^{n+1}, \nabla \Phi_r) = 0. \quad (4.1.6)$$

We remark that, although we analyze only the backward Euler method, the results are extendable to with the usual technical details. For the error assessment, we use the L^2 projections of $\mathbf{u}_r, T_r$ and C_r, respectively. The L^2 projection operators $P_{u,r} : L^2 \to$

$\mathbf{X}_r$, $P_{T,r} : L^2 \to W_r$, $P_{C,r} : L^2 \to \Psi_r$ are defined by (2.1.39) and (2.2.14). We first prove the stability of the solutions of (4.1.1)-(4.1.3).

Lemma 4.1.1 *(Stability) The POD-ROM approximation (4.1.1)-(4.1.3) is unconditionally stable in the following sense: for any $\Delta t > 0$,*

$$\begin{aligned}
&\|\mathbf{u}_r^M\|^2 + \sum_{n=0}^{M-1} \left(\|\mathbf{u}_r^{n+1} - \mathbf{u}_r^n\|^2 + 2\nu\Delta t\|\mathbb{D}\mathbf{u}_r^{n+1}\|^2 + Da^{-1}\Delta t\|\mathbf{u}_r^{n+1}\|^2\right) \\
&\quad \leq \quad \|\mathbf{u}_0\|^2 + C^*\|\mathbf{g}\|_\infty^2(\beta_T^2\gamma^{-1}\|T_0\|^2 + \beta_C^2 D_c^{-1}\|C_0\|^2), \qquad (4.1.7)
\end{aligned}$$

$$\|T_r^M\|^2 + \sum_{n=0}^{M-1} 2\Delta t\gamma\|\nabla T_r^n\|^2 \leq \|T_0\|^2, \qquad (4.1.8)$$

$$\|C_r^M\|^2 + \sum_{n=0}^{M-1} 2\Delta t D_c\|\nabla C_r^n\|^2 \leq \|C_0\|^2, \qquad (4.1.9)$$

where $C^* = \min\{\nu^{-1}, Da\}$.

Proof Choosing $S_r = T_r^{n+1}$ in (4.1.2) and using skew symmetry property, we have

$$\left(\frac{T_r^{n+1} - T_r^n}{\Delta t}, T_r^{n+1}\right) + \gamma(\nabla T_r^{n+1}, \nabla T_r^{n+1}) = 0, \qquad (4.1.10)$$

and multiplying both sides with Δt yields

$$\|T_r^{n+1}\|^2 + \gamma\Delta t\|\nabla T_r^n\|^2 = (T_r^n, T_r^{n+1}). \qquad (4.1.11)$$

Applying Cauchy-Schwarz and Young's inequality gives

$$\|T_r^{n+1}\|^2 + 2\gamma\Delta t\|\nabla T_r^n\|^2 \leq \|T_r^n\|^2, \qquad (4.1.12)$$

and finally summing over the time steps produces the stability result (4.1.8). In a similar manner, setting $\Phi_r = C_r^{n+1}$ in (4.1.3) yields (4.1.9). Letting $\mathbf{v}_r = \mathbf{u}_r^{n+1}$ in (4.1.1), we get

$$\begin{aligned}
&(\frac{\mathbf{u}_r^{n+1} - \mathbf{u}_r^n}{\Delta t}, \mathbf{u}_r^{n+1}) + 2\nu(\mathbb{D}\mathbf{u}_r^{n+1}, \mathbb{D}\mathbf{u}_r^{n+1}) + (Da^{-1}\mathbf{u}_r^{n+1}, \mathbf{u}_r^{n+1}) \\
&\quad = \quad \beta_T(\mathbf{g}T_r^{n+1}, \mathbf{u}_r^{n+1}) + \beta_C(\mathbf{g}C_r^{n+1}, \mathbf{u}_r^{n+1}). \qquad (4.1.13)
\end{aligned}$$

Using the Cauchy-Schwarz, Young's, Poincaré's inequality, polarization identity $(a - b, a) = \frac{1}{2}(\|a\|^2 - \|b\|^2 + \|a - b\|^2)$ gives

$$\begin{aligned}
&\frac{1}{2\Delta t}\|\mathbf{u}_r^{n+1}\|^2 + \frac{1}{2\Delta t}\|\mathbf{u}_r^{n+1} - \mathbf{u}_r^n\|^2 + \nu\|\mathbb{D}\mathbf{u}_r^{n+1}\|^2 + \frac{Da^{-1}}{2}\|\mathbf{u}_r^{n+1}\|^2 \\
&\quad \leq \quad \frac{1}{2\Delta t}\|\mathbf{u}_r^n\|^2 + K\|\mathbf{g}\|_\infty^2(\nu^{-1}\beta_T^2\|\nabla T_r^n\|^2 + Da\beta_C^2\|\nabla C_r^n\|^2). \qquad (4.1.14)
\end{aligned}$$

Multiplying $2\Delta t$ and summing over the time steps $n = 0, \ldots, M-1$ and using (4.1.8) and (4.1.9) gives

$$\begin{aligned}\|\mathbf{u}_r^M\|^2 + \sum_{n=0}^{M-1}\Big(\|\mathbf{u}_r^{n+1} - \mathbf{u}_r^n\|^2 + 2\nu\Delta t\|\mathbb{D}\mathbf{u}_r^{n+1}\|^2 + Da^{-1}\Delta t\|\mathbf{u}_r^{n+1}\|^2\Big)\\ \leq \|\mathbf{u}_0\|^2 + K\|\mathbf{g}\|_\infty^2(\nu^{-1}\beta_T^2\gamma^{-1}\|T_0\|^2 + Da\beta_C^2 D_c^{-1}\|C_0\|^2). \qquad (4.1.15)\end{aligned}$$

The result follows from (4.1.15) by taking minimum of ν^{-1} and Da.

The optimal asymptotic error estimation requires the following regularity assumptions for the true solution:

$$\begin{aligned}\mathbf{u} \in L^\infty(0,k;\mathbf{H}^{m+1}(\Omega)), \quad T,\ C \in L^\infty(0,k;H^{m+1}(\Omega)),\\ \mathbf{u}_{tt} \in L^2(0,k;\mathbf{H}^1(\Omega)), \quad T_{tt},\ C_{tt} \in L^2(0,k;H^1(\Omega)),\\ p \in L^\infty(0,k;H^m(\Omega)). \qquad (4.1.16)\end{aligned}$$

Theorem 4.1.2 *(Error Estimation) Suppose regularity assumptions (4.1.16) and Assumption 2.2.1 holds. Then for the sufficiently small Δt, i.e.*

$$\begin{aligned}\Delta t \leq \min\{&(\nu^{-3}|||\mathbb{D}\mathbf{u}|||_{\infty,0}^4 + \nu^{-1}\gamma^{-2}|||\nabla T|||_{\infty,0}^4\\ &+\nu^{-1}{D_c}^{-2}|||\nabla C|||_{\infty,0}^4)^{-1}, (\nu^{-1}\beta_T^2\|\mathbf{g}\|_\infty^2)^{-1}, (\nu^{-1}\beta_C^2\|\mathbf{g}\|_\infty^2)^{-1}\}. \qquad (4.1.17)\end{aligned}$$

the error satisfies

$$\begin{aligned}&\|\mathbf{u}^M - \mathbf{u}_r^M\|^2 + \|T^M - T_r^M\|^2 + \|C^M - C_r^M\|^2\\ &\leq K\Bigg(1 + h^{2m} + (\Delta t)^2 + (1 + \|S_{u,r}\|_2 + \|S_{T,r}\|_2 + \|S_{C,r}\|_2)h^{2m+2}\\ &\quad +\varepsilon_u^2 + \varepsilon_T^2 + \varepsilon_C^2 + \sum_{i=r_1+1}^{d}\lambda_i + \sum_{i=r_2+1}^{d}\mu_i + \sum_{i=r_3+1}^{d}\xi_i\Bigg). \qquad (4.1.18)\end{aligned}$$

Remark A similar result to (4.1.18) is expected for the BDF2 case, but with the Δt^2 replaced with Δt^4, following the same general steps and using the usual BDF2 analysis tools and regularity assumptions.

Proof Subtracting from (1.3.16), (1.3.18), (1.3.19) to (4.1.1),(4.1.2),(4.1.3) at time

t^{n+1}, respectively we have

$$\begin{aligned}\left(\mathbf{u}_t^{n+1} - \frac{\mathbf{u}_r^{n+1} - \mathbf{u}_r^n}{\Delta t}, \mathbf{v}_r\right) + 2\nu(\mathbb{D}(\mathbf{u}^{n+1} - \mathbf{u}_r^{n+1}), \mathbb{D}\mathbf{v}_r) + b_1(\mathbf{u}^{n+1}, \mathbf{u}^{n+1}, \mathbf{v}_r)\\ -b_1(\mathbf{u}_r^{n+1}, \mathbf{u}_r^{n+1}, \mathbf{v}_r) + (Da^{-1}(\mathbf{u} - \mathbf{u}_r^{n+1}), \mathbf{v}_r) - (p^{n+1}, \nabla \cdot \mathbf{v}_r)\\ = \beta_T(\mathbf{g}(T - T_r^{n+1}), \mathbf{v}_r) + \beta_C(\mathbf{g}(C - C_r^{n+1}), \mathbf{v}_r), \quad (4.1.19)\\ \left(T_t^{n+1} - \frac{T_r^{n+1} - T_r^n}{\Delta t}, S_r\right) + b_2(\mathbf{u}^{n+1}, T^{n+1}, S_r) - b_2(\mathbf{u}_r^{n+1}, T_r^{n+1}, S_r)\\ +\gamma(\nabla(T^{n+1} - T_r^{n+1}), \nabla S_r) = 0, \quad (4.1.20)\\ \left(C_t^{n+1} - \frac{C_r^{n+1} - C_r^n}{\Delta t}, \Phi_r\right) + b_3(\mathbf{u}^{n+1}, C^{n+1}, \Phi_r) - b_3(\mathbf{u}_r^{n+1}, C_r^{n+1}, \Phi_r)\\ +D_c(\nabla(C^{n+1} - C_r^{n+1}), \nabla\Phi_r) = 0. \quad (4.1.21)\end{aligned}$$

Define

$$\begin{aligned}\mathbf{u}^{n+1} - \mathbf{u}_r^{n+1} &= (\mathbf{u}^{n+1} - \tilde{\mathbf{u}}^{n+1}) - (\mathbf{u}_r^{n+1} - \tilde{\mathbf{u}}^{n+1}) &= \boldsymbol{\eta}_u^{n+1} - \boldsymbol{\phi}_{u,r}^{n+1},\\ T^{n+1} - T_r^{n+1} &= (T^{n+1} - \tilde{T}^{n+1}) - (T_r^{n+1} - \tilde{T}^{n+1}) &= \eta_T^{n+1} - \phi_{T,r}^{n+1}, \quad (4.1.22)\\ C^{n+1} - C_r^{n+1} &= (C^{n+1} - \tilde{C}^{n+1}) - (C_r^{n+1} - \tilde{C}^{n+1}) &= \eta_C^{n+1} - \phi_{C,r}^{n+1},\end{aligned}$$

where $(\tilde{\mathbf{u}}^{n+1}, \tilde{T}^{n+1}, \tilde{C}^{n+1})$ are L^2 projections of $(\mathbf{u}^{n+1}, T^{n+1}, C^{n+1})$ in $(\mathbf{X}_r, W_r, \Psi_r)$ at time t^{n+1}. We rewrite the temperature equation (4.1.20) as

$$\begin{aligned}\left(\frac{T^{n+1} - T^n}{\Delta t} - \frac{T_r^{n+1} - T_r^n}{\Delta t}, S_r\right) + b_2(\mathbf{u}^{n+1}, T^{n+1}, S_r) - b_2(\mathbf{u}_r^{n+1}, T_r^{n+1}, S_r)\\ +(T_t^{n+1} - \frac{T^{n+1} - T^n}{\Delta t}, S_r) + \gamma(\nabla(T^{n+1} - T_r^{n+1}), \nabla S_r) = 0. \quad (4.1.23)\end{aligned}$$

Using (4.1.22) and letting $S_r = \phi_{T,r}^{n+1}$ in (4.1.23) gives

$$\begin{aligned}\left(\frac{\phi_{T,r}^{n+1} - \phi_{T,r}^n}{\Delta t}, \phi_{T,r}^{n+1}\right) + \gamma(\nabla\phi_{T,r}^{n+1}, \nabla\phi_{T,r}^{n+1}) = (\frac{\eta_T^{n+1} - \eta_T^n}{\Delta t}, \phi_{T,r}^{n+1})\\ +\gamma(\nabla\eta_T^{n+1}, \nabla\phi_{T,r}^{n+1}) + b_2(\mathbf{u}^{n+1}, T^{n+1}, \phi_{T,r}^{n+1})\\ -b_2(\mathbf{u}_r^{n+1}, T_r^{n+1}, \phi_{T,r}^{n+1}) + (T_t^{n+1} - \frac{T^{n+1} - T^n}{\Delta t}, \phi_{T,r}^{n+1}). \quad (4.1.24)\end{aligned}$$

Adding and subtracting terms to the nonlinear terms in (4.1.24) leads to

$$\begin{aligned}b_2(\mathbf{u}^{n+1}, T^{n+1}, \phi_{T,r}^{n+1}) - b_2(\mathbf{u}_r^{n+1}, T_r^{n+1}, \phi_{T,r}^{n+1}) = b_2(\boldsymbol{\eta}_u{}^{n+1}, T^{n+1}, \phi_{T,r}^{n+1})\\ -b_2(\boldsymbol{\phi}_{u,r}^{n+1}, T^{n+1}, \phi_{T,r}^{n+1}) + b_2(\mathbf{u}_r^{n+1}, \eta_T{}^{n+1}, \phi_{T,r}^{n+1}) - b_2(\mathbf{u}_r^{n+1}, \phi_{T,r}^{n+1}, \phi_{T,r}^{n+1}).\end{aligned}$$

Note that $b_2(\mathbf{u}_r^{n+1}, \phi_{T,r}^{n+1}, \phi_{T,r}^{n+1}) = 0$. In addition, from the definition of L^2 projection (2.1.39) and (2.2.14), the first term in the right hand side of (4.1.24) vanishes. Using

Cauchy-Schwarz and Young's inequalities, we obtain

$$\begin{aligned}\frac{1}{2\Delta t}\|\phi_{T,r}^{n+1}\|^2-\frac{1}{2\Delta t}\|\phi_{T,r}^{n}\|^2+\gamma\|\nabla\phi_{T,r}^{n+1}\|^2=\gamma(\nabla{\eta_T}^{n+1},\nabla\phi_{T,r}^{n+1})\\ +b_2({\boldsymbol{\eta}_u}^{n+1},T^{n+1},\phi_{T,r}^{n+1})-b_2(\boldsymbol{\phi}_{u,r}^{n+1},T^{n+1},\phi_{T,r}^{n+1})\\ +b_2(\mathbf{u}_r^{n+1},{\eta_T}^{n+1},\phi_{T,r}^{n+1})+(T_t^{n+1}-\frac{T^{n+1}-T^n}{\Delta t},\phi_{T,r}^{n+1}).\end{aligned}\tag{4.1.25}$$

Next, we bound the first term in the right hand side of (4.1.25), by using Cauchy Schwarz, Young's and Poincaré's inequalities:

$$\gamma(\nabla{\eta_T}^{n+1},\nabla\phi_{T,r}^{n+1})\ \leq\ K\gamma\|\nabla{\eta_T}^{n+1}\|^2+\frac{\gamma}{10}\|\nabla\phi_{T,r}^{n+1}\|^2.\tag{4.1.26}$$

To bound the nonlinear terms we use Lemma 1.3.1 and Young's inequality,

$$b_2({\boldsymbol{\eta}_u}^{n+1},T^{n+1},\phi_{T,r}^{n+1})\ \leq\ K\gamma^{-1}\|\nabla{\boldsymbol{\eta}_u}^{n+1}\|^2\|\nabla T^{n+1}\|^2+\frac{\gamma}{10}\|\nabla\phi_{T,r}^{n+1}\|^2,\tag{4.1.27}$$

$$\begin{aligned}b_2(\boldsymbol{\phi}_{u,r}^{n+1},T^{n+1},\phi_{T,r}^{n+1})\ &\leq\ K\nu^{-1}\gamma^{-2}\|\boldsymbol{\phi}_{u,r}^{n+1}\|^2\|\nabla T^{n+1}\|^4+\frac{\nu}{2}\|\mathbb{D}\boldsymbol{\phi}_{u,r}^{n+1}\|^2\\ &\quad+\frac{\gamma}{10}\|\nabla\phi_{T,r}^{n+1}\|^2,\end{aligned}\tag{4.1.28}$$

$$b_2(\mathbf{u}_r^{n+1},{\eta_T}^{n+1},\phi_{T,r}^{n+1})\ \leq\ K\gamma^{-1}\|\nabla\mathbf{u}_r^{n+1}\|^2\|\nabla{\eta_T}^{n+1}\|^2+\frac{\gamma}{10}\|\nabla\phi_{T,r}^{n+1}\|^2.\tag{4.1.29}$$

For the last term in the right hand side of (4.1.25), we apply Cauchy Schwarz, Poincaré's and Young's inequalities along with the Taylor's remainder formula as

$$\begin{aligned}(T_t^{n+1}-\frac{T^{n+1}-T^n}{\Delta t},\phi_{T,r}^{n+1})\ &\leq\ K\gamma^{-1}\|T_t^{n+1}-\frac{T^{n+1}-T^n}{\Delta t}\|^2+\frac{\gamma}{10}\|\nabla\phi_{T,r}^{n+1}\|^2\\ &\leq\ K\gamma^{-1}\frac{1}{(\Delta t)^2}\|\int_{t_n}^{t_{n+1}}(t-t_n)T_{tt}\,\mathrm{d}t\|^2+\frac{\gamma}{10}\|\nabla\phi_{T,r}^{n+1}\|^2\\ &\leq\ K\gamma^{-1}\Delta t\|T_{tt}\|^2_{L^2(t^n,t^{n+1};H^1(\Omega))}+\frac{\gamma}{10}\|\nabla\phi_{T,r}^{n+1}\|^2\end{aligned}\tag{4.1.30}$$

Inserting (4.1.26)-(4.1.30) in (4.1.25), multiplying by $2\Delta t$ and summing over the time steps produces

$$\begin{aligned}\|\phi_{T,r}^{M}\|^2+\gamma\Delta t\sum_{n=0}^{M-1}\|\nabla\phi_{T,r}^{n+1}\|^2\leq\|\phi_{T,r}^{0}\|^2+K\Delta t\Big(\gamma\sum_{n=0}^{M-1}\|\nabla{\eta_T}^{n+1}\|^2\\ +\gamma^{-1}\sum_{n=0}^{M-1}\|\nabla{\boldsymbol{\eta}_u}^{n+1}\|^2\|\nabla T^{n+1}\|^2+\nu^{-1}\gamma^{-2}\sum_{n=0}^{M-1}\|\boldsymbol{\phi}_{u,r}^{n+1}\|^2\|\nabla T^{n+1}\|^4\\ +\gamma^{-1}\sum_{n=0}^{M-1}\|\nabla\mathbf{u}_r^{n+1}\|^2\|\nabla{\eta_T}^{n+1}\|^2+\frac{\nu}{2}\sum_{n=0}^{M-1}\|\mathbb{D}\boldsymbol{\phi}_{u,r}^{n+1}\|^2\\ +\gamma^{-1}\Delta t\|T_{tt}\|^2_{L^2(0,\tau;H^1(\Omega))}\Big).\end{aligned}\tag{4.1.31}$$

By using Lemma 2.1.4, Lemma 2.2.1, Lemma 4.1.1, Assumption 2.2.1 and regularity assumptions in (4.1.31) results in

$$\|\phi_{T,r}^{M}\|^2 + \gamma\Delta t \sum_{n=0}^{M-1} \|\nabla\phi_{T,r}^{n+1}\|^2 \leq \|\phi_{T,r}^{0}\|^2 + K\Big(h^{2m} + (\|S_{u,r}\|_2 + \|S_{T,r}\|_2)h^{2m+2} + \varepsilon_u^2 + \varepsilon_T^2 + \nu^{-1}\gamma^{-2}|||\nabla T|||_{\infty,0}^4 \Delta t \sum_{n=0}^{M-1} \|\boldsymbol{\phi}_{u,r}^{n+1}\|^2 + \frac{\nu\Delta t}{2} \sum_{n=0}^{M-1} \|\mathbb{D}\boldsymbol{\phi}_{u,r}^{n+1}\|^2 + (\Delta t)^2\Big). \tag{4.1.32}$$

Similarly, the error estimation for the concentration is given by

$$\|\phi_{C,r}^{M}\|^2 + D_c\Delta t \sum_{n=0}^{M-1} \|\nabla\phi_{C,r}^{n+1}\|^2 \leq \|\phi_{C,r}^{0}\|^2 + K\Big(h^{2m} + (\|S_{u,r}\|_2 + \|S_{C,r}\|_2)h^{2m+2} + \varepsilon_u^2 + \varepsilon_C^2 + \nu^{-1}{D_c}^{-2}|||\nabla C|||_{\infty,0}^4 \Delta t \sum_{n=0}^{M-1} \|\boldsymbol{\phi}_{u,r}^{n+1}\|^2 + \frac{\nu\Delta t}{2} \sum_{n=0}^{M-1} \|\mathbb{D}\boldsymbol{\phi}_{u,r}^{n+1}\|^2 + (\Delta t)^2\Big). \tag{4.1.33}$$

By using similar arguments as above, letting $\mathbf{v}_r = \boldsymbol{\phi}_{u,r}^{n+1}$ in (4.1.19), the velocity error equation becomes

$$\begin{aligned}
&\left(\frac{\boldsymbol{\phi}_{u,r}^{n+1} - \boldsymbol{\phi}_{u,r}^{n}}{\Delta t}, \boldsymbol{\phi}_{u,r}^{n+1}\right) + 2\nu(\mathbb{D}\boldsymbol{\phi}_{u,r}^{n+1}, \mathbb{D}\boldsymbol{\phi}_{u,r}^{n+1}) + (Da^{-1}\boldsymbol{\phi}_{u,r}^{n+1}, \boldsymbol{\phi}_{u,r}^{n+1}) \\
&= -\beta_T(\mathbf{g}(T - T_r^{n+1}), \boldsymbol{\phi}_{u,r}^{n+1}) - \beta_C(\mathbf{g}(C - C_r^{n+1}), \boldsymbol{\phi}_{u,r}^{n+1}) + \left(\frac{\boldsymbol{\eta}_u^{n+1} - \boldsymbol{\eta}_u^{n}}{\Delta t}, \boldsymbol{\phi}_{u,r}^{n+1}\right) \\
&\quad + 2\nu(\mathbb{D}{\boldsymbol{\eta}_u}^{n+1}, \mathbb{D}\boldsymbol{\phi}_{u,r}^{n+1}) + (Da^{-1}{\boldsymbol{\eta}_u}^{n+1}, \boldsymbol{\phi}_{u,r}^{n+1}) + b_1({\boldsymbol{\eta}_u}^{n+1}, \mathbf{u}^{n+1}, \boldsymbol{\phi}_{u,r}^{n+1}) \\
&\quad - b_1(\boldsymbol{\phi}_{u,r}^{n+1}, \mathbf{u}^{n+1}, \boldsymbol{\phi}_{u,r}^{n+1}) + b_1(\mathbf{u}_r^{n+1}, {\boldsymbol{\eta}_u}^{n+1}, \boldsymbol{\phi}_{u,r}^{n+1}) - (p^{n+1}, \nabla\cdot\boldsymbol{\phi}_{u,r}^{n+1}) \\
&\quad + (\mathbf{u}_t^{n+1} - \frac{\mathbf{u}^{n+1} - \mathbf{u}^{n}}{\Delta t}, \boldsymbol{\phi}_{u,r}^{n+1}).
\end{aligned} \tag{4.1.34}$$

Apply the polarization identity to get

$$\begin{aligned}
&\frac{1}{2\Delta t}\|\boldsymbol{\phi}_{u,r}^{n+1}\|^2 - \frac{1}{2\Delta t}\|\boldsymbol{\phi}_{u,r}^{n}\|^2 + \frac{1}{2\Delta t}\|\boldsymbol{\phi}_{u,r}^{n+1} - \boldsymbol{\phi}_{u,r}^{n}\|^2 + 2\nu\|\mathbb{D}\boldsymbol{\phi}_{u,r}^{n+1}\|^2 + Da^{-1}\|\boldsymbol{\phi}_{u,r}^{n+1}\|^2 \\
&\leq |\beta_T(\mathbf{g}(T - T_r^{n+1}), \boldsymbol{\phi}_{u,r}^{n+1})| + |\beta_C(\mathbf{g}(C - C_r^{n+1}), \boldsymbol{\phi}_{u,r}^{n+1})| + |(\frac{\boldsymbol{\eta}_u^{n+1} - \boldsymbol{\eta}_u^{n}}{\Delta t}, \boldsymbol{\phi}_{u,r}^{n+1})| \\
&\quad + 2\nu|(\mathbb{D}{\boldsymbol{\eta}_u}^{n+1}, \mathbb{D}\boldsymbol{\phi}_{u,r}^{n+1})| + Da^{-1}|({\boldsymbol{\eta}_u}^{n+1}, \boldsymbol{\phi}_{u,r}^{n+1})| + |b_1({\boldsymbol{\eta}_u}^{n+1}, \mathbf{u}^{n+1}, \boldsymbol{\phi}_{u,r}^{n+1})| \\
&\quad + |b_1(\boldsymbol{\phi}_{u,r}^{n+1}, \mathbf{u}^{n+1}, \boldsymbol{\phi}_{u,r}^{n+1})| + |b_1(\mathbf{u}_r^{n+1}, {\boldsymbol{\eta}_u}^{n+1}, \boldsymbol{\phi}_{u,r}^{n+1})| + |(p^{n+1} - q_h, \nabla\cdot\boldsymbol{\phi}_{u,r}^{n+1})| \\
&\quad + |(\mathbf{u}_t^{n+1} - \frac{\mathbf{u}^{n+1} - \mathbf{u}^{n}}{\Delta t}, \boldsymbol{\phi}_{u,r}^{n+1})|.
\end{aligned} \tag{4.1.35}$$

Note that $\left(\frac{\boldsymbol{\eta}_u^{n+1} - \boldsymbol{\eta}_u^{n}}{\Delta t}, \boldsymbol{\phi}_{u,r}^{n+1}\right) = 0$ due to the definition of the L^2 projection. Each of

the terms in (4.1.35) can be bounded in manner similar to what is done above

$$
\begin{aligned}
|\beta_T(\mathbf{g}(T-T_r^{n+1}),\boldsymbol{\phi}_{u,r}^{n+1})| &\leq K\nu^{-1}\beta_T^2\|\mathbf{g}\|_\infty^2(\|\eta_T^{n+1}\|^2+\|\phi_{T,r}^{n+1}\|^2)\\
&\quad+\frac{\nu}{8}\|\mathbb{D}\boldsymbol{\phi}_{u,r}^{n+1}\|^2, \qquad (4.1.36)\\
|\beta_C(\mathbf{g}(C-C_r^{n+1}),\boldsymbol{\phi}_{u,r}^{n+1})| &\leq K\nu^{-1}\beta_C^2\|\mathbf{g}\|_\infty^2(\|\eta_C^{n+1}\|^2+\|\phi_{C,r}^{n+1}\|^2)\\
&\quad+\frac{\nu}{8}\|\mathbb{D}\boldsymbol{\phi}_{u,r}^{n+1}\|^2, \qquad (4.1.37)\\
\nu|(\mathbb{D}\boldsymbol{\eta}_u^{n+1},\mathbb{D}\boldsymbol{\phi}_{u,r}^{n+1})| &\leq K\nu\|\mathbb{D}\boldsymbol{\eta}_u^{n+1}\|^2+\frac{\nu}{8}\|\mathbb{D}\boldsymbol{\phi}_{u,r}^{n+1}\|^2, \qquad (4.1.38)\\
Da^{-1}|(\boldsymbol{\eta}_u^{n+1},\boldsymbol{\phi}_{u,r}^{n+1})| &\leq KDa^{-1}\|\boldsymbol{\eta}_u^{n+1}\|^2+\frac{Da^{-1}}{2}\|\boldsymbol{\phi}_{u,r}^{n+1}\|^2, \qquad (4.1.39)\\
\left|(p^{n+1}-q_h,\nabla\cdot\boldsymbol{\phi}_{u,r}^{n+1})\right| &\leq K\nu^{-1}\left\|p^{n+1}-q_h\right\|^2+\frac{\nu}{8}\left\|\mathbb{D}\boldsymbol{\phi}_{u,r}^{n+1}\right\|^2, \qquad (4.1.40)\\
|(\mathbf{u}_t^{n+1}-\frac{\mathbf{u}^{n+1}-\mathbf{u}^n}{\Delta t},\boldsymbol{\phi}_{u,r}^{n+1})| &\leq K\nu^{-1}\|\mathbf{u}_t^{n+1}-\frac{\mathbf{u}^{n+1}-\mathbf{u}^n}{\Delta t}\|^2\\
&\quad+\frac{\nu}{8}\left\|\mathbb{D}\boldsymbol{\phi}_{u,r}^{n+1}\right\|^2. \qquad (4.1.41)
\end{aligned}
$$

The nonlinear terms are bounded by

$$
\begin{aligned}
b_1(\boldsymbol{\eta}_u^{n+1},\mathbf{u}^{n+1},\boldsymbol{\phi}_{u,r}^{n+1}) &\leq K\nu^{-1}\|\mathbb{D}\boldsymbol{\eta}_u^{n+1}\|^2\|\mathbb{D}\mathbf{u}^{n+1}\|^2+\frac{\nu}{8}\|\mathbb{D}\boldsymbol{\phi}_{u,r}^{n+1}\|^2, \qquad (4.1.42)\\
b_1(\boldsymbol{\phi}_{u,r}^{n+1},\mathbf{u}^{n+1},\boldsymbol{\phi}_{u,r}^{n+1}) &\leq K\nu^{-3}\|\boldsymbol{\phi}_{u,r}^{n+1}\|^2\|\mathbb{D}\mathbf{u}^{n+1}\|^4+\frac{\nu}{8}\|\mathbb{D}\boldsymbol{\phi}_{u,r}^{n+1}\|^2, \qquad (4.1.43)\\
b_1(\mathbf{u}_r^{n+1},\boldsymbol{\eta}_u^{n+1},\boldsymbol{\phi}_{u,r}^{n+1}) &\leq K\nu^{-1}\|\mathbb{D}\mathbf{u}_r^{n+1}\|^2\|\mathbb{D}\boldsymbol{\eta}_u^{n+1}\|^2+\frac{\nu}{8}\|\mathbb{D}\boldsymbol{\phi}_{u,r}^{n+1}\|^2. \qquad (4.1.44)
\end{aligned}
$$

We now insert (4.1.36)-(4.1.44) into (4.1.35) and use regularity assumptions (2.2.10) to get

$$
\begin{aligned}
&\frac{1}{2\Delta t}\|\boldsymbol{\phi}_{u,r}^{n+1}\|^2-\frac{1}{2\Delta t}\|\boldsymbol{\phi}_{u,r}^{n}\|^2+\frac{1}{2\Delta t}\|\boldsymbol{\phi}_{u,r}^{n+1}-\boldsymbol{\phi}_{u,r}^{n}\|^2+\nu\|\mathbb{D}\boldsymbol{\phi}_{u,r}^{n+1}\|^2+\frac{Da^{-1}}{2}\|\boldsymbol{\phi}_{u,r}^{n+1}\|^2\\
&\leq K\Big(\nu^{-1}\|\mathbf{g}\|_\infty^2(\beta_T^2\|\phi_{T,r}^{n+1}\|^2+\beta_C^2\|\phi_{C,r}^{n+1}\|^2)+\nu^{-3}\|\mathbb{D}\mathbf{u}^{n+1}\|^4\|\boldsymbol{\phi}_{u,r}^{n+1}\|^2\\
&\quad+\|\eta_T^{n+1}\|^2+\|\eta_C^{n+1}\|^2+\|\mathbb{D}\boldsymbol{\eta}_u{}^{n+1}\|^2(1+\|\mathbb{D}\mathbf{u}^{n+1}\|^2+\|\mathbb{D}\mathbf{u}_r^{n+1}\|^2)\\
&\quad+\|\boldsymbol{\eta}_u{}^{n+1}\|^2+\|p^{n+1}-q_h\|^2+\|\mathbf{u}_t^{n+1}-\frac{\mathbf{u}^{n+1}-\mathbf{u}^n}{\Delta t}\|^2\Big). \qquad (4.1.45)
\end{aligned}
$$

Dropping the third term in the left hand side of (4.1.45) and summing over the time

steps and multiplying by $2\Delta t$ gives

$$\begin{aligned}
&\|\boldsymbol{\phi}_{u,r}^{M}\|^2 + \Delta t \sum_{n=0}^{M-1} \Big(2\nu\|\mathbb{D}\boldsymbol{\phi}_{u,r}^{n+1}\|^2 + Da^{-1}\|\boldsymbol{\phi}_{u,r}^{n+1}\|^2\Big) \\
&\leq \|\boldsymbol{\phi}_{u,r}^{0}\|^2 + K\Delta t\Big(\nu^{-1}\|\mathbf{g}\|_\infty^2 \sum_{n=0}^{M-1} (\beta_T^2\|\phi_{T,r}^{n+1}\|^2 + \beta_C^2\|\phi_{C,r}^{n+1}\|^2) + \nu^{-3}\sum_{n=0}^{M-1}\|\mathbb{D}\mathbf{u}^{n+1}\|^4\|\boldsymbol{\phi}_{u,r}^{n+1}\|^2 \\
&\quad + \sum_{n=0}^{M-1}(\|\eta_T^{n+1}\|^2 + \|\eta_C^{n+1}\|^2) + \sum_{n=0}^{M-1}(\|\mathbb{D}\boldsymbol{\eta}_u{}^{n+1}\|^2(1 + \|\mathbb{D}\mathbf{u}^{n+1}\|^2 + \|\mathbb{D}\mathbf{u}_r^{n+1}\|^2)) \\
&\quad + \sum_{n=0}^{M-1}\|\boldsymbol{\eta}_u{}^{n+1}\|^2 + \sum_{n=0}^{M-1}\|p^{n+1} - q_h\|^2 + \sum_{n=0}^{M-1}\|\mathbf{u}_t^{n+1} - \frac{\mathbf{u}^{n+1}-\mathbf{u}^n}{\Delta t}\|^2\Big). \qquad (4.1.46)
\end{aligned}$$

Using Lemma 2.1.4, Lemma 2.2.1, Lemma 4.1.1, Assumption 2.1.1 in (4.1.46) and applying regularity assumptions leads to

$$\begin{aligned}
&\|\boldsymbol{\phi}_{u,r}^{M}\|^2 + \Delta t \sum_{n=0}^{M-1} \Big(2\nu\|\mathbb{D}\boldsymbol{\phi}_{u,r}^{n+1}\|^2 + Da^{-1}\|\boldsymbol{\phi}_{u,r}^{n+1}\|^2\Big) \\
&\leq \|\mathbf{u}_r^0 - \tilde{\mathbf{u}}^0\|^2 + K\Bigg(\nu^{-1}\beta_T^2\|\mathbf{g}\|_\infty^2\Delta t\sum_{n=0}^{M-1}\|\phi_{T,r}^{n+1}\|^2 + \nu^{-1}\beta_C^2\|\mathbf{g}\|_\infty^2\Delta t\sum_{n=0}^{M-1}\|\phi_{C,r}^{n+1}\|^2 \\
&\quad + h^{2m} + \Delta t^2 + h^{2m+2}\big(1 + \|S_{u,r}\|_2\big) + \sum_{i=r_1+1}^{d}\lambda_i + \sum_{i=r_2+1}^{d}\mu_i + \sum_{i=r_3+1}^{d}\xi_i + \varepsilon_u^2 \\
&\quad + \nu^{-3}|||\mathbb{D}\mathbf{u}|||_{\infty,0}^2\Delta t\sum_{n=0}^{M-1}\|\boldsymbol{\phi}_{u,r}^{n+1}\|^2\Bigg). \qquad (4.1.47)
\end{aligned}$$

Finally, we add (4.1.32), (4.1.33) and (4.1.47) to get

$$\begin{aligned}
&\|\boldsymbol{\phi}_{u,r}^{M}\|^2 + \|\phi_{T,r}^{M}\|^2 + \|\phi_{C,r}^{M}\|^2 + \sum_{n=0}^{M-1}\Big(\nu\Delta t\|\mathbb{D}\boldsymbol{\phi}_{u,r}^{n+1}\|^2 + Da^{-1}\Delta t\|\boldsymbol{\phi}_{u,r}^{n+1}\|^2\Big) \\
&\quad + \gamma\Delta t\sum_{n=0}^{M-1}\|\nabla\phi_{T,r}^{n+1}\|^2 + D_c\Delta t\sum_{n=0}^{M-1}\|\nabla\phi_{C,r}^{n+1}\|^2 \leq \|\mathbf{u}_r^0 - \tilde{\mathbf{u}}^0\|^2 + \|T_r^0 - \tilde{T}^0\|^2 \\
&\quad + \|C_r^0 - \tilde{C}^0\|^2 + K\Bigg(\nu^{-1}\beta_T^2\|\mathbf{g}\|_\infty^2\Delta t\sum_{n=0}^{M-1}\|\phi_{T,r}^{n+1}\|^2 + \nu^{-1}\beta_C^2\|\mathbf{g}\|_\infty^2\Delta t\sum_{n=0}^{M-1}\|\phi_{C,r}^{n+1}\|^2 \\
&\quad + (\nu^{-3}|||\mathbb{D}\mathbf{u}|||_{\infty,0}^2 + \nu^{-1}\gamma^{-2}|||\nabla T|||_{\infty,0}^4 + \nu^{-1}{D_c}^{-2}|||\nabla C|||_{\infty,0}^4)\Delta t\sum_{n=0}^{M-1}\|\boldsymbol{\phi}_{u,r}^{n+1}\|^2 \\
&\quad + h^{2m} + (\Delta t)^2 + h^{2m+2}\big(1 + \|S_{u,r}\|_2 + \|S_{T,r}\|_2 + \|S_{C,r}\|_2\big) \\
&\quad + \sum_{i=r_1+1}^{d}\lambda_i + \sum_{i=r_2+1}^{d}\mu_i + \sum_{i=r_3+1}^{d}\xi_i + \varepsilon_u^2 + \varepsilon_T^2 + \varepsilon_C^2\Bigg).
\end{aligned}$$

Application of the discrete Gronwall Lemma (1.2.8) requires an assumption on the time step size (4.1.17). The final error estimation can be obtained by using the assumption $(\mathbf{u}_r^0, T_r^0, C_r^0) = (\tilde{\mathbf{u}}^0, \tilde{T}^0, \tilde{C}^0)$, the triangle inequality, Assumption 2.1.1 and Assumption 2.2.1.

4.2 Numerical Analysis of Post-Processed VMS-POD Schemes for Double Diffusive Darcy-Brinkman system

In this section, the POD method is combined with VMS method similar to Chapter 3. VMS aims to model unresolved scales by adding an artificial viscosity to only resolved small-scales, as noted in Chapter 1. We consider adding the decoupled VMS-ROM stabilization from [21], where in effect additional viscosity gets added to the smaller R velocity modes in a post-processing step. Specifically, we post-process $\mathbf{u}_r^{n+1}$ by solving the algorithm:

Algorithm 4.2.1 *The post-processing VMS-POD approximation for double diffusive system (1.3.15) given as:*

***Step 1**: Find* $(\mathbf{w}_r^{n+1}, T_r^{n+1}, C_r^{n+1}) \in (\mathbf{X}_r, W_r, \Psi_r)$ *satisfying*

$$\begin{aligned}(\frac{\mathbf{w}_r^{n+1}-\mathbf{u}_r^n}{\Delta t}, \mathbf{v}_r) + 2\nu(\mathbb{D}\mathbf{w}_r^{n+1}, \mathbb{D}\mathbf{v}_r) + b_1(\mathbf{w}_r^{n+1}, \mathbf{w}_r^{n+1}, \mathbf{v}_r)\\ +(Da^{-1}\mathbf{w}_r^{n+1}, \mathbf{v}_r) = \beta_T(\mathbf{g}T_r^{n+1}, \mathbf{v}_r) + \beta_C(\mathbf{g}C_r^{n+1}, \mathbf{v}_r),\end{aligned} \tag{4.2.1}$$

$$(\frac{T_r^{n+1}-T_r^n}{\Delta t}, S_r) + b_2(\mathbf{w}_r^{n+1}, T_r^{n+1}, S_r) + \gamma(\nabla T_r^{n+1}, \nabla S_r) = 0, \tag{4.2.2}$$

$$(\frac{C_r^{n+1}-C_r^n}{\Delta t}, \Phi_r) + b_3(\mathbf{w}_r^{n+1}, C_r^{n+1}, \Phi_r) + D_c(\nabla C_r^{n+1}, \nabla \Phi_r) = 0, \tag{4.2.3}$$

for all $(\mathbf{v}_r, S_r, \Phi_r) \in (\mathbf{X}_r, W_r, \Psi_r)$.

***Step 2**: Find* $\mathbf{u}_r^{n+1} \in \mathbf{X}_r$, $\forall \mathbf{v}_r \in \mathbf{X}_r$*:*

$$\left(\frac{\mathbf{w}_r^{n+1}-\mathbf{u}_r^{n+1}}{\Delta t}, \mathbf{v}_r\right) = \left(\nu_T(I-P_R)\nabla\frac{(\mathbf{u}_r^{n+1}+\mathbf{w}_r^{n+1})}{2}, (I-P_R)\nabla\mathbf{v}_r\right), \tag{4.2.4}$$

where P_R *is the* L^2 *projection into* $\mathbf{X}_R$*, which is the subset of* $\mathbf{X}_r$ *that is the span of the first* R *(*$< r$*) velocity modes.*

This section states two important results; the stability and convergence of the algorithm (4.2.1)-(4.2.4).

Lemma 4.2.1 *(Stability) The post-processed VMS-POD approximation (4.2.1)-(4.2.4)*

is unconditionally stable in the following sense: for any $\Delta t > 0$*,*

$$\begin{aligned}
&\|\mathbf{u}_r^M\|^2 + \sum_{n=0}^{M-1}\Bigg[2\nu_T\Delta t\left\|(I-P_R)\nabla\frac{(\mathbf{w}_r^{n+1}+\mathbf{u}_r^{n+1})}{2}\right\|^2 \\
&\qquad +\|\mathbf{w}_r^{n+1}-\mathbf{u}_r^n\|^2 + 2\nu\Delta t\|\mathbb{D}\mathbf{w}_r^{n+1}\|^2 + Da^{-1}\Delta t\|\mathbf{w}_r^{n+1}\|^2\Bigg] \\
&\quad\leq \|\mathbf{u}_0\|^2 + C^*\|\mathbf{g}\|_\infty^2(\beta_T^2\gamma^{-1}\|T_0\|^2 + \beta_C^2 D_c^{-1}\|C_0\|^2). \qquad (4.2.5)
\end{aligned}$$

$$\|T_r^M\|^2 + \sum_{n=0}^{M-1} 2\Delta t\gamma\|\nabla T_r^n\|^2 \leq \|T_0\|^2, \qquad (4.2.6)$$

$$\|C_r^M\|^2 + \sum_{n=0}^{M-1} 2\Delta t D_c\|\nabla C_r^n\|^2 \leq \|C_0\|^2, \qquad (4.2.7)$$

where $C^* = \min\{\nu^{-1}, Da\}$.

Proof Letting $S_r = T_r^{n+1}$ in (4.2.2) and using skew symmetry property and applying Cauchy-Schwarz and Young's inequality produces

$$\|T_r^{n+1}\|^2 + 2\gamma\Delta t\|\nabla T_r^n\|^2 \leq \|T_r^n\|^2, \qquad (4.2.8)$$

and finally summing over the time steps yields the stability result (4.2.6). In a similar manner, setting $\Phi_r = C_r^{n+1}$ in (4.2.3) yields (4.2.7). Finally, choosing $\mathbf{v}_r = \mathbf{w}_r^{n+1}$ in (4.2.1), using the polarization identity, and multiply both sides by $2\Delta t$ yields

$$\begin{aligned}
&\|\mathbf{w}_r^{n+1}\|^2 - \|\mathbf{u}_r^n\|^2 + \|\mathbf{w}_r^{n+1}-\mathbf{u}_r^n\|^2 + 4\nu\Delta t\|\mathbb{D}\mathbf{w}_r^{n+1}\|^2 + 2Da^{-1}\Delta t\|\mathbf{w}_r^{n+1}\|^2 \\
&\quad = 2\Delta t\beta_T(\mathbf{g}T_r^{n+1}, \mathbf{w}_r^{n+1}) + 2\Delta t\beta_C(\mathbf{g}C_r^{n+1}, \mathbf{w}_r^{n+1}). \qquad (4.2.9)
\end{aligned}$$

Note that if we let $\mathbf{v}_r = \frac{(\mathbf{w}_r^{n+1}+\mathbf{u}_r^{n+1})}{2}$ in (4.2.4), we have

$$\|\mathbf{w}_r^{n+1}\|^2 = \|\mathbf{u}_r^{n+1}\|^2 + 2\nu_T\Delta t\left\|(I-P_R)\nabla\frac{(\mathbf{w}_r^{n+1}+\mathbf{u}_r^{n+1})}{2}\right\|^2. \qquad (4.2.10)$$

Insert (4.2.10) in (4.2.9), and apply Cauchy-Schwarz, Young's inequality and Poincaré's inequality, which provides

$$\begin{aligned}
&\|\mathbf{u}_r^{n+1}\|^2 - \|\mathbf{u}_r^n\|^2 + 2\nu_T\Delta t\left\|(I-P_R)\nabla\frac{(\mathbf{w}_r^{n+1}+\mathbf{u}_r^{n+1})}{2}\right\|^2 \\
&\qquad +\|\mathbf{w}_r^{n+1}-\mathbf{u}_r^n\|^2 + 2\nu\Delta t\|\mathbb{D}\mathbf{w}_r^{n+1}\|^2 + Da^{-1}\Delta t\|\mathbf{w}_r^{n+1}\|^2 \\
&\quad\leq C^*\|\mathbf{g}\|_\infty^2(\beta_T^2\Delta t\|\nabla T_r^{n+1}\|^2 + \beta_C^2\Delta t\|\nabla C_r^{n+1}\|^2) \qquad (4.2.11)
\end{aligned}$$

where $C^* = \min\{\nu^{-1}, Da^{-1}\}$. Summing over the time steps yields the stated result (4.2.5).

The optimal asymptotic error estimation is given as follows with its proof.

Theorem 4.2.2 *(Error Estimation) Suppose regularity assumptions (4.1.16) holds. Then for the sufficiently small Δt, the error satisfies*

$$\begin{aligned}
&\|\mathbf{u}^M - \mathbf{u}_r^M\|^2 + \|T^M - T_r^M\|^2 + \|C^M - C_r^M\|^2 \\
&\leq K\Bigg(1 + h^{2m} + (\Delta t)^2 + (1 + \|S_{u,r}\|_2 \\
&\quad + \|S_{u,R}\|_2 + \|S_{T,r}\|_2 + \|S_{C,r}\|_2)h^{2m+2} \\
&\quad + \sum_{i=r_1+1}^{d} (\|\boldsymbol{\psi}_i\|_1^2 + 1)\lambda_i + \sum_{i=r_2+1}^{d} (\|\phi_i\|_1^2 + 1)\mu_i \\
&\quad + \sum_{i=r_3+1}^{d} (\|\eta_i\|_1^2 + 1)\xi_i + \sum_{i=R+1}^{d} \|\boldsymbol{\psi}_i\|_1^2 \lambda_i \Bigg). \qquad (4.2.12)
\end{aligned}$$

Proof We begin the proof by deriving error equations, subtracting from (1.3.16), (1.3.18), (1.3.19) to (4.2.1), (4.2.2), (4.2.3) at time t^{n+1}, respectively we have

$$\begin{aligned}
&\left(\mathbf{u}_t^{n+1} - \frac{\mathbf{w}_r^{n+1} - \mathbf{u}_r^n}{\Delta t}, \mathbf{v}_r\right) + 2\nu(\mathbb{D}(\mathbf{u}^{n+1} - \mathbf{w}_r^{n+1}), \mathbb{D}\mathbf{v}_r) + b_1(\mathbf{u}^{n+1}, \mathbf{u}^{n+1}, \mathbf{v}_r) \\
&\quad - b_1(\mathbf{w}_r^{n+1}, \mathbf{w}_r^{n+1}, \mathbf{v}_r) + (Da^{-1}(\mathbf{u} - \mathbf{w}_r^{n+1}), \mathbf{v}_r) - (p^{n+1}, \nabla \cdot \mathbf{v}_r) \\
&\quad = \beta_T(\mathbf{g}(T - T_r^{n+1}), \mathbf{v}_r) + \beta_C(\mathbf{g}(C - C_r^{n+1}), \mathbf{v}_r), \qquad (4.2.13) \\
&\left(T_t^{n+1} - \frac{T_r^{n+1} - T_r^n}{\Delta t}, S_r\right) + b_2(\mathbf{u}^{n+1}, T^{n+1}, S_r) - b_2(\mathbf{u}_r^{n+1}, T_r^{n+1}, S_r) \\
&\quad + \gamma(\nabla(T^{n+1} - T_r^{n+1}), \nabla S_r) = 0, \qquad (4.2.14) \\
&\left(C_t^{n+1} - \frac{C_r^{n+1} - C_r^n}{\Delta t}, \Phi_r\right) + b_3(\mathbf{u}^{n+1}, C^{n+1}, \Phi_r) - b_3(\mathbf{u}_r^{n+1}, C_r^{n+1}, \Phi_r) \\
&\quad + D_c(\nabla(C^{n+1} - C_r^{n+1}), \nabla\Phi_r) = 0. \qquad (4.2.15)
\end{aligned}$$

The notations that are used in the proof are defined as

$$\begin{aligned}
\boldsymbol{\eta}_{\mathbf{u}}^n &:= \mathbf{u}^n - \mathcal{U}^n, \quad \boldsymbol{\phi}_{\mathbf{u},r}^n := \mathbf{w}_r^n - \mathcal{U}^n, \quad \boldsymbol{\theta}_{\mathbf{u},r}^n := \mathbf{u}_r^n - \mathcal{U}^n, \\
\mathbf{e}_{\mathbf{u},r}^n &= \mathbf{u}^n - \mathbf{u}_r^n, \quad \boldsymbol{\varepsilon}_{\mathbf{u},r}^n := \mathbf{u}^n - \mathbf{w}_r^n, \\
\eta_T^{n+1} &= T^{n+1} - \tilde{T}, \quad \phi_{T,r}^{n+1} := T_r^{n+1} - \tilde{T}^{n+1}, \\
\eta_C^{n+1} &= \eta_C^{n+1}, \quad \phi_{C,r}^{n+1} := C_r^{n+1} - \tilde{C}^{n+1}
\end{aligned}$$

where $(\mathcal{U}^{\mathbf{n}}, \tilde{T}^{n+1}, \tilde{C}^{n+1})$ are L^2 projections of $(\mathbf{u}^{n+1}, T^{n+1}, C^{n+1})$ in $(\mathbf{X}_r, W_r, \Psi_r)$ at time t^{n+1}.

Letting $S_r = T_r^{n+1}$ in (4.2.14), and reorganizing it similarly (4.1.31), we get

$$\begin{aligned}\|\phi_{T,r}^{M}\|^2 + \gamma\Delta t\sum_{n=0}^{M-1}\|\nabla\phi_{T,r}^{n+1}\|^2 \leq \|\phi_{T,r}^{0}\|^2 + K\Delta t\Big(\gamma\sum_{n=0}^{M-1}\|\nabla {\eta_T}^{n+1}\|^2\\ +\gamma^{-1}\sum_{n=0}^{M-1}\|\nabla {\boldsymbol{\eta}_u}^{n+1}\|^2\|\nabla T^{n+1}\|^2 + \nu^{-1}\gamma^{-2}\sum_{n=0}^{M-1}\|\boldsymbol{\phi}_{u,r}^{n+1}\|^2\|\nabla T^{n+1}\|^4\\ +\gamma^{-1}\sum_{n=0}^{M-1}\|\nabla\mathbf{u}_r^{n+1}\|^2\|\nabla {\eta_T}^{n+1}\|^2 + \frac{\nu}{2}\sum_{n=0}^{M-1}\|\mathbb{D}\boldsymbol{\phi}_{u,r}^{n+1}\|^2\\ +\gamma^{-1}\Delta t\|T_{tt}\|^2_{L^2(0,\tau;H^1(\Omega))}\Big).\end{aligned} \tag{4.2.16}$$

By using Lemma 2.1.4, Lemma 2.2.1, Lemma 4.1.1, Assumption 2.2.1 and regularity assumptions in (4.2.16) results in

$$\begin{aligned}\|\phi_{T,r}^{M}\|^2 + \gamma\Delta t\sum_{n=0}^{M-1}\|\nabla\phi_{T,r}^{n+1}\|^2 \leq \|\phi_{T,r}^{0}\|^2 + K\Big(h^{2m} + (\|S_{u,r}\|_2\\ +\|S_{T,r}\|_2)h^{2m+2} + \varepsilon_u^2 + \varepsilon_T^2 + \nu^{-1}\gamma^{-2}|||\nabla T|||^4_{\infty,0}\Delta t\sum_{n=0}^{M-1}\|\boldsymbol{\phi}_{u,r}^{n+1}\|^2\\ +\frac{\nu\Delta t}{2}\sum_{n=0}^{M-1}\|\mathbb{D}\boldsymbol{\phi}_{u,r}^{n+1}\|^2 + (\Delta t)^2\Big).\end{aligned} \tag{4.2.17}$$

Similarly, the error estimation for the concentration is given by

$$\begin{aligned}\|\phi_{C,r}^{M}\|^2 + D_c\Delta t\sum_{n=0}^{M-1}\|\nabla\phi_{C,r}^{n+1}\|^2 \leq \|\phi_{C,r}^{0}\|^2 + K\Big(h^{2m} + (\|S_{u,r}\|_2\\ +\|S_{C,r}\|_2)h^{2m+2} + \varepsilon_u^2 + \varepsilon_C^2 + \nu^{-1}{D_c}^{-2}|||\nabla C|||^4_{\infty,0}\Delta t\sum_{n=0}^{M-1}\|\boldsymbol{\phi}_{u,r}^{n+1}\|^2\\ +\frac{\nu\Delta t}{2}\sum_{n=0}^{M-1}\|\mathbb{D}\boldsymbol{\phi}_{u,r}^{n+1}\|^2 + (\Delta t)^2\Big).\end{aligned} \tag{4.2.18}$$

In a similar manner, setting $\mathbf{v}_r = \boldsymbol{\phi}_{\mathbf{u},r}^{n+1}$ in the (4.2.13), we have

$$\begin{aligned}&\left(\frac{\boldsymbol{\phi}_{\mathbf{u},r}^{n+1} - \boldsymbol{\theta}_{\mathbf{u},r}^{n}}{\Delta t}, \boldsymbol{\phi}_{\mathbf{u},r}^{n+1}\right) + 2\nu\|\mathbb{D}\boldsymbol{\phi}_{\mathbf{u},r}^{n+1}\|^2 + Da^{-1}\|\boldsymbol{\phi}_{\mathbf{u},r}^{n+1}\|^2\\ &= \left(\frac{\boldsymbol{\eta}_{\mathbf{u}}^{n+1} - \boldsymbol{\eta}_{\mathbf{u}}^{n}}{\Delta t}, \boldsymbol{\phi}_{\mathbf{u},r}^{n+1}\right) + 2\nu(\mathbb{D}\boldsymbol{\eta}_{\mathbf{u}}^{n+1}, \mathbb{D}\boldsymbol{\phi}_{\mathbf{u},r}^{n+1})\\ &\quad +[b(\mathbf{u}^{n+1}, \mathbf{u}^{n+1}, \boldsymbol{\phi}_{\mathbf{u},r}^{n+1}) - b(\mathbf{w}_r^{n+1}, \mathbf{w}_r^{n+1}, \boldsymbol{\phi}_{\mathbf{u},r}^{n+1})] + (Da^{-1}\boldsymbol{\eta}_{\mathbf{u}}^{n+1}, \boldsymbol{\phi}_{\mathbf{u},r}^{n+1})\\ &\quad -(p^{n+1}, \nabla\cdot\boldsymbol{\phi}_{\mathbf{u},r}^{n+1}) + \left(\mathbf{u}_t^{n+1} - \frac{\mathbf{u}^{n+1} - \mathbf{u}^{n}}{\Delta t}, \boldsymbol{\phi}_{\mathbf{u},r}^{n+1}\right)\\ &\quad +\beta_T(\mathbf{g}(T^{n+1} - T_r^{n+1}), \boldsymbol{\phi}_{\mathbf{u},r}^{n+1}) + \beta_C(\mathbf{g}(C^{n+1} - C_r^{n+1}), \boldsymbol{\phi}_{\mathbf{u},r}^{n+1}).\end{aligned} \tag{4.2.19}$$

Note that, we get $(\boldsymbol{\eta}_{\mathbf{u}}^{n}, \boldsymbol{\phi}_{\mathbf{u},r}^{n+1}) = 0$ and $(\boldsymbol{\eta}_{\mathbf{u}}^{n+1}, \boldsymbol{\phi}_{\mathbf{u},r}^{n+1}) = 0$ using the L^2 projection (2.1.50). Using this along with the polarization identity and that $\boldsymbol{\phi}_{\mathbf{u},r}^{n+1} \in \mathbf{X}^r \subset \mathbf{V}^h$,

and inserting all bounds (3.1.11)-(3.1.14) and (4.1.36)-(4.1.37) for the right hand side terms of (4.2.19) and multiplying both sides by $2\Delta t$ gives

$$
\begin{aligned}
&(\|\boldsymbol{\phi}_{\mathbf{u},r}^{n+1}\|^2 - \|\boldsymbol{\theta}_{\mathbf{u},r}^{n}\|^2) + \nu\Delta t\|\nabla\boldsymbol{\phi}_{\mathbf{u},r}^{n+1}\|^2 + Da^{-1}\|\boldsymbol{\phi}_{\mathbf{u},r}^{n+1}\|^2 \leq K\Big(\nu\Delta t\|\nabla\boldsymbol{\eta}_{\mathbf{u}}^{n+1}\|^2 \\
&+\nu^{-1}\Delta t\|\boldsymbol{\eta}_{\mathbf{u}}^{n+1}\|\|\nabla\boldsymbol{\eta}_{\mathbf{u}}^{n+1}\|\|\nabla\mathbf{u}^{n+1}\|^2 + Da^{-1}\|\boldsymbol{\eta}_{\mathbf{u}}^{n+1}\|^2 + \frac{\Delta t}{\nu^3}\|\boldsymbol{\phi}_{\mathbf{u},r}^{n+1}\|^2\|\nabla\mathbf{u}^{n+1}\|^4 \\
&+\nu^{-1}\Delta t\|\mathbf{w}_r^{n+1}\|\|\nabla\mathbf{w}_r^{n+1}\|\|\nabla\boldsymbol{\eta}_{\mathbf{u}}^{n+1}\|^2 + \nu^{-1}\Delta t\|p^{n+1} - q_h\|^2 + \nu^{-1}\Delta t\|\mathbf{u}_t^{n+1} - \frac{\mathbf{u}^{n+1} - \mathbf{u}^n}{\Delta t}\|^2 \\
&+\nu^{-1}\beta_T^2\|\mathbf{g}\|_\infty^2(\|\eta_T^{n+1}\|^2 + \|\phi_{T,r}^{n+1}\|^2) + \nu^{-1}\beta_C^2\|\mathbf{g}\|_\infty^2(\|\eta_C^{n+1}\|^2 + \|\phi_{C,r}^{n+1}\|^2)\Big). \qquad (4.2.20)
\end{aligned}
$$

To get a bound for $\|\boldsymbol{\phi}_r^{n+1}\|^2$, write (4.2.4) by adding and subtracting the true solution projection $\mathcal{U}^{n+1}$ on both sides and we have

$$
\left(\frac{\boldsymbol{\phi}_{\mathbf{u},r}^{n+1} - \boldsymbol{\theta}_{\mathbf{u},r}^{n+1}}{\Delta t}, \boldsymbol{\psi}\right) = (\nu_T(I - P_R)\nabla\frac{(\boldsymbol{\phi}_{\mathbf{u},r}^{n+1} + \boldsymbol{\theta}_{\mathbf{u},r}^{n+1} + 2\mathcal{U}^{n+1})}{2}, (I - P_R)\nabla\boldsymbol{\psi}), \quad (4.2.21)
$$

and then choosing $\boldsymbol{\psi} = \dfrac{(\boldsymbol{\phi}_{\mathbf{u},r}^{n+1} + \boldsymbol{\theta}_{\mathbf{u},r}^{n+1})}{2}$ in (4.2.21), we get

$$
\begin{aligned}
\|\boldsymbol{\phi}_{\mathbf{u},r}^{n+1}\|^2 \quad &= \quad \|\boldsymbol{\theta}_{\mathbf{u},r}^{n+1}\|^2 + \frac{1}{2}\Delta t\nu_T\|(I - P_R)\nabla(\boldsymbol{\phi}_{\mathbf{u},r}^{n+1} + \boldsymbol{\theta}_{\mathbf{u},r}^{n+1})\|^2 \\
&\quad +\Delta t(\nu_T(I - P_R)\nabla\mathcal{U}^{n+1}, (I - P_R)\nabla(\boldsymbol{\phi}_{\mathbf{u},r}^{n+1} + \boldsymbol{\theta}_{\mathbf{u},r}^{n+1})). \quad (4.2.22)
\end{aligned}
$$

Noting $\mathcal{U}^{n+1} = \mathbf{u}^{n+1} - \boldsymbol{\eta}_{\mathbf{u}}^{n+1}$ and inserting (4.2.22) into (4.2.20) results into

$$
\begin{aligned}
&\|\boldsymbol{\theta}_{\mathbf{u},r}^{n+1}\|^2 - \|\boldsymbol{\theta}_{\mathbf{u},r}^{n}\|^2 + \frac{1}{2}\Delta t\nu_T\|(I - P_R)\nabla(\boldsymbol{\phi}_{\mathbf{u},r}^{n+1} + \boldsymbol{\theta}_{\mathbf{u},r}^{n+1})\|^2 + \nu\Delta t\|\nabla\boldsymbol{\phi}_{\mathbf{u},r}^{n+1}\|^2 \\
&\quad +Da^{-1}\|\boldsymbol{\phi}_{\mathbf{u},r}^{n+1}\|^2 \\
&\leq \; C\nu\Delta t\|\nabla\boldsymbol{\eta}_{\mathbf{u}}^{n+1}\|^2 + \frac{C\Delta t}{\nu}\|\boldsymbol{\eta}_{\mathbf{u}}^{n+1}\|\|\nabla\boldsymbol{\eta}_{\mathbf{u}}^{n+1}\|\|\nabla\mathbf{u}^{n+1}\|^2 \\
&\quad +\frac{C\Delta t}{\nu^3}\|\nabla\mathbf{u}^{n+1}\|^4\Big[\|\boldsymbol{\theta}_{\mathbf{u},r}^{n+1}\|^2 + \frac{1}{2}\Delta t\nu_T\|(I - P_R)\nabla(\boldsymbol{\phi}_{\mathbf{u},r}^{n+1} + \boldsymbol{\theta}_{\mathbf{u},r}^{n+1})\|^2 \\
&\quad +\Delta t(\nu_T(I - P_R)\nabla(\mathbf{u}^{n+1} - \boldsymbol{\eta}_{\mathbf{u}}^{n+1}), (I - P_R)\nabla(\boldsymbol{\phi}_{\mathbf{u},r}^{n+1} + \boldsymbol{\theta}_{\mathbf{u},r}^{n+1}))\Big] \\
&\quad +\Delta t(\nu_T(I - P_R)\nabla(\boldsymbol{\eta}_{\mathbf{u}}^{n+1} - \mathbf{u}^{n+1}), (I - P_R)\nabla(\boldsymbol{\phi}_{\mathbf{u},r}^{n+1} + \boldsymbol{\theta}_{\mathbf{u},r}^{n+1})) \\
&\quad +\frac{C\Delta t}{\nu}\|\mathbf{w}_r^{n+1}\|\|\nabla\mathbf{w}_r^{n+1}\|\|\nabla\boldsymbol{\eta}_{\mathbf{u}}^{n+1}\|^2 + \frac{C\Delta t}{\nu}\|p^{n+1} - q_h\|^2 \\
&\quad +\frac{C\Delta t}{\nu}\|\mathbf{u}_t^{n+1} - \frac{\mathbf{u}^{n+1} - \mathbf{u}^n}{\Delta t}\|^2 + \nu^{-1}\beta_T^2\|\mathbf{g}\|_\infty^2(\|\eta_T^{n+1}\|^2 + \|\phi_{T,r}^{n+1}\|^2) \\
&\quad +\nu^{-1}\beta_C^2\|\mathbf{g}\|_\infty^2(\|\eta_C^{n+1}\|^2 + \|\phi_{C,r}^{n+1}\|^2)\Big). \qquad (4.2.23)
\end{aligned}
$$

Assume now $\Delta t \leq \dfrac{1}{8C}\Big[\frac{\|\nabla\mathbf{u}\|^4}{\nu^3}\Big]^{-1}$. Substitute the bounds (3.1.19)-(3.1.20) into (4.2.23)

and sum from $n = 0$ to $M - 1$. This gives

$$\begin{aligned}
&\|\boldsymbol{\theta}_r^M\|^2 + \sum_{n=0}^{M-1}\left[\frac{1}{8}\Delta t\nu_T\|(I-P_R)\nabla(\boldsymbol{\phi}_r^{n+1}+\boldsymbol{\theta}_r^{n+1})\|^2 + \nu\Delta t\|\nabla\boldsymbol{\phi}_r^{n+1}\|^2 + Da^{-1}\|\boldsymbol{\phi}_{\mathbf{u},r}^{n+1}\|^2\right] \\
&\leq \|\boldsymbol{\theta}_r^0\|^2 + C\sum_{n=0}^{M-1}\left[\nu\Delta t\|\nabla\boldsymbol{\eta}_{\mathbf{u}}^{n+1}\|^2 + \frac{\Delta t}{\nu}\|\nabla\mathbf{u}^{n+1}\|^2\|\nabla\boldsymbol{\eta}_{\mathbf{u}}^{n+1}\|^2\right. \\
&\quad +\Delta t\nu_T\|(I-P_R)\nabla(\mathbf{u}^{n+1}-\boldsymbol{\eta}_{\mathbf{u}}^{n+1})\|^2 + \frac{\Delta t}{\nu}\|\mathbf{w}_r^{n+1}\|\|\nabla\mathbf{w}_r^{n+1}\|\|\nabla\boldsymbol{\eta}_{bu}^{n+1}\|^2 \\
&\quad +\frac{\Delta t}{\nu}\|p^{n+1}-q_h\|^2 + \frac{\Delta t}{\nu}\|\mathbf{u}_t^{n+1} - \frac{\mathbf{u}^{n+1}-\mathbf{u}^n}{\Delta t}\|^2 + \nu^{-1}\beta_T^2\|\mathbf{g}\|_\infty^2(\|\eta_T^{n+1}\|^2 + \|\phi_{T,r}^{n+1}\|^2) \\
&\quad \left.+\nu^{-1}\beta_C^2\|\mathbf{g}\|_\infty^2(\|\eta_C^{n+1}\|^2 + \|\phi_{C,r}^{n+1}\|^2)\right] + \frac{C\Delta t}{\nu^3}\sum_{n=0}^{M-1}\|\nabla\mathbf{u}^{n+1}\|^4\|\boldsymbol{\theta}_r^{n+1}\|^2. \qquad (4.2.24)
\end{aligned}$$

Collecting all the bounds (3.1.22)-(3.1.29) for (4.2.24) and using Lemma 2.1.4, Lemma 2.2.1, Lemma 3.1.1, Assumption 2.2.1 in (4.1.46) and applying regularity assumptions leads to

$$\begin{aligned}
&\|\boldsymbol{\theta}_r^M\|^2 + \sum_{n=0}^{M-1}\left[\frac{1}{8}\Delta t\nu_T\|(I-P_R)\nabla(\boldsymbol{\phi}_r^{n+1}+\boldsymbol{\theta}_r^{n+1})\|^2 + \nu\Delta t\|\nabla\boldsymbol{\phi}_r^{n+1}\|^2\right. \\
&\quad \left.+Da^{-1}\|\boldsymbol{\phi}_{\mathbf{u},r}^{n+1}\|^2\right] \leq K\left[\nu\left(\left(h^{2m}+\|S_{u,r}\|_2h^{2m+2}\right)|||\mathbf{u}|||_{2,m+1}^2 + \sum_{j=r+1}^{d}\|\boldsymbol{\psi}_j\|_1^2\lambda_j\right)\right. \\
&\quad +\nu^{-1}|||\nabla\mathbf{u}|||_{2,0}^2\left(\left(h^{2m}+\|S_{u,r}\|_2h^{2m+2}\right)|||\mathbf{u}|||_{2,m+1}^2 + \sum_{j=r+1}^{d}\|\boldsymbol{\psi}_j\|_1^2\lambda_j\right) \\
&\quad +\nu_T\left(\left(h^{2m}+(\|S_{u,R}\|_2+\|S_{u,r}\|_2)h^{2m+2}\right)|||\mathbf{u}|||_{2,m+1}^2\right. \\
&\quad \left.+\sum_{j=R+1}^{d}\|\boldsymbol{\psi}_j\|_1^2\lambda_j + \sum_{j=r+1}^{d}\|\boldsymbol{\psi}_j\|_1^2\lambda_j\right) + \nu^{-2}(\|\mathbf{u}_r^0\|^2 + \nu^{-1}|||\mathbf{f}|||_{2,-1}^2) \\
&\quad \times\left(\left(h^{2m}+\|S_{u,r}\|_2h^{2m+2}\right)|||\mathbf{u}|||_{2,m+1}^2 + \sum_{j=r+1}^{d}\|\boldsymbol{\psi}_j\|_1^2\lambda_j\right) \\
&\quad +\nu^{-1}h^{2m}|||p|||_{2,m}^2 + \nu^{-1}(\Delta t)^2\|\mathbf{u}_{tt}\|_{L^2(0,T;H^1(\Omega))}^2 \\
&\quad +\nu^{-1}\beta_T^2\|\mathbf{g}\|_\infty^2\left(h^{2m+2}|||T|||_{2,m+1}^2 + \sum_{i=r_2+1}^{d}\mu_i\right) \\
&\quad \left.+\nu^{-1}\beta_C^2\|\mathbf{g}\|_\infty^2\left(h^{2m+2}|||C|||_{2,m+1}^2 + \sum_{i=r_3+1}^{d}\xi_i\right)\right] \\
&\quad +K\nu^{-1}\beta_T^2\|\mathbf{g}\|_\infty^2\Delta t\sum_{n=0}^{M-1}\|\phi_{T,r}^{n+1}\|^2 + K\nu^{-1}\beta_C^2\|\mathbf{g}\|_\infty^2\Delta t\sum_{n=0}^{M-1}\|\phi_{C,r}^{n+1}\|^2 \\
&\quad +\frac{K\Delta t}{\nu^3}\sum_{n=0}^{M-1}|||\nabla\mathbf{u}|||_{\infty,0}^4\|\boldsymbol{\theta}_r^{n+1}\|^2 \qquad (4.2.25)
\end{aligned}$$

Applying Gronwall inequality for sufficiently small time step,

$$\Delta t \leq \min\{(K\nu^{-1}(\nu^{-2}+\gamma^{-2}+{D_c}^{-2}))^{-1}, (K\nu^{-1}\beta_T^2)^{-1}, (K\nu^{-1}\beta_C^2)^{-1}\} \qquad (4.2.26)$$

and adding (4.2.17) and (4.2.18) to (4.2.25) we have

$$
\begin{aligned}
&\|\boldsymbol{\phi}_{u,r}^{M}\|^2 + \|\phi_{T,r}^{M}\|^2 + \|\phi_{C,r}^{M}\|^2 + \sum_{n=0}^{M-1}\left(\nu\Delta t\|\mathbb{D}\boldsymbol{\phi}_{u,r}^{n+1}\|^2 + Da^{-1}\Delta t\|\boldsymbol{\phi}_{u,r}^{n+1}\|^2\right)\\
&\quad+\gamma\Delta t\sum_{n=0}^{M-1}\|\nabla\phi_{T,r}^{n+1}\|^2 + D_c\Delta t\sum_{n=0}^{M-1}\|\nabla\phi_{C,r}^{n+1}\|^2\\
&\quad\le \|\mathbf{u}_r^0 - \tilde{\mathbf{u}}^0\|^2 + \|T_r^0 - \tilde{T}^0\|^2 + \|C_r^0 - \tilde{C}^0\|^2 + K\Bigg(\nu^{-1}\beta_T^2\|\mathbf{g}\|_\infty^2\Delta t\sum_{n=0}^{M-1}\|\phi_{T,r}^{n+1}\|^2\\
&\quad+\nu^{-1}\beta_C^2\|\mathbf{g}\|_\infty^2\Delta t\sum_{n=0}^{M-1}\|\phi_{C,r}^{n+1}\|^2 + (\nu^{-3}|||\mathbb{D}\mathbf{u}|||_{\infty,0}^2 + \nu^{-1}\gamma^{-2}|||\nabla T|||_{\infty,0}^4\\
&\quad+\nu^{-1}{D_c}^{-2}|||\nabla C|||_{\infty,0}^4)\Delta t\sum_{n=0}^{M-1}\|\boldsymbol{\phi}_{u,r}^{n+1}\|^2\\
&\quad+h^{2m} + (\Delta t)^2 + h^{2m+2}(1 + \|S_{u,r}\|_2 + \|S_{T,r}\|_2 + \|S_{C,r}\|_2)\\
&\quad+\sum_{i=r_1+1}^{d}\lambda_i + \sum_{i=r_2+1}^{d}\mu_i + \sum_{i=r_3+1}^{d}\xi_i + \varepsilon_u^2 + \varepsilon_T^2 + \varepsilon_C^2\Bigg).
\end{aligned}
$$

4.3 Numerical Studies

In this section we present results of numerical tests using the POD-ROM studied above. Here we use (4.1.4)-(4.1.6), which is the BDF2 temporal discretization with POD-ROM.

4.3.1 Problem Description

For our numerical tests, we consider a test problem from [18, 62]. The domain Ω is the rectangular box $[0,1]\times[0,2]$, the time domain is from $t = 0$ to $t = 1$, and we consider the boundary conditions

$$\mathbf{u} = \mathbf{0} \text{ on } \partial\Omega,$$

$$T = 0,\ C = 0 \text{ for } x = 0,$$

$$T = 1,\ C = 1 \text{ for } x = 1.$$

$$\nabla T\cdot n = 0,\ \nabla C\cdot n = 0 \text{ for } y = 0, y = 2,$$

We run tests using Lewis number $Le = 2$, Prandtl number $Pr = 1$, and buoyancy ratio $N = 0.8$, and test the method with different Rayleigh numbers: $Ra = 10^4$, 10^5 and 10^6. We consider the case of Darcy number $Da = \infty$, which corresponds to no porosity. We take kinematic viscosity $\nu = 1$, $\beta_T = -\frac{Ra}{Pr}$, $\beta_C = \frac{Ra \cdot N}{Pr}$, $\mathbf{g} = \mathbf{e}_2$, $\gamma = \frac{1}{Pr}$, $D_c = \frac{1}{Le \cdot Pr}$. The initial conditions are $u_0 = T_0 = C_0 = 0$.

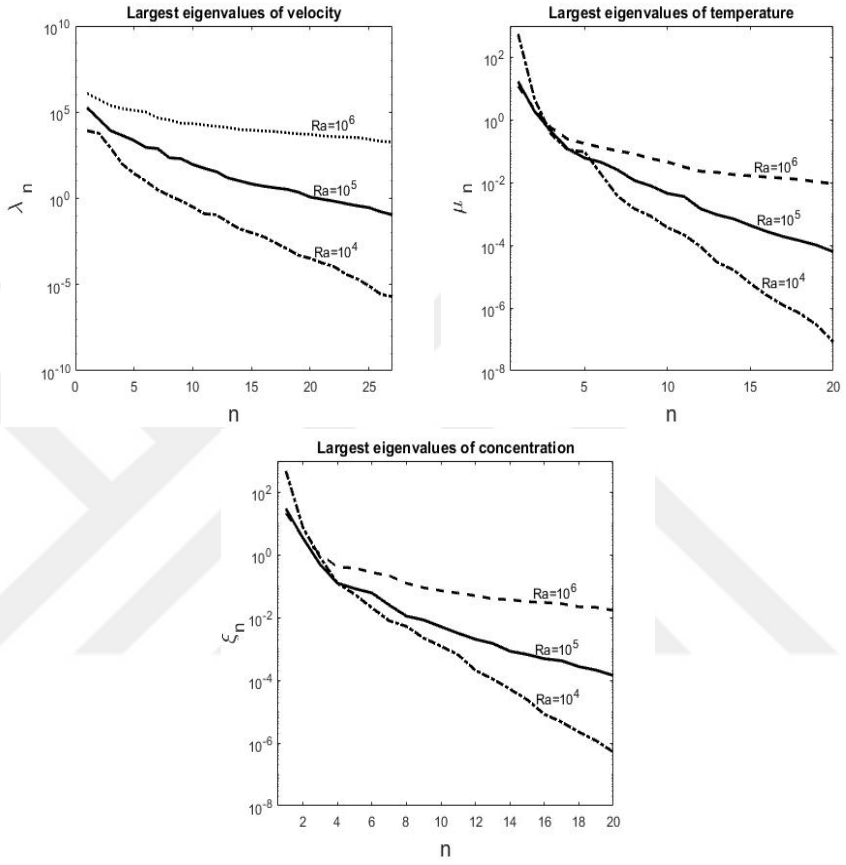

Figure 4.1: The eigenvalues for the velocity, temperature and concentration for different Ra

The fine mesh solution used to create the snapshots for each Ra was computed using a BDF2 finite element scheme, using a time step of $\Delta t = 0.00025$, and with a 30×60 uniform triangulation that was further refined near the boundary. This provided a total of $59,255$ degrees of freedom with Taylor-Hood velocity-pressure elements, and continuous quadratic elements used for the transported quantities. Solutions at each time step (i.e. snapshots) were saved, and following the procedure described above (see e.g. [14] for a more detailed description), the matrices of snapshots were

decomposed into the eigenvalues and eigenmodes.

Plots of the eigenvalues of the snapshot matrices for the different Ra simulations are shown in Figure 4.1, and we see a fairly rapid decay for $Ra = 10^4$, a slower decay for $Ra = 10^5$, but for $Ra = 10^6$ we observe that even the 50^{th} largest mode has a corresponding eigenvalue that is only three orders of magnitude smaller than the largest one.

4.3.2 Convergence Rates with Respect to Δt and the POD-ROM cutoff

The dominant error source in a POD-ROM typically comes from the basis truncation. The convergence rates in the velocity, the temperature and the concentration are given in Table 4.1. To scaling this test, we fix $T = 0.1$, $Ra = 10^6$.

Table 4.1: Convergence rates of velocity, temperature and concentration for varying Δt.

r	Δt	$\|\nabla(\mathbf{u}-\mathbf{u}_r)\|_{L^2(H^1)}$	rate	$\|\nabla(T-T_r)\|_{L^2(H^1)}$	rate	$\|\nabla(C-C_r)\|_{L^2(H^1)}$	rate
10	2.5e-04	6.7080e+02	-	0.6141	-	0.8925	-
10	1.25e-04	3.9079e+02	0.78	0.3444	0.83	0.4662	0.94
10	6.25e-05	2.5724e+02	0.60	0.2222	0.63	0.2896	0.69
10	3.125e-05	1.3594e+02	0.92	0.1235	0.85	0.1483	0.97
10	1.5625e-05	46.7776	1.54	0.0455	1.44	0.0529	1.49
10	7.8125e-06	14.8303	1.66	0.0195	1.22	0.0212	1.32
20	2.5e-04	5.3497e+02	-	0.4975	-	0.7248	-
20	1.25e-04	3.3729e+02	0.67	0.3132	0.67	0.4428	0.71
20	6.25e-05	2.0351e+02	0.73	0.1772	0.82	0.2289	0.95
20	3.125e-05	1.1922e+02	0.77	0.1027	0.79	0.1277	0.84
20	1.5625e-05	48.6892	1.29	0.0498	1.04	0.0531	1.27
20	7.8125e-06	10.6756	2.19	0.0147	1.76	0.0173	1.62

We observe that as the number of POD basis r increases, the error in the velocity, the temperature and the concentration decreases, that is, more modes used for POD gives more accurate solutions. In addition, we note that the convergence rates in velocity error for varying Δt are consistent with second order for $r = 20$. In a similar

manner, as r increases, the convergence rates in temperature and concentration increase, however, they are not close enough to second order even for high r in Table 4.1. Our analysis predicts that temporal and spatial error are negligible compared to the POD truncation errors, ε_u, ε_T, ε_C. Thus, we only pay attention convergence rates for varying R, which are evaluated in Table 4.2, Table 4.3, and Table 4.4.

Table 4.2: Convergence of velocity for varying r.

r	ε_u	$\|\nabla(\mathbf{u}-\mathbf{u}_r)\|_{L^2(H^1)}$	rate
3	35.646	0.5215	-
5	13.524	0.2254	0.87
7	6.4511	0.1087	0.99
9	3.2584	0.0697	0.65
11	1.8444	0.0408	0.94
13	0.9870	0.0286	0.57

Table 4.3: Convergence of temperature for varying r.

r	ε_T	$\|\nabla(T-T_r)\|_{L^2(H^1)}$	rate
3	2.0381	0.0501	-
5	0.5569	0.0211	0.67
7	0.2836	0.0122	0.81
9	0.1364	0.0068	0.79
11	0.0553	0.0048	0.39
13	0.0255	0.0040	0.23

The error contributions of the velocity, temperature, concentration defined by (2.2.19). In the analysis error (in $L^2(0,T;H^1(\Omega))$ norm) will scale like $O(\varepsilon_u^{1/2}+\varepsilon_T^{1/2}+\varepsilon_C^{1/2})$ when temporal and spatial error are negligible. In Table 4.2, Table 4.3 and Table 4.4, we compute errors for $Ra = 10^4$ using $\Delta t = 0.000015625$, $T = 0.01$, and varying r (fixing $r_1 = r_2 = r_3 = r$). Here we take the solution of the fine mesh BDF2 finite element scheme as the true solution, calculate ε_u, ε_T, ε_C for each r, and display these

Table 4.4: Convergence of concentration for varying r.

r	ε_C	$\|\nabla(C - C_r)\|_{L^2(H^1)}$	rate
3	2.1881	0.0706	-
5	0.8746	0.0283	1.00
7	0.4369	0.0168	0.75
9	0.2646	0.0113	0.79
11	0.1244	0.0080	0.46
13	0.0541	0.0053	0.50

quantities and the scaling of the error with respect to them in the tables. Note that, the rates in the tables consistent with the 0.5 rate as expected by analysis.

4.3.3 Captured Energy with Respect to the Different POD-ROM cutoff

In this test, to create POD basis, 4000 snapshots are used in the time interval [0, 1]. The correlation matrix are constructed using snapshots. Captured energy for the velocity (E_u), temperature (E_T), concentration (E_C) can be defined as

$$E_u = \frac{\sum_{j=1}^{r} \lambda_j}{\sum_{j=1}^{M} \lambda_j} \times 100, \quad E_T = \frac{\sum_{j=1}^{r} \mu_j}{\sum_{j=1}^{M} \mu_j} \times 100, \quad E_C = \frac{\sum_{j=1}^{r} \xi_j}{\sum_{j=1}^{M} \xi_j} \times 100.$$

The percent of captured energy with respect to the different POD modes number for the velocity, temperature and concentration are shown in Table 4.5, Table 4.6 and Table 4.7, respectively.

When we select POD modes number $r = 12$ for $Ra = 10^4$ and $r = 20$ for $Ra = 10^5$, 99.999% of the total energy is captured. On the other hand, for $Ra = 10^6$, and it would take many more modes than this to capture a sufficiently large portion of the system energy; hence for this test it was necessary to use a stabilization to get good numerical results.

Table 4.5: Percent of captured energy for the velocity, temperature and concentration with Ra = 10^4 varying r

r	E_u	E_T	E_C
4	99.7151	99.9782	99.9809
6	99.9608	99.9987	99.9963
8	99.9911	99.9997	99.9990
10	99.9979	99.9999	99.9997
12	99.9994	99.9999	99.9999

Table 4.6: Percent of captured energy for the velocity, temperature and concentration with Ra = 10^5 varying r

r	E_u	E_T	E_C
8	99.8173	99.8942	99.9304
12	99.9781	99.9845	99.9852
16	99.9939	99.9966	99.9955
20	99.9985	99.9992	99.9985
24	99.9995	99.9997	99.9994

Table 4.7: Percent of captured energy for the velocity, temperature and concentration with Ra = 10^6 varying r

r	E_u	E_T	E_C
8	93.0866	97.6547	97.4737
16	97.4949	99.1031	98.9494
24	98.9831	99.5758	99.4581
32	99.4980	99.7838	99.6876
40	99.7096	99.8793	99.8065

4.3.4 POD Performance for Different Ra

We consider now the ability of the POD for $Ra = 10^4$, $Ra = 10^5$, and $Ra = 10^6$. The computation times for full order solutions, POD basis functions and POD solutions for varying Ra are presented in Table 4.8. The following speed-up factor can be used as a measurement for the computational efficiency of the POD over DNS

$$\text{Speed-up} = \frac{\text{Process time in DNS}}{\text{Process time in POD}}.$$

The computed speed-up values are listed in Table 4.8. For this test, we fix $T = 0.01$, $\Delta t = 0.00025$, and $r = 7$.

Table 4.8: CPU times (in seconds) for DNS, POD basis and POD, and speed-up of POD for different Ra

Ra	DNS	POD basis	POD	Speed-up
10^4	1186.973710	869.562297	62.812477	18.89
10^5	1285.602149	967.813853	66.644541	19.29
10^6	966.318515	860.485202	135.498313	7.13

We see that the reduced order model is significantly faster than the full order model for $Ra = 10^4$ and $Ra = 10^5$, however, the efficiency of POD slightly drops for $Ra = 10^6$. Note that, the computational cost decreases remarkably for all Ra.

In the next test, we aim to show the decreasing behaviour of L^2 and H^1 errors for varying Ra. Hence, we calculate the errors at each time step and plot them versus time. We choose $r = 20$ for $Ra = 10^4$ and $Ra = 10^5$, $r = 40$ for $Ra = 10^6$.

The variations of L^2 error and H^1 error with respect to time are shown for $Ra = 10^4$ and $Ra = 10^5$ in Figure 4.2 and Figure 4.3, respectively. As seen in Figure 4.2 and Figure 4.3, the L^2 errors and the H^1 errors become close to zero as the time increase. It gives that our solution matches DNS for $Ra = 10^4$ and $Ra = 10^5$. We also observe the error plots for $Ra = 10^5$ to be significantly larger than for $Ra = 10^4$, so it is no surprise, as Ra increases, more modes are needed to obtain a good solution.

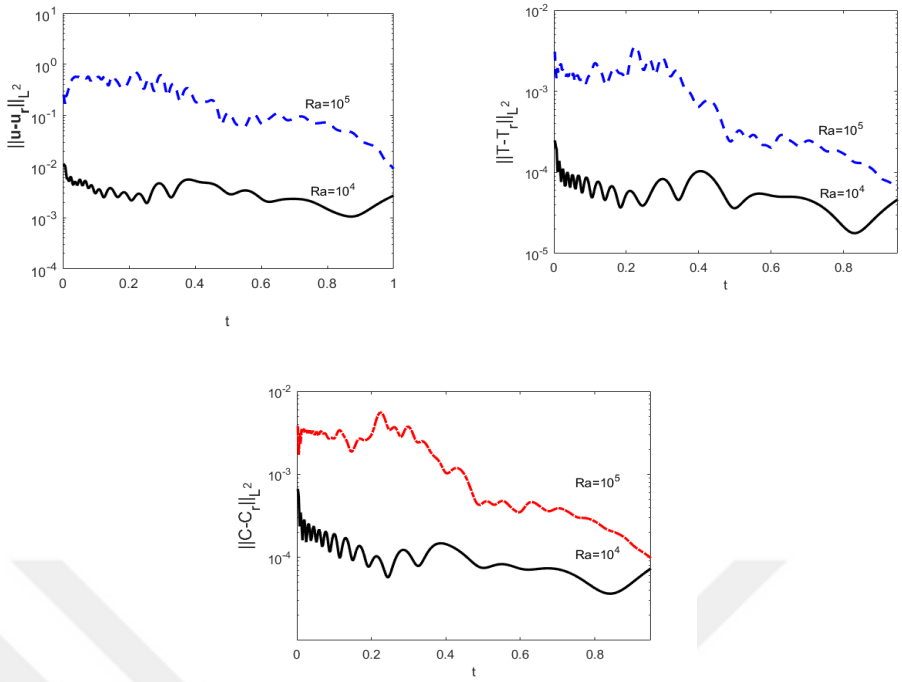

Figure 4.2: The L^2 error in the velocity, temperature and concentration for $Ra = 10^4$ and $Ra = 10^5$.

We also check the ability of the POD for $Ra = 10^4$ by comparing with DNS solution in Figure 4.4. First column indicate the DNS solution, second column indicate the POD solution. We observe no visual difference in the $t = 0.5$ solutions. We note that POD solutions matches the DNS solution qualitatively quite well. We consider also the same numerical test with $Ra = 10^5$ in the Figure 4.5. We obtain same results. POD solution matches well with DNS solution.

For a final test, we consider the same test but with higher Rayleigh number, $Ra = 10^6$. Here, even with 40 modes, the POD-ROM is unable to give a good solution (see Figure 4.6 and Figure 4.7), which is expected since Figure 4.1 shows a very slow decay of the eigenvalues of the snapshot matrix. We use Algorithm 4.2.1 which is obtained adding the decoupled VMS-ROM stabilization, then the effect of additional viscosity is added to the smaller R velocity modes in a post-processing step. After running several tests to optimize parameters R and ν_T, we found that $R = 20$, $\nu_T = 1$ is a near optimal choice that gives a much better solution than the unstabilized POD-

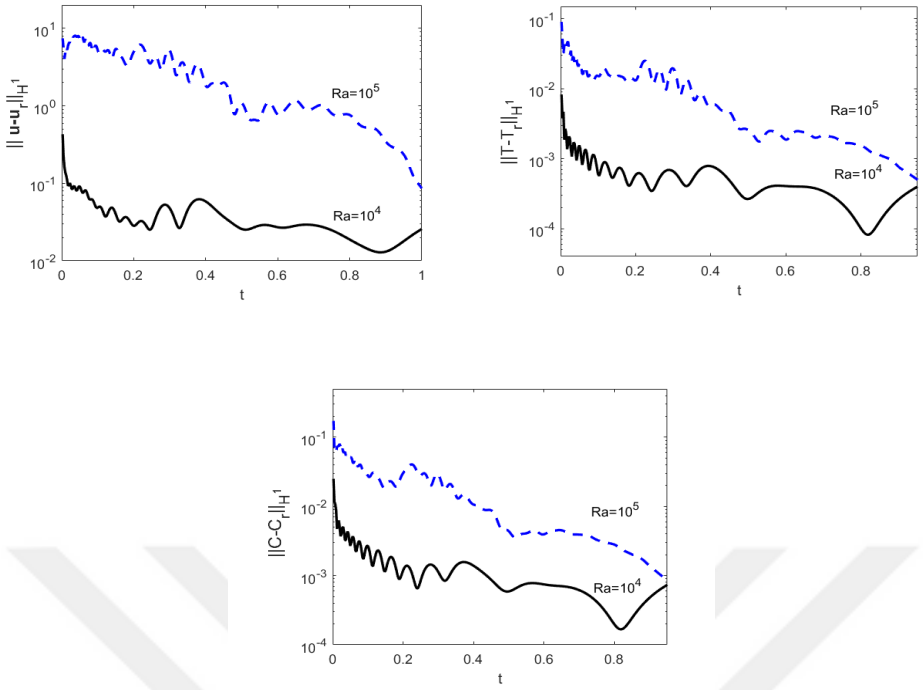

Figure 4.3: The H^1 error in the velocity, temperature and concentration for Ra = 10^4 and Ra = 10^5.

ROM, see Figure 4.6 and Figure 4.7. We note that no stabilization was added to the transport equations in these results.

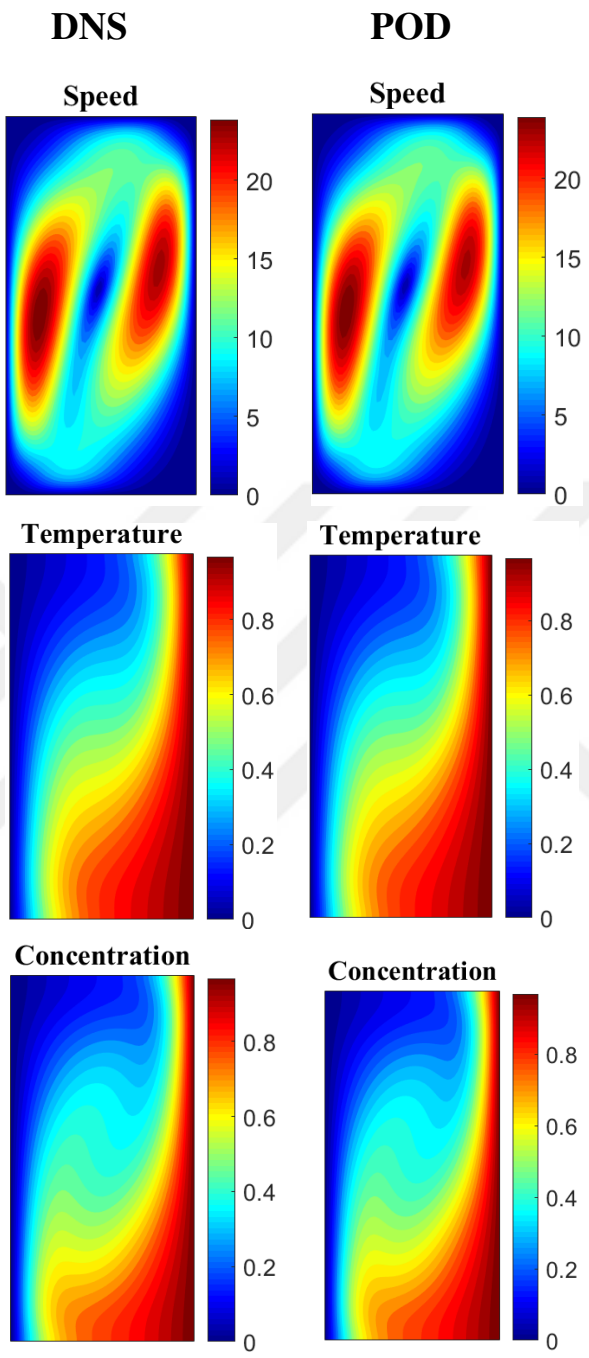

Figure 4.4: Shown above are $Ra = 10^4$ solution plots for the simulations using DNS and POD using 8 modes at $t = 0.5$.

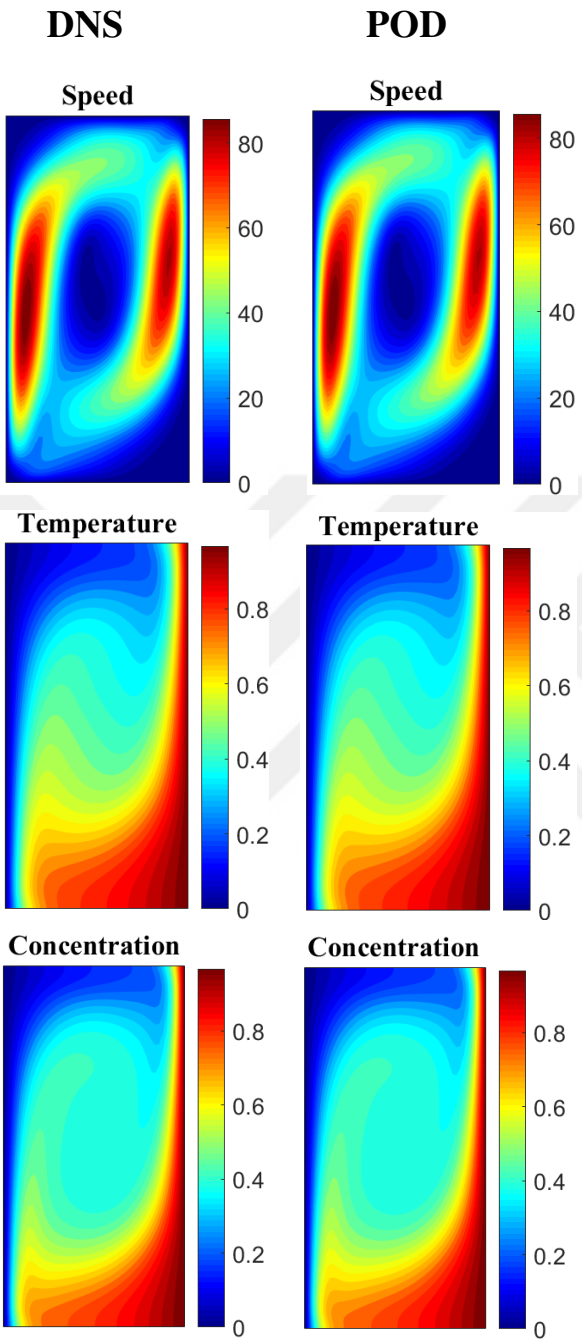

Figure 4.5: Shown above are $Ra = 10^5$ solution plots for the simulations using DNS and POD using 10 modes at $t = 0.5$.

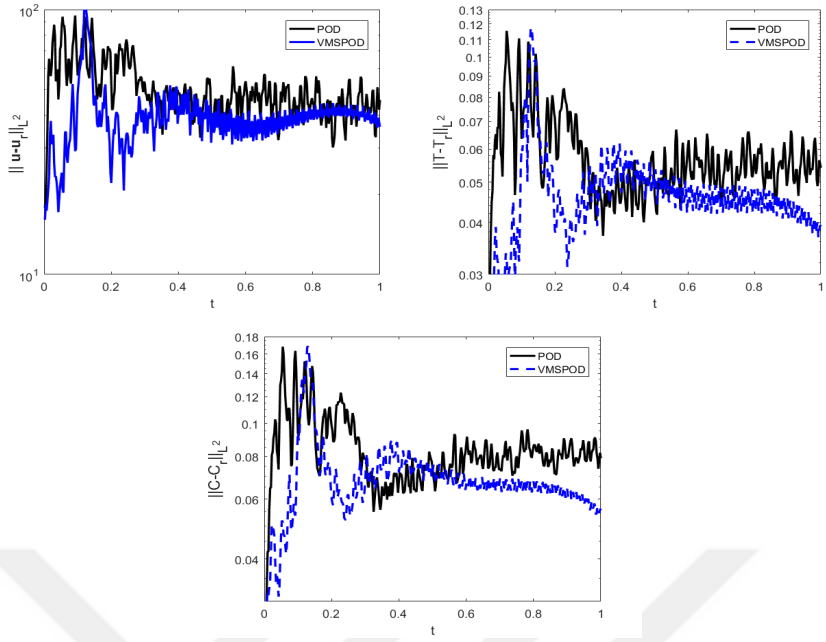

Figure 4.6: The L^2 error in the velocity, temperature and concentration for $Ra = 10^6$.

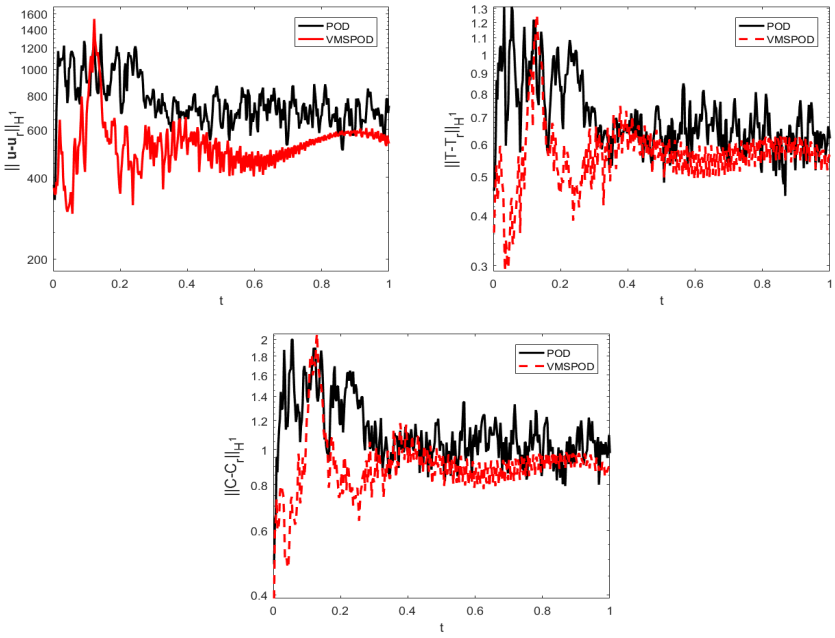

Figure 4.7: The H^1 error in the velocity, temperature and concentration for $Ra = 10^6$.

CHAPTER 5

THE EXTRAPOLATED CRANK NICHOLSON VMS-POD METHOD FOR DARCY BRINKMAN EQUATIONS

In this chapter, we extend [22] with VMS-POD methodology for the Darcy Brinkman system. The scheme obtains POD solutions with a projection based VMS stabilization introduced in [40, 55] for the fluid velocity, temperature and concentration. The finite element method is considered for space variables and Crank Nicholson time discretization method for time variables. In addition, to obtain a fully linear system at each time level, the nonlinear terms are treated with the extrapolated Crank Nicholson method of Baker's [5].

This chapter is arranged as follows. In Section 2, the full order model for Darcy Brinkman system is introduced. A review of POD and VMS methods are given in Section 3. Section 4 is devoted to the numerical analysis of the VMS-POD formulation. In Section 5, analytical results are verified with numerical experiments.

5.1 Preliminaries

In this section, some preliminaries are given about VMS-POD setting for Darcy-Brinkman with double diffusive convection. The artificial diffusions are added to the smaller R_1, R_2, R_3 velocity, temperature, concentration modes affecting only small scales. Therefore, the following spaces are used for VMS-POD setting

$$\begin{aligned}
\mathbf{X}_R &= span\{\boldsymbol{\psi}_k\}_{k=1}^{R_1}, \quad \mathbf{L}_{R,\mathbf{u}} = \nabla \mathbf{X}_R := \{\nabla \boldsymbol{\psi}_k\}_{k=1}^{R_1}, \\
W_R &= span\{\boldsymbol{\phi}_k\}_{k=1}^{R_2}, \quad \mathbf{L}_{R,T} = \nabla W_R := \{\nabla \boldsymbol{\phi}_k\}_{k=1}^{R_2}, \\
\Psi_R &= span\{\eta_k\}_{k=1}^{R_3}, \quad \mathbf{L}_{R,C} = \nabla \Psi_R := \{\nabla \eta_k\}_{k=1}^{R_3}.
\end{aligned}$$

with $R_1 < r_1$, $R_2 < r_2$ and $R_3 < r_3$. Here R_1, R_2 and R_3 denote the POD modes numbers for each fluid variables used in the projections for VMS method. The following relations between finite element spaces and POD spaces are provided by construction,

$$\mathbf{X}_R \subset \mathbf{X}_r \subset \mathbf{V}_h \subset \mathbf{X}, \quad W_R \subset W_r \subset W_h \subset W, \quad \text{and} \quad \Psi_R \subset \Psi_r \subset \Psi_h \subset \Psi.$$

In the VMS formulation, we will use the L^2 projection operator

$$P_{u,R} : L^2 \to \mathbf{L}_{R,\mathbf{u}}, \quad P_{T,R} : L^2 \to \mathbf{L}_{R,T}, \quad P_{C,R} : L^2 \to \mathbf{L}_{R,C}$$

which are defined as

$$(\mathbf{u} - P_{u,R}\mathbf{u}, \mathbf{v}_R) = 0, \quad (T - P_{T,R}T, S_R) = 0, \quad (C - P_{C,R}C, \zeta_R) = 0, \quad (5.1.1)$$

for all $(\mathbf{v}_R, S_R, \zeta_R) \in (\mathbf{L}_{R,\mathbf{u}}, \mathbf{L}_{R,T}, \mathbf{L}_{R,C})$. Therefore, VMS-POD formulation of the (1.3.15) with a Crank Nicholson temporal discretization becomes: Find $\mathbf{u}_r : [0,\tau] \to \mathbf{X}_r, \quad T_r : [0,\tau] \to W_r, \quad C_r : [0,\tau] \to \Psi_r$ for every $(\mathbf{v}_r, S_r, \Phi_r), \in (\mathbf{X}_r, W_r, \Psi_r)$

$$\begin{aligned}
&\left(\frac{\mathbf{u}_r^{n+1} - \mathbf{u}_r^n}{\Delta t}, \mathbf{v}_r\right) + 2\nu(\mathbb{D}\mathbf{u}_r^{n/2}, \mathbb{D}\mathbf{v}_r) + b_1(\mathcal{X}(\mathbf{u}_r^n), \mathbf{u}_r^{n/2}, \mathbf{v}_r) \\
&\quad + \alpha_1\Big((I - P_{\mathbf{u},R})\mathbb{D}\mathbf{u}_r^{n/2}, (I - P_{\mathbf{u},R})\mathbb{D}\mathbf{v}_r\Big) + Da^{-1}(\mathbf{u}_r^{n/2}, \mathbf{v}_r) \\
&= \beta_T(\mathbf{g}T_r^{n/2}, \mathbf{v}_r) + \beta_C(\mathbf{g}C_r^{n/2}, \mathbf{v}_r),
\end{aligned} \quad (5.1.2)$$

$$\begin{aligned}
&\left(\frac{T_r^{n+1} - T_r^n}{\Delta t}, S_r\right) + \gamma(\nabla T_r^{n/2}, \nabla S_r) + b_2(\mathcal{X}(\mathbf{u}_r^n), T_r^{n/2}, S_r) \\
&\quad + \alpha_2\Big((I - P_{T,R})\nabla T_r^{n/2}, (I - P_{T,R})\nabla S_r\Big) = 0,
\end{aligned} \quad (5.1.3)$$

$$\begin{aligned}
&\left(\frac{C_r^{n+1} - C_r^n}{\Delta t}, \varsigma_r\right) + D_c(\nabla C_r^{n/2}, \nabla \varsigma_r) + b_3(\mathcal{X}(\mathbf{u}_r^n), C_r^{n/2}, \varsigma_r) \\
&\quad + \alpha_3\Big((I - P_{C,R})\nabla C_r^{n/2}, (I - P_{C,R})\nabla \varsigma_r\Big) = 0.
\end{aligned} \quad (5.1.4)$$

where $P_{\mathbf{u},R}$, $P_{T,R}$ and $P_{C,R}$ are the L^2 projection into $(\mathbf{X}_R, W_R, \Psi_R)$ and

$$\mathcal{X}(\mathbf{u}_r^n) = \frac{3}{2}\mathbf{u}_r^n - \frac{1}{2}\mathbf{u}_r^{n-1}, \ \mathbf{u}_r^{n/2} = \frac{\mathbf{u}_r^{n+1} + \mathbf{u}_r^n}{2}, \ T_r^{n/2} = \frac{T_r^{n+1} + T_r^n}{2}, \ C_r^{n/2} = \frac{C_r^{n+1} + C_r^n}{2}.$$

Note that in algorithm (5.1.2)-(5.1.4), the linear extrapolation of the velocity, temperature and concentration are used, [20]. Thus, the solution of the system requires one linear system per time.

5.2 Numerical analysis of VMS-POD double diffusive Darcy Brinkman scheme

In this section, we present the stability analysis and convergence result for the solutions of (5.1.2)-(5.1.4).

Lemma 5.2.1 *The VMS-POD approximation (5.1.2)-(5.1.4) is unconditionally stable in the following sense: for any* $\Delta t > 0$

$$\begin{aligned}
&\|\mathbf{u}_r^M\| + 4\nu\Delta t \sum_{n=0}^{M-1} \|\mathbb{D}\mathbf{u}_r^{n/2}\|^2 + 2Da^{-1}\Delta t \sum_{n=0}^{M-1} \|\mathbf{u}_r^{n/2}\|^2 \\
&\qquad +2\alpha_1\Delta t \sum_{n=0}^{M-1} \|(I - P_{\mathbf{u},R})\mathbb{D}\mathbf{u}_r^{n/2}\|^2 \\
&\leq \|\mathbf{u}_r^0\|^2 + K\|\mathbf{g}\|_\infty^2(\beta_T^2\nu^{-1}\gamma^{-1}\|T_r^0\|^2 + \beta_C^2 DaD_c^{-1}\|C_r^0\|^2) \qquad (5.2.1)\\
&\|T_r^M\|^2 + 2\gamma\Delta t \sum_{n=0}^{M-1} \|\nabla T_r^{n/2}\| + 2\alpha_2\Delta t \sum_{n=0}^{M-1} \|(I - P_{T,R})\nabla T_r^{n/2}\|^2 \\
&\leq \|T_r^0\|^2 \qquad (5.2.2)\\
&\|C_r^M\|^2 + 2D_c\Delta t \sum_{n=0}^{M-1} \|\nabla C_r^{n/2}\| + 2\alpha_3\Delta t \sum_{n=0}^{M-1} \|(I - P_{C,R})\nabla C_r^{n/2}\|^2 \\
&\leq \|C_r^0\|^2 \qquad (5.2.3)
\end{aligned}$$

Proof Letting $S_r = T_r^{n/2} = \dfrac{T_r^{n+1} + T_r^n}{2}$ in (5.1.3), and using the skew symmetry, we get $b_2(\mathcal{X}(\mathbf{u}_r^n), T_r^{n/2}, T_r^{n/2}) = 0$. Then (5.1.3) becomes

$$\|T_r^{n+1}\|^2 + 2\gamma\Delta t\|\nabla T_r^{n/2}\| + 2\alpha_2\Delta t\|(I - P_{T,R})\nabla T_r^{n/2}\|^2 = \|T_r^n\|^2. \qquad (5.2.4)$$

Summing over the time steps $n = 0, \ldots, M-1$ yields

$$\|T_r^M\|^2 + 2\gamma\Delta t \sum_{n=0}^{M-1} \|\nabla T_r^{n/2}\| + 2\alpha_2\Delta t \sum_{n=0}^{M-1} \|(I - P_{T,R})\nabla T_r^{n/2}\|^2 \leq \|T_r^0\|^2. \quad (5.2.5)$$

Similarly, setting $\varsigma_r = C_r^{n/2}$ in (5.1.4) and summing over the time steps produces

$$\|C_r^M\|^2 + 2D_c\Delta t \sum_{n=0}^{M-1} \|\nabla C_r^{n/2}\| + 2\alpha_3\Delta t \sum_{n=0}^{M-1} \|(I - P_{C,R})\nabla C_r^{n/2}\|^2 \leq \|C_r^0\|^2. \quad (5.2.6)$$

Choosing $\mathbf{v}_r = \mathbf{u}_r^{n/2}$ and using $b_1(\mathcal{X}(\mathbf{u}_r^n), \mathbf{u}_r^{n/2}, \mathbf{u}_r^{n/2}) = 0$ in (5.1.2) gives

$$\begin{aligned}
&\|\mathbf{u}_r^{n+1}\| + 4\nu\Delta t\|\mathbb{D}\mathbf{u}_r^{n/2}\|^2 + 2\alpha_1\Delta t\|(I - P_{u,R})\mathbb{D}\mathbf{u}_r^{n/2}\|^2 + 2Da^{-1}\Delta t\|\mathbf{u}_r^{n/2}\|^2 \\
&\qquad = \|\mathbf{u}_r^n\|^2 + 2\beta_T\Delta t(\mathbf{g}T_r^{n/2}, \mathbf{u}_r^{n/2}) + 2\beta_C\Delta t(\mathbf{g}C_r^{n/2}, \mathbf{u}_r^{n/2}). \quad (5.2.7)
\end{aligned}$$

Applying Cauchy-Schwarz inequality and Young's inequality yields

$$\|\mathbf{u}_r^{n+1}\| + 4\nu\Delta t\|\mathbb{D}\mathbf{u}_r^{n/2}\|^2 + 2\alpha_1\Delta t\|(I - P_{u,R})\mathbb{D}\mathbf{u}_r^{n/2}\|^2 + 2Da^{-1}\Delta t\|\mathbf{u}_r^{n/2}\|^2$$
$$\leq \|\mathbf{u}_r^n\|^2 + K\|\mathbf{g}\|_\infty^2(\beta_T^2\nu^{-1}\Delta t\|\nabla T_r^{n/2}\| + \beta_C^2 Da\Delta t\|\nabla C_r^{n/2}\|^2) \quad (5.2.8)$$

Summing over the time steps $n = 0, \ldots, M-1$ gives

$$\|\mathbf{u}_r^M\| + 4\nu\Delta t\sum_{n=0}^{M-1}\|\mathbb{D}\mathbf{u}_r^{n/2}\|^2 + 2\alpha_1\Delta t\sum_{n=0}^{M-1}\|(I - P_{u,R})\mathbb{D}\mathbf{u}_r^{n/2}\|^2$$
$$+2Da^{-1}\Delta t\sum_{n=0}^{M-1}\|\mathbf{u}_r^{n/2}\|^2$$
$$\leq \|\mathbf{u}_r^0\|^2 + K\|\mathbf{g}\|_\infty^2(\beta_T^2\nu^{-1}\Delta t\sum_{n=0}^{M-1}\|\nabla T_r^{n/2}\| + \beta_C^2 Da\Delta t\sum_{n=0}^{M-1}\|\nabla C_r^{n/2}\|^2) \quad (5.2.9)$$

Inserting (5.2.4) and (5.2.6) in (5.2.8) gives the stated result (5.2.1).

Hence the method is stable without any time step restriction. The next question is: how fast approximate solutions converge to true solutions. To answer this question, we now consider the error analysis of VMS-POD.

Theorem 5.2.2 *(Error Estimation) Suppose regularity assumptions* $\mathbf{u}, T, C \in L^\infty(0,\tau;H^{m+1})$, $p \in L^\infty(0,\tau;H^m)$ *holds. Then for the sufficiently small* Δt*, the error satisfies*

$$\|\mathbf{u}^M - \mathbf{u}_r^M\|^2 + \|T^M - T_r^M\|^2 + \|C^M - C_r^M\|^2$$
$$\leq K\Bigg(1 + h^{2m} + (\Delta t)^4 + (1 + \|S_{u,r}\|_2 + \|S_{u,R}\|_2$$
$$+\|S_{T,r}\|_2 + \|S_{T,R}\|_2 + \|S_{C,r}\|_2 + \|S_{C,R}\|_2)h^{2m+2}$$
$$+\sum_{i=r_1+1}^{d}(\|\boldsymbol{\psi}_i\|_1^2 + 1)\lambda_i + \sum_{i=r_2+1}^{d}(\|\phi_i\|_1^2 + 1)\mu_i + \sum_{i=r_3+1}^{d}(\|\eta_i\|_1^2 + 1)\xi_i$$
$$+\sum_{i=R_1+1}^{d}\|\boldsymbol{\psi}_i\|_1^2\lambda_i + \sum_{i=R_2+1}^{d}\|\phi_i\|_1^2\mu_i + \sum_{i=R_3+1}^{d}\|\eta_i\|_1^2\xi_i\Bigg). \quad (5.2.10)$$

Proof We begin the proof by deriving error equations, subtracting from (1.3.16), (1.3.18), (1.3.19) to (5.1.2), (5.1.3), (5.1.4) at time $t^{n/2}$, respectively we have

$$\Big(\mathbf{u}_t^{n/2} - \frac{\mathbf{u}_r^{n+1} - \mathbf{u}_r^n}{\Delta t}, \mathbf{v}_r\Big) + 2\nu(\mathbb{D}(\mathbf{u}^{n/2} - \mathbf{u}_r^{n/2}), \mathbb{D}\mathbf{v}_r) + b_1(\mathbf{u}^{n/2}, \mathbf{u}^{n/2}, \mathbf{v}_r)$$
$$-b_1(\mathcal{X}(\mathbf{u}_r^n), \mathbf{u}_r^{n/2}, \mathbf{v}_r) + (Da^{-1}(\mathbf{u}^{n/2} - \mathbf{u}_r^{n/2}), \mathbf{v}_r) - (p^{n+1}, \nabla\cdot\mathbf{v}_r)$$
$$+\alpha_1\Big((I - P_{\mathbf{u},R})\mathbb{D}(\mathbf{u}^{n/2} - \mathbf{u}_r^{n/2}), (I - P_{\mathbf{u},R})\mathbb{D}\mathbf{v}_r\Big)$$

$$
\begin{aligned}
&= \beta_T(\mathbf{g}(T^{n/2} - T_r^{n/2}), \mathbf{v}_r) + \beta_C(\mathbf{g}(C^{n/2} - C_r^{n/2}), \mathbf{v}_r) \\
&\quad + \alpha_1\Big((I - P_{\mathbf{u},R})\mathbb{D}\mathbf{u}^{n/2}, (I - P_{\mathbf{u},R})\mathbb{D}\mathbf{v}_r\Big), \qquad (5.2.11)
\end{aligned}
$$

$$
\begin{aligned}
&\Big(T_t^{n/2} - \frac{T_r^{n+1} - T_r^n}{\Delta t}, S_r\Big) + \gamma(\nabla(T^{n/2} - T_r^{n/2}), \nabla S_r) + b_2(\mathbf{u}^{n/2}, T^{n/2}, S_r) \\
&\quad - b_2(\mathcal{X}(\mathbf{u}_r^n), T_r^{n/2}, S_r) + \alpha_2\Big((I - P_{T,R})\nabla(T^{n/2} - T_r^{n/2}), (I - P_{T,R})\nabla S_r\Big) \\
&= \alpha_2\Big((I - P_{T,R})\nabla T^{n/2}, (I - P_{T,R})\nabla S_r\Big), \qquad (5.2.12)
\end{aligned}
$$

$$
\begin{aligned}
&\Big(C_t^{n/2} - \frac{C_r^{n+1} - C_r^n}{\Delta t}, \Phi_r\Big) + D_c(\nabla(C^{n/2} - C_r^{n/2}), \nabla\Phi_r) + b_3(\mathbf{u}^{n/2}, C^{n/2}, \Phi_r) \\
&\quad - b_3(\mathcal{X}(\mathbf{u}_r^n), C_r^{n/2}, \Phi_r) + \alpha_3\Big((I - P_{C,R})\nabla(C^{n/2} - C_r^{n/2}), (I - P_{C,R})\nabla\varsigma_r\Big) \\
&= \alpha_3\Big((I - P_{C,R})\nabla C^{n/2}, (I - P_{C,R})\nabla\varsigma_r\Big). \qquad (5.2.13)
\end{aligned}
$$

for all $(\mathbf{v}_r, S_r, \Phi_r) \in (\mathbf{X}_r, W_r, \Psi_r)$. We use the following notations for the decomposition of the errors.

$$
\begin{aligned}
\boldsymbol{\eta}_{\mathbf{u}}^n &:= \mathbf{u}^n - \tilde{\mathbf{u}}^n, \quad \boldsymbol{\phi}_{\mathbf{u},r}^n &:= \mathbf{u}_r^n - \tilde{\mathbf{u}}^n, \\
\eta_T^n &= T^n - \tilde{T}^n, \quad \phi_{T,r}^n &:= T_r^n - \tilde{T}^n, \\
\eta_C^n &= C^n - \tilde{C}^n, \quad \phi_{C,r}^n &:= C_r^n - \tilde{C}^n
\end{aligned} \qquad (5.2.14)
$$

Hence the errors can be denoted by

$$
\mathbf{e}_{\mathbf{u},r}^n = \boldsymbol{\eta}_{\mathbf{u}}^n - \boldsymbol{\phi}_{\mathbf{u},r}^n, \quad e_{T,r}^n := \eta_T^n - \phi_{T,r}^n, \quad e_{C,r}^n := \eta_C^n - \phi_{C,r}^n \qquad (5.2.15)
$$

where $\tilde{\mathbf{u}}^n$, $\tilde{T}^n$, $\tilde{C}^n$ are L^2 projections of $\mathbf{u}^n$, T^n, C^n in $\mathbf{X}_r$, W_r, Ψ_r at time t^n, respectively.

We first derive the error estimation for the temperature. To do that, the error equation for the temperature is rewritten as

$$
\begin{aligned}
&\Big(\frac{T(t^{n+1}) - T(t^n)}{\Delta t} - \frac{T_r^{n+1} - T_r^n}{\Delta t}, S_r\Big) + \gamma(\nabla(T(t^{n/2}) - T_r^{n/2}), \nabla S_r) \\
&\quad + b_2(\mathbf{u}(t^{n/2}), T(t^{n/2}), S_r) - b_2(\mathcal{X}(\mathbf{u}_r^n), T_r^{n/2}, S_r) \\
&\quad + \alpha_2\Big((I - P_{T,R})\nabla(T(t^{n/2}) - T_r^{n/2}), (I - P_{T,R})\nabla S_r\Big) \\
&\quad + (T_t(t^{n/2}) - \frac{T(t^{n+1}) - T(t^n)}{\Delta t}, S_r) \\
&= \alpha_2\Big((I - P_{T,R})\nabla T(t^{n/2}), (I - P_{T,R})\nabla S_r\Big), \qquad (5.2.16)
\end{aligned}
$$

Adding and subtracting

$$
\gamma(\nabla(\frac{T(t^{n+1}) + T(t^n)}{\Delta t}), \nabla S_r) + \alpha_2\Big((I - P_{T,R})\nabla(\frac{T(t^{n+1}) + T(t^n)}{\Delta t}), (I - P_{T,R})\nabla S_r\Big)
$$

terms in (5.2.16) and utilizing (5.2.14) and setting $S_r = \phi_{T,r}^{n/2}$ in (5.2.16) gives

$$\begin{aligned}
&\left(\frac{\phi_{T,r}^{n+1}-\phi_{T,r}^{n}}{\Delta t},\phi_{T,r}^{n+1}\right)+\gamma\|\nabla\phi_{T,r}^{n/2}\|^2+\alpha_2\|(I-P_{T,R})\nabla\phi_{T,r}^{n/2}\|^2\\
&\leq\ |(\frac{\eta_T^{n+1}-\eta_T^{n}}{\Delta t},\phi_{T,r}^{n+1})|+\gamma|(\nabla\eta_T^{n/2},\nabla\phi_{T,r}^{n/2})|\\
&\quad+\gamma|(\nabla(\frac{T(t^{n+1})+T(t^n)}{\Delta t}-T(t^{n/2})),\nabla\phi_{T,r}^{n/2})|^2\\
&\quad+|b_2(\mathbf{u}(t^{n/2}),T(t^{n/2}),\phi_{T,r}^{n/2})-b_2(\mathcal{X}(\mathbf{u}_r^n),T_r^{n/2},\phi_{T,r}^{n/2})|\\
&\quad+\alpha_2|\Big((I-P_{T,R})\nabla\eta_T^{n/2},(I-P_{T,R})\nabla\phi_{T,r}^{n/2}\Big)|\\
&\quad+|(\frac{T(t^{n+1})-T(t^n)}{\Delta t}-T_t(t^{n/2})),\phi_{T,r}^{n/2})|\\
&\quad+\alpha_2|\Big((I-P_{T,R})\nabla T(t^{n/2}),(I-P_{T,R})\nabla S_r\Big)|\\
&\quad+\alpha_2|\Big((I-P_{T,R})\nabla(\frac{T(t^{n+1})+T(t^n)}{\Delta t}-T(t^{n/2})),(I-P_{T,R})\nabla S_r\Big)|
\end{aligned}\tag{5.2.17}$$

Using the fact that $(\eta_T^{n+1},\phi_{T,r}^{n+1})=0$, and $(\eta_T^{n},\phi_{T,r}^{n+1})=0$ from the definition of L^2 projection in (5.2.17), we get

$$\begin{aligned}
&\frac{1}{2\Delta t}\|\phi_{T,r}^{n+1}\|^2+\gamma\|\nabla\phi_{T,r}^{n/2}\|^2+\alpha_2\|(I-P_{T,R})\nabla\phi_{T,r}^{n/2}\|^2\\
&\leq\ \frac{1}{2\Delta t}\|\phi_{T,r}^{n}\|+\gamma|(\nabla\eta_T^{n/2},\nabla\phi_{T,r}^{n/2})|+\gamma|(\nabla(\frac{T(t^{n+1})+T(t^n)}{\Delta t}-T(t^{n/2})),\nabla\phi_{T,r}^{n/2})|^2\\
&\quad+|b_2(\mathbf{u}(t^{n/2}),T(t^{n/2}),\phi_{T,r}^{n/2})-b_2(\mathcal{X}(\mathbf{u}_r^n),T_r^{n/2},\phi_{T,r}^{n/2})|\\
&\quad+\alpha_2|\Big((I-P_{T,R})\nabla\eta_T^{n/2},(I-P_{T,R})\nabla\phi_{T,r}^{n/2}\Big)|\\
&\quad+\alpha_2|\Big((I-P_{T,R})\nabla T(t^{n/2}),(I-P_{T,R})\nabla\phi_{T,r}^{n/2}\Big)|\\
&\quad+\alpha_2|\Big((I-P_{T,R})\nabla(\frac{T(t^{n+1})+T(t^n)}{\Delta t}-T(t^{n/2})),(I-P_{T,R})\nabla\phi_{T,r}^{n/2}\Big)|\\
&\quad+|(\frac{T(t^{n+1})-T(t^n)}{\Delta t}-T_t(t^{n/2})),\phi_{T,r}^{n/2})|.
\end{aligned}\tag{5.2.18}$$

Adding and subtracting terms

$$b_2(\mathbf{u}(t^{n/2})+\mathcal{X}(\mathbf{u}_r^n)+\mathcal{X}(\mathbf{u}(t^n)),\frac{T(t^{n+1})+T(t^n)}{2},\phi_{T,r}^{n/2})$$

to the nonlinear terms in (5.2.18) leads to

$$\begin{aligned}
&b_2(\mathbf{u}(t^{n/2}),T(t^{n/2}),\phi_{T,r}^{n/2})-b_2(\mathcal{X}(\mathbf{u}_r^n),T_r^{n/2},\phi_{T,r}^{n/2})\\
&=\ b_2(\mathcal{X}(\mathbf{u}_r^n),{\eta_T}^{n/2},\phi_{T,r}^{n/2})-b_2(\mathcal{X}(\mathbf{u}_r^n),\phi_{T,r}^{n/2},\phi_{T,r}^{n/2})\\
&\quad+b_2(\mathcal{X}(\mathbf{e}_{\mathbf{u},r}^n),\frac{T(t^{n+1})+T(t^n)}{2},\phi_{T,r}^{n/2})
\end{aligned}$$

$$
\begin{aligned}
&+b_2(\mathbf{u}(t^{n/2}), \frac{T(t^{n+1})+T(t^n)}{2} - T_{n/2}, \phi_{T,r}^{n/2}) \\
&+b_2(\mathbf{u}(t^{n/2}) - \mathcal{X}(\mathbf{u}(t^n)), \frac{T(t^{n+1})+T(t^n)}{2}, \phi_{T,r}^{n/2}) \\
&+b_2(\mathbf{u}(t^{n/2}), T(t^{n/2}) - \frac{T(t^{n+1})+T(t^n)}{2}, \phi_{T,r}^{n/2})
\end{aligned}
$$

Note that $b_2(\mathbf{u}^{n/2}, \phi_{T,r}^{n+1}, \phi_{T,r}^{n+1}) = 0$. Using Cauchy-Schwarz and Young's inequalities, we obtain

$$
\begin{aligned}
&\frac{1}{2\Delta t}\|\phi_{T,r}^{n+1}\|^2 + \gamma\|\nabla\phi_{T,r}^{n/2}\|^2 + \alpha_2\|(I-P_{T,R})\nabla\phi_{T,r}^{n/2}\|^2 \leq \frac{1}{2\Delta t}\|\phi_{T,r}^{n}\|^2 \\
&\quad +\gamma|(\nabla {\eta_T}^{n/2}, \nabla\phi_{T,r}^{n/2})| + \gamma|(\nabla(\frac{T(t^{n+1})+T(t^n)}{\Delta t} - T(t^{n/2})), \nabla\phi_{T,r}^{n/2})|^2 \\
&\quad +|b_2(\mathcal{X}(\mathbf{u}_r^n), {\eta_T}^{n/2}, \phi_{T,r}^{n/2})| + |b_2(\mathcal{X}(\mathbf{e}_{\mathbf{u},r}^n), \frac{T(t^{n+1})+T(t^n)}{2}, \phi_{T,r}^{n/2})| \\
&\quad +|b_2(\mathbf{u}(t^{n/2}), \frac{T(t^{n+1})+T(t^n)}{2} - T_{n/2}, \phi_{T,r}^{n/2})| \\
&\quad +|b_2(\mathbf{u}(t^{n/2}) - \mathcal{X}(\mathbf{u}(t^n)), \frac{T(t^{n+1})+T(t^n)}{2}, \phi_{T,r}^{n/2})| \\
&\quad +|b_2(\mathbf{u}(t^{n/2}), T(t^{n/2}) - \frac{T(t^{n+1})+T(t^n)}{2}, \phi_{T,r}^{n/2})| \\
&\quad +\alpha_2|\Big((I-P_{T,R})\nabla\eta_T^{n/2}, (I-P_{T,R})\nabla\phi_{T,r}^{n/2}\Big)| \\
&\quad +\alpha_2|\Big((I-P_{T,R})\nabla T(t^{n/2}), (I-P_{T,R})\nabla\phi_{T,r}^{n/2}\Big)| \\
&\quad +\alpha_2|\Big((I-P_{T,R})\nabla(\frac{T(t^{n+1})+T(t^n)}{\Delta t} - T(t^{n/2})), (I-P_{T,R})\nabla\phi_{T,r}^{n/2}\Big)| \\
&\quad +|(\frac{T(t^{n+1})-T(t^n)}{\Delta t} - T_t(t^{n/2}), \phi_{T,r}^{n/2})|. \qquad (5.2.19)
\end{aligned}
$$

Next, we bound the second and third term in the right hand side of (5.2.19), by using Lemma 1.2.13, Cauchy Schwarz, Young's and Poincaré's inequalities:

$$
\gamma|(\nabla {\eta_T}^{n/2}, \nabla\phi_{T,r}^{n/2})| \leq K\gamma\|\nabla {\eta_T}^{n/2}\|^2 + \frac{\gamma}{6}\|\nabla\phi_{T,r}^{n/2}\|^2. \qquad (5.2.20)
$$

$$
\begin{aligned}
\gamma|(\nabla(\frac{T(t^{n+1})+T(t^n)}{\Delta t} - T(t^{n/2})), \nabla\phi_{T,r}^{n/2})|^2 &\leq K\gamma\Delta t^4\|\nabla T_{tt}(t^*)\|^2 \\
&\quad +\frac{\gamma}{6}\|\nabla\phi_{T,r}^{n/2}\|^2 \qquad (5.2.21)
\end{aligned}
$$

The first nonlinear term right hand side of (5.2.19) can be rearranged adding and subtracting the term $b_2(\mathcal{X}(\mathbf{u}(t^n)), {\eta_T}^{n/2}, \phi_{T,r}^{n/2})$ as

$$
\begin{aligned}
b_2(\mathcal{X}(\mathbf{u}_r^n), {\eta_T}^{n/2}, \phi_{T,r}^{n/2}) &\leq |b_2(\mathcal{X}(\eta_{\mathbf{u}}^n), {\eta_T}^{n/2}, \phi_{T,r}^{n/2})| + |b_2(\mathcal{X}(\phi_{\mathbf{u},r}), {\eta_T}^{n/2}, \phi_{T,r}^{n/2})| \\
&\quad +|b_2(\mathcal{X}(\mathbf{u}(t^n)), {\eta_T}^{n/2}, \phi_{T,r}^{n/2})| \qquad (5.2.22)
\end{aligned}
$$

To bound this nonlinear terms in the right hand side of (5.2.22), we use Lemma 1.3.1 and Young's inequality

$$\begin{aligned}
|b_2(\mathcal{X}(\eta_{\mathbf{u}}^n), {\eta_T}^{n/2}, \phi_{T,r}^{n/2})| &\leq K\gamma^{-1}(\|\mathbb{D}\eta_{\mathbf{u}}^n\|^2 + \|\mathbb{D}\eta_{\mathbf{u}}^{n-1}\|^2)\|\nabla\eta_T^{n/2}\|^2 \\
&\quad + \frac{\gamma}{6}\|\nabla\phi_{T,r}^{n/2}\|^2 \\
|b_2(\mathcal{X}(\phi_{\mathbf{u},r}), {\eta_T}^{n/2}, \phi_{T,r}^{n/2})| &\leq K\gamma^{-1}h^{-1}(\|\phi_{\mathbf{u},r}^n\|^2 + \|\phi_{\mathbf{u},r}^{n-1}\|^2)\|\nabla\eta_T^{n/2}\|^2 \\
&\quad + \frac{\gamma}{6}\|\nabla\phi_{T,r}^{n/2}\|^2 \\
|b_2(\mathcal{X}(\mathbf{u}(t^n)), {\eta_T}^{n/2}, \phi_{T,r}^{n/2})| &\leq K\gamma^{-1}(\|\mathbb{D}\mathbf{u}(t^n)\|^2 + \|\mathbb{D}\mathbf{u}(t^{n-1})\|^2)\|\nabla\eta_T^{n/2}\|^2 \\
&\quad + \frac{\gamma}{6}\|\nabla\phi_{T,r}^{n/2}\|^2
\end{aligned}$$

Using similar techniques for the other nonlinear terms in the right hand side of (5.2.19), we get

$$\begin{aligned}
&|b_2(\mathcal{X}(\mathbf{e}_{\mathbf{u}}^n), \frac{T(t^{n+1}) + T(t^n)}{2}, \phi_{T,r}^{n/2})| \\
&\quad \leq K\gamma^{-1}(\|\mathbb{D}\eta_{\mathbf{u}}^n\|^2 + \|\mathbb{D}\eta_{\mathbf{u}}^{n-1}\|^2 + h^{-1}(\|\phi_{\mathbf{u},r}^n\|^2 + \|\phi_{\mathbf{u},r}^{n-1})\|^2)\|\nabla(\frac{T(t^{n+1}) + T(t^n)}{2})\|^2 \\
&\qquad + \frac{\gamma}{6}\|\nabla(\phi_{T,r}^{n/2})\|^2 \\
&|b_2(\mathbf{u}(t^{n/2}), \frac{T(t^{n+1}) + T(t^n)}{2} - T(t^{n/2}), \phi_{T,r}^{n/2})| \\
&\quad \leq K\gamma^{-1}\Delta t^4\|\mathbb{D}(\mathbf{u}(t^{n/2}))\|^2\|\nabla T_{tt}(t^*)\|^2 + \frac{\gamma}{6}\|\nabla\phi_{T,r}^{n/2}\|^2 \\
&|b_2(\mathcal{X}(\mathbf{u}(t^n)) - \mathbf{u}(t^{n/2}), \frac{T(t^{n+1}) + T(t^n)}{2}, \phi_{T,r}^{n/2})| \\
&\quad \leq K\gamma^{-1}\|\nabla(\mathcal{X}(\mathbf{u}(t^n)) - \mathbf{u}(t^{n/2}))\|^2\|\nabla(\frac{T(t^{n+1}) + T(t^n)}{2})\|^2 + \frac{\gamma}{6}\|\nabla\phi_{T,r}^{n/2}\|^2 \\
&|b_2(\mathbf{u}(t^{n/2}), \frac{T(t^{n+1}) + T(t^n)}{2} - T(t^{n/2}), \phi_{T,r}^{n/2})| \\
&\quad \leq K\gamma^{-1}\Delta t^4\|\nabla\mathbf{u}(t^{n/2})\|^2\|\nabla T_{tt}(t^*)\|^2 + \frac{\gamma}{6}\|\nabla\phi_{T,r}^{n/2}\|^2 \qquad (5.2.23)
\end{aligned}$$

The ninth, tenth, eleventh terms in (5.2.19) are bounded by using the fact that $\|(I -$

$P_{T,R})\nabla w\|^2 \leq \|\nabla w\|^2$

$$\begin{aligned}
&\alpha_2|\Big((I-P_{T,R})\nabla(\frac{T(t^{n+1})+T(t^n)}{\Delta t}-T(t^{n/2})),(I-P_{T,R})\nabla\phi_{T,r}^{n/2}\Big)|\\
&\quad+\alpha_2|\Big((I-P_{T,R})\nabla\eta_T^{n/2},(I-P_{T,R})\nabla\phi_{T,r}^{n/2}\Big)|\\
&\quad+\alpha_2|\Big((I-P_{T,R})\nabla T^{n/2},(I-P_{T,R})\nabla\phi_{T,r}^{n/2}\Big)|\\
&\leq\ \alpha_2\|\nabla\eta_T^{n/2}\|^2+\alpha_2\|(I-P_{T,R})\nabla T^{n/2}\|^2+\alpha_2\Delta t^4\|(I-P_{T,R})\nabla T_{tt}\|^2\\
&\quad+\frac{\alpha_2}{2}\|(I-P_{T,R})\nabla\phi_{T,r}^{n/2}\|^2 \qquad (5.2.24)
\end{aligned}$$

For the last term in the right hand side of (5.2.19), we apply Cauchy Schwarz, Poincaré's, Young's inequalities and Lemma 1.2.13 as

$$(\frac{T(t^{n+1})-T(t^n)}{\Delta t}-T_t(t^{n/2}),\phi_{T,r}^{n/2}) \ \leq\ K\gamma^{-1}\Delta t^4\|T_{ttt}(t^*)\|^2+\frac{\gamma}{6}\|\nabla\phi_{T,r}^{n/2}\|^2 \qquad (5.2.25)$$

Inserting (5.2.20)-(5.2.25) in (5.2.19), multiplying by $2\Delta t$ and summing over the time steps produces

$$\begin{aligned}
&\|\phi_{T,r}^M\|^2+\gamma\Delta t\sum_{n=0}^{M-1}\|\nabla\phi_{T,r}^{n/2}\|^2+\alpha_2\Delta t\sum_{n=0}^{M-1}\|(I-P_{T,R})\nabla\phi_{T,r}^{n/2}\|^2\leq\|\phi_{T,r}^0\|^2\\
&+K\Delta t\Big((\gamma+\alpha_2)\sum_{n=0}^{M-1}\|\nabla{\eta_T}^{n/2}\|^2+\gamma^{-1}h^{-1}\sum_{n=0}^{M-1}(\|\phi_{\mathbf{u},r}^n\|^2+\|\phi_{\mathbf{u},r}^{n-1}\|^2)\|\nabla\eta_T^{n/2}\|^2\\
&+\gamma^{-1}\sum_{n=0}^{M-1}(1+\|\mathbb{D}\eta_{\mathbf{u}}^n\|^2+\|\mathbb{D}\eta_{\mathbf{u}}^{n-1}\|^2)\|\nabla\eta_T^{n/2}\|^2+\gamma^{-1}\Big(\|\mathbb{D}\eta_{\mathbf{u}}^n\|^2+\|\mathbb{D}\eta_{\mathbf{u}}^{n-1}\|^2\\
&+h^{-1}(\|\phi_{\mathbf{u},r}^n\|^2+\|\phi_{\mathbf{u},r}^{n-1}\|)^2\Big)+\Delta t^4\Big((\gamma+\gamma^{-1}\|\mathbb{D}(\mathbf{u}(t^{n/2}))\|^2)\|\nabla T_{tt}(t^*)\|^2\\
&+\gamma^{-1}\|T_{ttt}(t^*)\|^2+\alpha_2\|(I-P_{T,R})\nabla T_{tt}(t^*)\|^2\Big)+\alpha_2\|(I-P_{T,R})\nabla T(t^{n/2})\|^2\Big) \qquad (5.2.26)
\end{aligned}$$

By using Lemma 2.1.4, Lemma 5.2.1, Assumption 2.2.1 and regularity assumptions in (5.2.26) results in

$$\begin{aligned}
&\|\phi_{T,r}^M\|^2+\gamma\Delta t\sum_{n=0}^{M-1}\|\nabla\phi_{T,r}^{n/2}\|^2+\alpha_2\Delta t\sum_{n=0}^{M-1}\|(I-P_{T,R})\nabla\phi_{T,r}^{n/2}\|^2\\
&\leq\ \|\phi_{T,r}^0\|^2+K\Big(h^{2m}+(\|S_{T,r}\|_2+\|S_{T,R}\|_2)h^{2m+2}+\varepsilon_{T,r}^2+\varepsilon_{T,R}^2\\
&\quad+(1+h^{2m}+\|S_{\mathbf{u},r}\|_2h^{2m+2}+\varepsilon_{\mathbf{u},r}^2)(h^{2m}+\|S_{T,r}\|_2h^{2m+2}+\varepsilon_{T,r}^2)\\
&\quad+(\Delta t)^4+\gamma^{-1}h^{-1}\sum_{n=0}^{M-1}(\|\phi_{\mathbf{u},r}^n\|^2+\|\phi_{\mathbf{u},r}^{n-1}\|^2)\|\nabla\eta_T^{n/2}\|^2\Big). \qquad (5.2.27)
\end{aligned}$$

Similarly, the error estimation for the concentration is given by

$$\begin{aligned}
&\|\phi_{C,r}^{M}\|^2 + D_c\Delta t\sum_{n=0}^{M-1}\|\nabla\phi_{C,r}^{n/2}\|^2 + \alpha_3\Delta t\sum_{n=0}^{M-1}\|(I-P_{C,R})\nabla\phi_{C,r}^{n/2}\|^2\\
&\leq \|\phi_{C,r}^{0}\|^2 + K\Big(h^{2m} + (\|S_{C,r}\|_2 + \|S_{C,R}\|_2)h^{2m+2} + \varepsilon_{C,r}^2 + \varepsilon_{C,R}^2\\
&\quad +(1+h^{2m}+\|S_{\mathbf{u},r}\|_2 h^{2m+2} + \varepsilon_{\mathbf{u},r}^2)(h^{2m}+\|S_{C,r}\|_2 h^{2m+2} + \varepsilon_{C,r}^2)\\
&\quad +(\Delta t)^4 + D_c^{-1}h^{-1}\sum_{n=0}^{M-1}(\|\phi_{\mathbf{u},r}^{n}\|^2 + \|\phi_{\mathbf{u},r}^{n-1}\|^2)\|\nabla\eta_C^{n/2}\|^2\Big). \qquad (5.2.28)
\end{aligned}$$

To obtain an estimation for the velocity we use similar arguments as above. Thus, in a similar manner, for the velocity we add and subtract

$$\begin{aligned}
&2\nu(\mathbb{D}(\frac{\mathbf{u}(t^{n+1})+\mathbf{u}(t^n)}{2}),\mathbb{D}\mathbf{v}_r) + (Da^{-1}(\frac{\mathbf{u}(t^{n+1})+\mathbf{u}(t^n)}{2}),\mathbf{v}_r)\\
&-(\frac{p(t^{n+1})+p(t^n)}{2},\nabla\cdot\mathbf{v}_r)\\
&+\alpha_1\Big((I-P_{\mathbf{u},R})\mathbb{D}(\frac{\mathbf{u}(t^{n+1})+\mathbf{u}(t^n)}{2}),(I-P_{\mathbf{u},R})\mathbb{D}\mathbf{v}_r\Big)\\
&-\beta_T(\mathbf{g}(\frac{T(t^{n+1})+T(t^n)}{2}),\mathbf{v}_r) - \beta_C(\mathbf{g}(\frac{C(t^{n+1})+C(t^n)}{2}),\mathbf{v}_r)\\
&b_1(\mathbf{u}(t^{n/2}) + \mathcal{X}(\mathbf{u}_r{}^n) + \mathcal{X}(\mathbf{u}(t^n)),\frac{\mathbf{u}(t^{n+1})+\mathbf{u}(t^n)}{2},\mathbf{v}_r)
\end{aligned}$$

to (5.2.11) and letting $\mathbf{v}_r = \boldsymbol{\phi}_{\mathbf{u},r}^{n/2}$ in (5.1.2), and applying the polarization identity to get

$$\begin{aligned}
&\frac{1}{2\Delta t}\|\boldsymbol{\phi}_{\mathbf{u},r}^{n+1}\|^2 - \frac{1}{2\Delta t}\|\boldsymbol{\phi}_{\mathbf{u},r}^{n}\|^2 + \frac{1}{2\Delta t}\|\boldsymbol{\phi}_{\mathbf{u},r}^{n+1}-\boldsymbol{\phi}_{\mathbf{u},r}^{n}\|^2 + 2\nu\|\mathbb{D}\boldsymbol{\phi}_{\mathbf{u},r}^{n/2}\|^2\\
&\quad +\alpha_1\|(I-P_{\mathbf{u},R})\mathbb{D}\boldsymbol{\phi}_{\mathbf{u},r}^{n/2}\|^2 + Da^{-1}\|\boldsymbol{\phi}_{\mathbf{u},r}^{n/2}\|^2\\
&\leq |\beta_T(\mathbf{g}(\eta_T^{n/2}),\boldsymbol{\phi}_{\mathbf{u},r}^{n/2})| + |\beta_C(\mathbf{g}(\eta_C^{n/2}),\boldsymbol{\phi}_{\mathbf{u},r}^{n/2})| + |\beta_T(\mathbf{g}(\phi_{T,r}^{n/2}),\boldsymbol{\phi}_{\mathbf{u},r}^{n/2})|\\
&\quad +|\beta_C(\mathbf{g}(\phi_{C,r}^{n/2}),\boldsymbol{\phi}_{\mathbf{u},r}^{n/2})| + |\beta_T(\mathbf{g}(\frac{T(t^{n+1})+T(t^n)}{2} - T^{n/2}),\boldsymbol{\phi}_{\mathbf{u},r}^{n/2})|\\
&\quad +|\beta_C(\mathbf{g}(\frac{C(t^{n+1})+C(t^n)}{2} - C^{n/2}),\boldsymbol{\phi}_{\mathbf{u},r}^{n/2})| + |(\frac{\boldsymbol{\eta}_u^{n+1}-\boldsymbol{\eta}_u^{n}}{\Delta t},\boldsymbol{\phi}_{\mathbf{u},r}^{n/2})|\\
&\quad +2\nu|(\mathbb{D}\boldsymbol{\eta}_{\mathbf{u}}{}^{n/2},\mathbb{D}\boldsymbol{\phi}_{\mathbf{u},r}^{n/2})| + 2\nu|(\mathbb{D}(\frac{\mathbf{u}(t^{n+1})+\mathbf{u}(t^n)}{2}) - \mathbb{D}\mathbf{u}(t^{n/2}),\mathbb{D}\boldsymbol{\phi}_{\mathbf{u},r}^{n/2})|\\
&\quad +Da^{-1}|(\boldsymbol{\eta}_{\mathbf{u}}{}^{n/2},\boldsymbol{\phi}_{\mathbf{u},r}^{n/2})| + Da^{-1}|\Big((\frac{\mathbf{u}(t^{n+1})+\mathbf{u}(t^n)}{2}) - \mathbf{u}(t^{n/2}),\boldsymbol{\phi}_{\mathbf{u},r}^{n/2}\Big)|\\
&\quad +\alpha_1|\Big((I-P_{\mathbf{u},R})\nabla\eta_{\mathbf{u}}^{n/2},(I-P_{\mathbf{u},R})\mathbb{D}\phi_{\mathbf{u},r}^{n/2}\Big)|\\
&\quad +\alpha_1|\Big((I-P_{\mathbf{u},R})\mathbb{D}\mathbf{u}(t^{n/2}),(I-P_{\mathbf{u},R})\mathbb{D}\boldsymbol{\phi}_{\mathbf{u},r}^{n/2}\Big)|
\end{aligned}$$

$$
\begin{aligned}
&+\alpha_1|\Big((I-P_{\mathbf{u},R})\mathbb{D}(\frac{\mathbf{u}(t^{n+1})+\mathbf{u}(t^n)}{2}-\mathbf{u}(t^{n/2}),(I-P_{\mathbf{u},R})\mathbb{D}\boldsymbol{\phi}_{\mathbf{u},r}^{n/2}\Big)|\\
&+|b_1(\mathcal{X}(\mathbf{u}_r^n),\eta_{\mathbf{u}}{}^{n/2},\phi_{\mathbf{u},r}^{n/2})|+|b_1((\mathcal{X}(\boldsymbol{\eta}_{\mathbf{u}}^n),\frac{\mathbf{u}(t^{n+1})+\mathbf{u}(t^n)}{2},\phi_{\mathbf{u},r}^{n/2})|\\
&+|b_1((\mathcal{X}(\boldsymbol{\phi}_{\mathbf{u},r}^n),\frac{\mathbf{u}(t^{n+1})+\mathbf{u}(t^n)}{2},\phi_{\mathbf{u},r}^{n/2})|\\
&+|b_1(\mathbf{u}(t^{n/2}),\frac{\mathbf{u}(t^{n+1})+\mathbf{u}(t^n)}{2}-\mathbf{u}(t^{n/2}),\phi_{\mathbf{u},r}^{n/2})|\\
&+|b_1((\mathcal{X}(\mathbf{u}(t^n))-\mathbf{u}(t^{n/2}),\frac{\mathbf{u}(t^{n+1})+\mathbf{u}(t^n)}{2},\phi_{\mathbf{u},r}^{n/2})|\\
&+|(\frac{p(t^{n+1})+p(t^n)}{2}-p(t^{n/2}),\nabla\cdot\boldsymbol{\phi}_{\mathbf{u},r}^{n/2})|\\
&+|(\frac{p(t^{n+1})+p(t^n)}{2}-q_h,\nabla\cdot\boldsymbol{\phi}_{\mathbf{u},r}^{n/2})|+|(\frac{\mathbf{u}^{n+1}-\mathbf{u}^n}{\Delta t}-\mathbf{u}_t^{n+1},\boldsymbol{\phi}_{\mathbf{u},r}^{n/2})|. \qquad (5.2.29)
\end{aligned}
$$

Note that $\left(\frac{\boldsymbol{\eta}_u^{n+1}-\boldsymbol{\eta}_u^n}{\Delta t},\boldsymbol{\phi}_{\mathbf{u},r}^{n/2}\right)=0$ due to the definition of the L^2 projection. Each of the terms in (5.2.29) can be bounded in a similar manner. Thus, one gets

$$
\begin{aligned}
&|\beta_T(\mathbf{g}(\eta_T^{n/2}),\boldsymbol{\phi}_{\mathbf{u},r}^{n/2})|+|\beta_C(\mathbf{g}(\eta_C^{n/2}),\boldsymbol{\phi}_{\mathbf{u},r}^{n/2})|+|\beta_T(\mathbf{g}(\phi_{T,r}^{n/2}),\boldsymbol{\phi}_{\mathbf{u},r}^{n/2})|\\
&\quad+|\beta_C(\mathbf{g}(\phi_{C,r}^{n/2}),\boldsymbol{\phi}_{\mathbf{u},r}^{n/2})|+|\beta_T(\mathbf{g}(\frac{T(t^{n+1})+T(t^n)}{2}-T(t^{n/2})),\boldsymbol{\phi}_{\mathbf{u},r}^{n/2})|\\
&\quad+|\beta_C(\mathbf{g}(\frac{C(t^{n+1})+C(t^n)}{2}-C(t^{n/2})),\boldsymbol{\phi}_{\mathbf{u},r}^{n/2})|\\
&\leq\ K\nu^{-1}\|\mathbf{g}\|_\infty^2\Big(\beta_T^2(\|\eta_T^{n/2}\|^2+\|\phi_{T,r}^{n/2}\|^2+\Delta t^4\|T_{tt}(\cdot,\tilde{t})\|^2)\\
&\quad+\beta_C^2(\|\eta_C^{n/2}\|^2+\|\phi_{C,r}^{n/2}\|^2+\Delta t^4\|C_{tt}(t^*)\|^2)\Big)+\frac{\nu}{10}\|\mathbb{D}\boldsymbol{\phi}_{\mathbf{u},r}^{n/2}\|^2, \qquad (5.2.30)
\end{aligned}
$$

$$
\begin{aligned}
&2\nu|(\mathbb{D}\boldsymbol{\eta}_{\mathbf{u}}^{n/2},\mathbb{D}\boldsymbol{\phi}_{\mathbf{u},r}^{n/2})|+2\nu|(\mathbb{D}(\frac{\mathbf{u}(t^{n+1})+\mathbf{u}(t^n)}{2})-\mathbb{D}\mathbf{u}(t^{n/2}),\mathbb{D}\boldsymbol{\phi}_{\mathbf{u},r}^{n/2})|\\
&\leq\ K\nu\Big(\|\mathbb{D}\boldsymbol{\eta}_{\mathbf{u}}^{n/2}\|^2+\Delta t^4\|\mathbb{D}\mathbf{u}_{tt}(\cdot,\tilde{t})\|^2\Big)+\frac{\nu}{10}\|\mathbb{D}\boldsymbol{\phi}_{\mathbf{u},r}^{n/2}\|^2, \qquad (5.2.31)
\end{aligned}
$$

$$
\begin{aligned}
&Da^{-1}|(\boldsymbol{\eta}_{\mathbf{u}}^{n/2},\boldsymbol{\phi}_{\mathbf{u},r}^{n/2})|+Da^{-1}|\Big((\frac{\mathbf{u}(t^{n+1})+\mathbf{u}(t^n)}{2})-\mathbf{u}(t^{n/2}),\boldsymbol{\phi}_{\mathbf{u},r}^{n/2}\Big)|\\
&\leq\ KDa^{-1}\Big(\|\boldsymbol{\eta}_{\mathbf{u}}^{n/2}\|^2+\Delta t^4\|\mathbf{u}_{tt}(t^*)\|^2\Big)+\frac{Da^{-1}}{2}\|\boldsymbol{\phi}_{\mathbf{u},r}^{n/2}\|^2, \qquad (5.2.32)
\end{aligned}
$$

$$
\begin{aligned}
&|(\frac{p(t^{n+1})+p(t^n)}{2}-p(t^{n/2}),\nabla\cdot\boldsymbol{\phi}_{\mathbf{u},r}^{n/2})|+|(\frac{p(t^{n+1})+p(t^n)}{2}-q_h,\nabla\cdot\boldsymbol{\phi}_{\mathbf{u},r}^{n/2})|\\
&\leq\ K\nu^{-1}(\Delta t^4\left\|p_{tt}(t^*)\right\|^2+\left\|\frac{p(t^{n+1})+p(t^n)}{2}-q_h\right\|^2)+\frac{\nu}{10}\left\|\mathbb{D}\boldsymbol{\phi}_{\mathbf{u},r}^{n/2}\right\|^2, \qquad (5.2.33)
\end{aligned}
$$

$$|(\mathbf{u}_t^{n+1} - \frac{\mathbf{u}^{n+1}-\mathbf{u}^n}{\Delta t}, \boldsymbol{\phi}_{\mathbf{u},r}^{n/2})| \le K\nu^{-1}\Delta t^4 \|\mathbf{u}_{ttt}(t^*)\|^2 + \frac{\nu}{10}\left\|\mathbb{D}\boldsymbol{\phi}_{\mathbf{u},r}^{n/2}\right\|^2, \tag{5.2.34}$$

$$\begin{aligned}
&\alpha_1\Big|\Big((I-P_{\mathbf{u},R})\mathbb{D}(\frac{\mathbf{u}(t^{n+1})+\mathbf{u}(t^n)}{2} - \mathbf{u}(t^{n/2})), (I-P_{\mathbf{u},R})\mathbb{D}\boldsymbol{\phi}_{\mathbf{u},r}^{n/2}\Big)\Big| \\
&\quad +\alpha_1\Big|\Big((I-P_{\mathbf{u},R})\nabla\eta_{\mathbf{u}}^{n/2}, (I-P_{\mathbf{u},R})\mathbb{D}\phi_{\mathbf{u},r}^{n/2}\Big)\Big| \\
&\quad +\alpha_1\Big|\Big((I-P_{\mathbf{u},R})\mathbb{D}\mathbf{u}(t^{n/2}), (I-P_{\mathbf{u},R})\mathbb{D}\boldsymbol{\phi}_{\mathbf{u},r}^{n/2}\Big)\Big| \\
\le\ & K\alpha_1\Big(\Delta t^4\|(I-P_{\mathbf{u},R})\mathbb{D}\mathbf{u}_{tt}(t^*)\|^2 + \|\nabla\eta_{\mathbf{u}}^{n/2}\|^2 + \|(I-P_{\mathbf{u},R})\mathbb{D}\mathbf{u}(t^{n/2})\|^2\Big) \\
&\quad +\frac{\alpha_1}{2}\|(I-P_{\mathbf{u},R})\mathbb{D}\phi_{\mathbf{u},r}^{n/2}\|^2.
\end{aligned} \tag{5.2.35}$$

The first nonlinear terms are organized as

$$\begin{aligned}
|b_1(\mathcal{X}(\mathbf{u}_r^n), {\eta_{\mathbf{u}}}^{n/2}, \phi_{\mathbf{u},r}^{n/2})| &\le |b_1(\mathcal{X}(\mathbf{u}(t^n)), {\eta_{\mathbf{u}}}^{n/2}, \phi_{\mathbf{u},r}^{n/2})| \\
&+|b_1(\mathcal{X}(\eta_{\mathbf{u}}^n), {\eta_{\mathbf{u}}}^{n/2}, \phi_{\mathbf{u},r}^{n/2})| + |b_1(\mathcal{X}(\phi_{\mathbf{u},r}^n), {\eta_{\mathbf{u}}}^{n/2}, \phi_{\mathbf{u},r}^{n/2})|
\end{aligned} \tag{5.2.36}$$

The nonlinear terms in (5.2.36) are bounded as before:

$$\begin{aligned}
&|b_1(\mathcal{X}(\mathbf{u}(t^n)), {\eta_{\mathbf{u}}}^{n/2}, \phi_{\mathbf{u},r}^{n/2})| \\
&\quad\le K\nu^{-1}(\|\mathbb{D}\mathbf{u}(t^n)\|^2 + \|\mathbb{D}\mathbf{u}(t^{n-1})\|^2)\|\mathbb{D}{\eta_{\mathbf{u}}}^{n/2}\|^2 + \frac{\nu}{10}\|\mathbb{D}\boldsymbol{\phi}_{\mathbf{u},r}^{n/2}\|^2 \\
&|b_1(\mathcal{X}(\eta_{\mathbf{u}}^n), {\eta_{\mathbf{u}}}^{n/2}, \phi_{\mathbf{u},r}^{n/2})| \\
&\quad\le K\nu^{-1}(\|\mathbb{D}\eta_{\mathbf{u}}^n\|^2 + \|\mathbb{D}\eta_{\mathbf{u}}^{n-1}\|^2)\|\mathbb{D}{\eta_{\mathbf{u}}}^{n/2}\|^2 + \frac{\nu}{10}\|\mathbb{D}\boldsymbol{\phi}_{\mathbf{u},r}^{n/2}\|^2 \\
&|b_1(\mathcal{X}(\phi_{\mathbf{u},r}^n), {\eta_{\mathbf{u}}}^{n/2}, \phi_{\mathbf{u},r}^{n/2})| \\
&\quad\le K\nu^{-1}h^{-1}(\|\phi_{\mathbf{u},r}^n\|^2 + \|\phi_{\mathbf{u},r}^{n-1}\|^2)\|\mathbb{D}{\eta_{\mathbf{u}}}^{n/2}\|^2 + \frac{\nu}{10}\|\mathbb{D}\boldsymbol{\phi}_{\mathbf{u},r}^{n/2}\|^2
\end{aligned}$$

Similarly, the other nonlinear terms can be bounded as

$$\begin{aligned}
&|b_1((\mathcal{X}(\boldsymbol{\eta}_{\mathbf{u}}^n), \frac{\mathbf{u}(t^{n+1})+\mathbf{u}(t^n)}{2}, \phi_{\mathbf{u},r}^{n/2})| + |b_1((\mathcal{X}(\boldsymbol{\phi}_{\mathbf{u},r}^n), \frac{\mathbf{u}(t^{n+1})+\mathbf{u}(t^n)}{2}, \phi_{\mathbf{u},r}^{n/2})| \\
&\quad\le K\nu^{-1}\Big(\|\mathbb{D}\boldsymbol{\eta}_{\mathbf{u}}^n\|^2 + \|\mathbb{D}\boldsymbol{\eta}_{\mathbf{u}}^{n-1}\|^2 + h^{-1}(\|\boldsymbol{\phi}_{\mathbf{u},r}^n\|^2 + \|\boldsymbol{\phi}_{\mathbf{u},r}^{n-1}\|^2)\Big)\|\mathbb{D}(\frac{\mathbf{u}(t^{n+1})+\mathbf{u}(t^n)}{2})\|^2 \\
&\qquad +\frac{\nu}{10}\|\mathbb{D}\boldsymbol{\phi}_{\mathbf{u},r}^{n/2}\|^2 \\
&|b_1(\mathbf{u}(t^{n/2}), \frac{\mathbf{u}(t^{n+1})+\mathbf{u}(t^n)}{2} - \mathbf{u}(t^{n/2}), \phi_{\mathbf{u},r}^{n/2})| \\
&\quad\le K\nu^{-1}\Delta t^4\|\mathbb{D}\mathbf{u}(t^{n/2})\|^2\|\mathbb{D}\mathbf{u}_{tt}(t^*)\|^2 + \frac{\nu}{10}\|\mathbb{D}\boldsymbol{\phi}_{\mathbf{u},r}^{n/2}\|^2 \\
&b_1((\mathcal{X}(\mathbf{u}(t^n)) - \mathbf{u}(t^{n/2}), \frac{\mathbf{u}(t^{n+1})+\mathbf{u}(t^n)}{2}, \phi_{\mathbf{u},r}^{n/2})| \\
&\quad\le K\nu^{-1}\|\mathbb{D}(\mathcal{X}(\mathbf{u}(t^n)) - \mathbf{u}(t^{n/2}))\|^2\|\mathbb{D}(\frac{\mathbf{u}(t^{n+1})+\mathbf{u}(t^n)}{2})\|^2 + \frac{\nu}{10}\|\mathbb{D}\boldsymbol{\phi}_{\mathbf{u},r}^{n/2}\|^2
\end{aligned} \tag{5.2.37}$$

We now insert (5.2.30)-(5.2.37) into (5.2.29) and use regularity assumptions to get

$$
\begin{aligned}
&\frac{1}{2\Delta t}\|\boldsymbol{\phi}_{\mathbf{u},r}^{n+1}\|^2-\frac{1}{2\Delta t}\|\boldsymbol{\phi}_{\mathbf{u},r}^{n}\|^2+\frac{1}{2\Delta t}\|\boldsymbol{\phi}_{\mathbf{u},r}^{n+1}-\boldsymbol{\phi}_{\mathbf{u},r}^{n}\|^2\\
&\quad+\nu\|\mathbb{D}\boldsymbol{\phi}_{\mathbf{u},r}^{n/2}\|^2+\frac{Da^{-1}}{2}\|\boldsymbol{\phi}_{\mathbf{u},r}^{n/2}\|^2+\frac{\alpha_1}{2}\|(I-P_{\mathbf{u},R})\mathbb{D}\phi_{\mathbf{u},r}^{n/2}\|^2\\
&\leq\ K\Big(\nu^{-1}\|\mathbf{g}\|_\infty^2(\beta_T^2\|\phi_{T,r}^{n/2}\|^2+\beta_C^2\|\phi_{C,r}^{n/2}\|^2)+\|\eta_T^{n/2}\|^2+\|\eta_C^{n/2}\|^2\\
&\quad+\|\boldsymbol{\eta}_{\mathbf{u}}{}^{n/2}\|^2+\|\mathbb{D}\boldsymbol{\eta}_{\mathbf{u}}{}^{n/2}\|^2(1+\|\mathbb{D}\boldsymbol{\eta}_{\mathbf{u}}^{n}\|^2+\|\mathbb{D}\boldsymbol{\eta}_{\mathbf{u}}^{n-1}\|^2)\\
&\quad+\nu^{-1}h^{-1}(\|\mathbb{D}\boldsymbol{\eta}_{\mathbf{u}}{}^{n/2}\|^2+\|\mathbb{D}(\frac{\mathbf{u}(t^{n+1})+\mathbf{u}(t^n)}{2})\|^2)(\|\boldsymbol{\phi}_{\mathbf{u},r}^{n}\|^2+\|\boldsymbol{\phi}_{\mathbf{u},r}^{n-1}\|^2)\\
&\quad+\alpha_1\|(I-P_{\mathbf{u},R})\mathbb{D}\mathbf{u}(t^{n/2})\|^2+\|\frac{p(t^{n+1})+p(t^n)}{2}-q_h\|^2\\
&\quad+\nu^{-1}\|\mathbf{g}\|_\infty^2\Delta t^4\Big(\beta_T^2\|T_{tt}(\cdot,\tilde{t})\|^2+\beta_C^2\|C_{tt}(t^*)\|^2\Big)\\
&\quad+(\nu+\nu^{-1}\|\mathbb{D}\mathbf{u}(t^{n/2})\|^2)\Delta t^4\|\mathbb{D}\mathbf{u}_{tt}(\cdot,\tilde{t})\|^2+Da^{-1}\Delta t^4\|\mathbf{u}_{tt}(t^*)\|^2\\
&\quad+\nu^{-1}\Delta t^4\left\|p_{tt}(t^*)\right\|^2+\nu^{-1}\Delta t^4\|\mathbf{u}_{ttt}(t^*)\|^2\\
&\quad+\Delta t^4\alpha_1\|(I-P_{\mathbf{u},R})\mathbb{D}\mathbf{u}_{tt}(t^*)\|^2\Big).
\end{aligned}
\tag{5.2.38}
$$

Dropping the third term in the left hand side of (5.2.38) and summing over the time steps and multiplying by $2\Delta t$ gives

$$
\begin{aligned}
&\|\boldsymbol{\phi}_{\mathbf{u},r}^{M}\|^2+\Delta t\sum_{n=0}^{M-1}\Big(2\nu\|\mathbb{D}\boldsymbol{\phi}_{\mathbf{u},r}^{n/2}\|^2+Da^{-1}\|\boldsymbol{\phi}_{\mathbf{u},r}^{n/2}\|^2+\alpha_1\|(I-P_{\mathbf{u},R})\mathbb{D}\phi_{\mathbf{u},r}^{n/2}\|^2\Big)\\
&\leq\ \|\boldsymbol{\phi}_{\mathbf{u},r}^{0}\|^2+K\Delta t\Big(\nu^{-1}\|\mathbf{g}\|_\infty^2\sum_{n=0}^{M-1}(\beta_T^2\|\phi_{T,r}^{n/2}\|^2+\beta_C^2\|\phi_{C,r}^{n/2}\|^2)\\
&\quad+\sum_{n=0}^{M-1}(\|\eta_T^{n/2}\|^2+\|\eta_C^{n/2}\|^2+\|\boldsymbol{\eta}_{\mathbf{u}}{}^{n/2}\|^2)\\
&\quad+\sum_{n=0}^{M-1}\|\mathbb{D}\boldsymbol{\eta}_{\mathbf{u}}{}^{n/2}\|^2(1+\|\mathbb{D}\boldsymbol{\eta}_{\mathbf{u}}^{n}\|^2+\|\mathbb{D}\boldsymbol{\eta}_{\mathbf{u}}^{n-1}\|^2)\\
&\quad+\nu^{-1}h^{-1}\sum_{n=0}^{M-1}\Big(\|\mathbb{D}\boldsymbol{\eta}_{\mathbf{u}}{}^{n/2}\|^2+\|\mathbb{D}(\frac{\mathbf{u}(t^{n+1})+\mathbf{u}(t^n)}{2})\|^2\Big)(\|\boldsymbol{\phi}_{\mathbf{u},r}^{n}\|^2+\|\boldsymbol{\phi}_{\mathbf{u},r}^{n-1}\|^2)\\
&\quad+\alpha_1\sum_{n=0}^{M-1}\|(I-P_{\mathbf{u},R})\mathbb{D}\mathbf{u}(t^{n/2})\|^2+\sum_{n=0}^{M-1}\|\frac{p(t^{n+1})+p(t^n)}{2}-q_h\|^2\\
&\quad+\Delta t^4\Big(\nu^{-1}\|\mathbf{g}\|_\infty^2\sum_{n=0}^{M-1}\big(\beta_T^2\|T_{tt}(\cdot,\tilde{t})\|^2+\beta_C^2\|C_{tt}(t^*)\|^2\big)\\
&\quad+\sum_{n=0}^{M-1}(\nu+\nu^{-1}\|\mathbb{D}\mathbf{u}(t^{n/2})\|^2)\|\mathbb{D}\mathbf{u}_{tt}(\cdot,\tilde{t})\|^2+Da^{-1}\sum_{n=0}^{M-1}\|\mathbf{u}_{tt}(t^*)\|^2\\
&\quad+\nu^{-1}\sum_{n=0}^{M-1}\left\|p_{tt}(t^*)\right\|^2+\nu^{-1}\sum_{n=0}^{M-1}\|\mathbf{u}_{ttt}(t^*)\|^2+\alpha_1\sum_{n=0}^{M-1}\|(I-P_{\mathbf{u},R})\mathbb{D}\mathbf{u}_{tt}(t^*)\|^2\Big)\Big).
\end{aligned}
\tag{5.2.39}
$$

Using Lemma 2.1.4, Lemma 5.2.1, Assumption 2.2.1 in (5.2.39) and applying regu-

larity assumptions leads to

$$
\begin{aligned}
&\|\boldsymbol{\phi}_{\mathbf{u},r}^{M}\|^2+\Delta t\sum_{n=0}^{M-1}(2\nu\|\mathbb{D}\boldsymbol{\phi}_{\mathbf{u},r}^{n/2}\|^2+Da^{-1}\|\boldsymbol{\phi}_{\mathbf{u},r}^{n/2}\|^2)\\
&\quad+\alpha_1\sum_{n=0}^{M-1}\|(I-P_{\mathbf{u},R})\mathbb{D}\phi_{\mathbf{u},r}^{n/2}\|^2\\
&\leq\ \|\phi_{\mathbf{u},r}^{0}\|^2+K\Bigg(\nu^{-1}\beta_T^2\|\mathbf{g}\|_\infty^2\Delta t\sum_{n=0}^{M-1}\|\phi_{T,r}^{n/2}\|^2+\nu^{-1}\beta_C^2\|\mathbf{g}\|_\infty^2\Delta t\sum_{n=0}^{M-1}\|\phi_{C,r}^{n/2}\|^2\\
&\quad+h^{2m}+(1+\|S_{\mathbf{u},r}\|_2+\|S_{\mathbf{u},R}\|_2)h^{2m+2}+\varepsilon_{\mathbf{u},r}^2+\varepsilon_{\mathbf{u},R}^2+\sum_{i=r_1+1}^{d}\lambda_i+\sum_{i=r_2+1}^{d}\mu_i\\
&\quad+\sum_{i=r_3+1}^{d}\xi_i+(\Delta t)^4+(h^{2m}+(\|S_{\mathbf{u},r}\|_2+\|S_{\mathbf{u},R}\|_2)h^{2m+2}+\varepsilon_{\mathbf{u},r}^2)^2\\
&\quad+\nu^{-1}h^{-1}\Big(h^{2m}+\|S_{\mathbf{u},r}\|h^{2m+2}+\varepsilon_{\mathbf{u},r}+\|\mathbb{D}\mathbf{u}\|_\infty^2\Big)\sum_{n=0}^{M-1}(\|\boldsymbol{\phi}_{\mathbf{u},r}^{n}\|^2)\Bigg).
\end{aligned}
\tag{5.2.39}
$$

Finally, we add (5.2.27), (5.2.28) and (5.2.39) to get

$$
\begin{aligned}
&\|\boldsymbol{\phi}_{\mathbf{u},r}^{M}\|^2+\|\phi_{T,r}^{M}\|^2+\|\phi_{C,r}^{M}\|^2+\sum_{n=0}^{M-1}\Big(2\nu\Delta t\|\mathbb{D}\boldsymbol{\phi}_{\mathbf{u},r}^{n/2}\|^2+Da^{-1}\Delta t\|\boldsymbol{\phi}_{\mathbf{u},r}^{n/2}\|^2\Big)\\
&\quad+\gamma\Delta t\sum_{n=0}^{M-1}\|\nabla\phi_{T,r}^{n/2}\|^2+D_c\Delta t\sum_{n=0}^{M-1}\|\nabla\phi_{C,r}^{n/2}\|^2+\alpha_1\|(I-P_{\mathbf{u},R})\mathbb{D}\phi_{\mathbf{u},r}^{n/2}\|^2\\
&\quad+\alpha_2\Delta t\sum_{n=0}^{M-1}\|(I-P_{T,R})\nabla\phi_{T,r}^{n/2}\|^2+\alpha_3\Delta t\sum_{n=0}^{M-1}\|(I-P_{C,R})\nabla\phi_{C,r}^{n/2}\|^2\\
&\leq\ \|\mathbf{u}_r^0-\tilde{\mathbf{u}}^0\|^2+\|T_r^0-\tilde{T}^0\|^2+\|C_r^0-\tilde{C}^0\|^2+K\Bigg(\nu^{-1}\beta_T^2\|\mathbf{g}\|_\infty^2\Delta t\sum_{n=0}^{M-1}\|\phi_{T,r}^{n/2}\|^2\\
&\quad+\nu^{-1}\beta_C^2\|\mathbf{g}\|_\infty^2\Delta t\sum_{n=0}^{M-1}\|\phi_{C,r}^{n+1}\|^2+h^{2m}+(\|S_{\mathbf{u},r}\|_2+\|S_{\mathbf{u},R}\|_2+\|S_{T,r}\|_2+\|S_{T,R}\|_2\\
&\quad+\|S_{C,r}\|_2+\|S_{C,R}\|_2)h^{2m+2}+\varepsilon_{\mathbf{u},r}^2+\varepsilon_{\mathbf{u},R}^2+\varepsilon_{T,r}^2+\varepsilon_{T,R}^2+\varepsilon_{C,r}^2+\varepsilon_{C,R}^2+(\Delta t)^4\\
&\quad+(h^{2m}+\|S_{\mathbf{u},r}\|_2h^{2m+2}+\varepsilon_{\mathbf{u},r}^2)\times\Big(h^{2m}+(\|S_{\mathbf{u},r}\|_2+\|S_{T,r}\|_2+\|S_{C,r}\|_2)h^{2m+2}\\
&\quad+\varepsilon_{\mathbf{u},r}^2+\varepsilon_{T,r}^2+\varepsilon_{C,r}^2\Big)+\sum_{i=r_1+1}^{d}\lambda_i+\sum_{i=r_2+1}^{d}\mu_i+\sum_{i=r_3+1}^{d}\xi_i\\
&\quad+\Big((\nu^{-1}+\gamma^{-1}+D_c^{-1})h^{2m-1}+(\|S_{\mathbf{u},r}\|+\|S_{T,r}\|+\|S_{C,r}\|)h^{2m+1}\\
&\quad+\nu^{-1}h^{-1}\varepsilon_{\mathbf{u},r}+\gamma^{-1}h^{-1}\varepsilon_{T,r}+D_c^{-1}h^{-1}\varepsilon_{C,r}+\|\mathbb{D}\mathbf{u}\|_\infty^2\Big)\sum_{n=0}^{M-1}\|\boldsymbol{\phi}_{\mathbf{u},r}^{n}\|^2\Bigg).
\end{aligned}
$$

We remark that the application of the discrete Gronwall inequality requires an assumption on the time step size. The final error estimation can be obtained by using the assumption $(\mathbf{u}_r^0, T_r^0, C_r^0) = (\tilde{\mathbf{u}}^0, \tilde{T}^0, \tilde{C}^0)$, the triangle inequality, Assumption 2.1.1 and Assumption 2.2.1.

5.3 Numerical Experiments

In this section, the numerical experiments for the linearly extrapolated schemes described by (5.1.2)-(5.1.4) are illustrated. The numerical experiments include a convergence test experiment with respect to VMS-POD modes R and a comparison test experiment by considering POD and VMS-POD solutions.

5.3.1 Problem description

In the numerical experiments, we choose the same test problem with Chapter 4. We also select the time step $\Delta t = 1.5625e-05$, POD basis number $r = 12$, the kinematic viscosity $\nu = 1$. Recall that we use snapshots come from DNS obtained by finite element spatial discretization. Thus, to get fine mesh solution for snapshots, we use BDF2 finite element method with $Ra = 10^4$ and $\Delta t = 0.00025$ with 30×60 uniform triangulation. In this case, one gets 59,255 total degrees of freedom for Taylor-Hood elements and piecewise quadratics for both temperature and concentration.

5.3.2 Test 1: Convergence rates with respect to R

We evaluate the convergence rates of VMS-POD solution to measure the effect of the error sources. POD and VMS cutoffs become dominant sources when the spatial error and the temporal error are neglected. Our special interest is the scaling of the error with respect to R. The VMS contributions for the velocity, the temperature, and the concentration are defined by

$$\varepsilon_{\mathbf{u},R} = \sqrt{\sum_{j=R+1}^{d} \|\psi_j\|_1^2 \lambda_j}, \quad \varepsilon_{T,R} = \sqrt{\sum_{j=R+1}^{d} \|\phi_j\|_1^2 \mu_j}, \quad \varepsilon_{C,R} = \sqrt{\sum_{j=R+1}^{d} \|\eta_j\|_1^2 \xi_j}.$$

We choose the artificial viscosities $\alpha_1 = 2$, $\alpha_2 = \frac{1}{8}$, $\alpha_3 = \frac{1}{8}$ for the velocity, the temperature and the concentration, respectively. The results of this test are shown in Table 5.1.

Table 5.1: Convergence of the VMS-POD for varying R

r	R	ε_u	$\|\nabla(\mathbf{u}-\mathbf{u}_r)\|_{L^2(H^1)}$	rate	ε_T	$\|\nabla(T-T_r)\|_{L^2(H^1)}$	rate
12	4	21.8237	0.63196	-	1.5694	0.01427	-
12	6	8.8818	0.22636	1.14	0.4319	0.00823	0.42
12	8	4.4168	0.13008	0.79	0.1842	0.00416	0.80

r	R	ε_C	$\|\nabla(C-C_r)\|_{L^2(H^1)}$	rate
12	4	1.5529	0.02991	-
12	6	0.6768	0.01468	0.85
12	8	0.3858	0.00927	0.81

As seen in Table 5.1, the rates of error in $L^2(0,T;H^1(\Omega))$ consistent with 0.5 expected by the analysis.

5.3.3 Test 2: Comparison of POD solution and VMS-POD solution

In this test, we check the ability of VMS method. We fix $R = 5$, $\alpha_1 = \alpha_2 = \alpha_3 = 10^{-3}$. Figure 5.1 shows decreasing behaviours of L^2 errors in the velocity, the temperature, and the concentration. These figures indicate that the L^2 errors in VMS-POD solutions improve the behaviour of the errors for each fluid variables compared with the POD solutions.

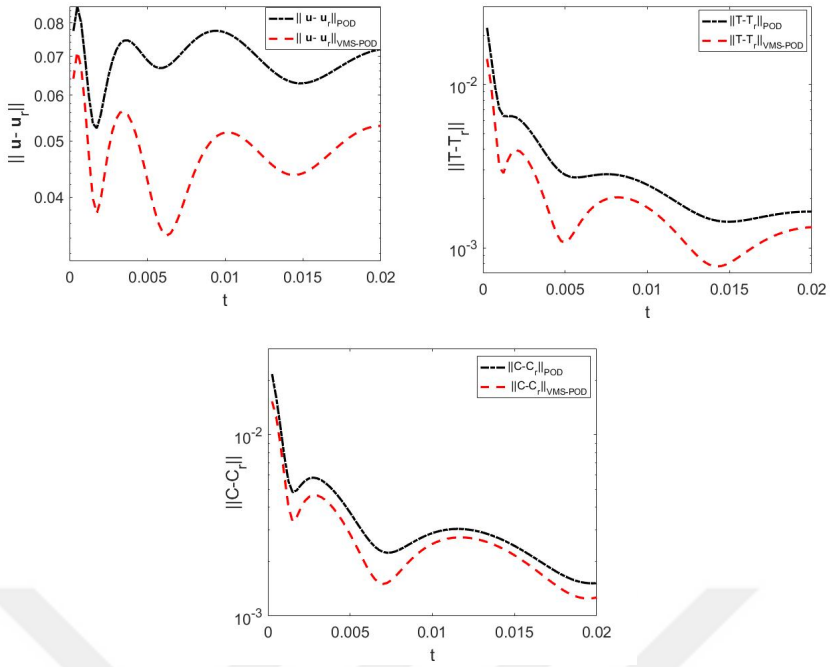

Figure 5.1: L^2 errors of stabilized and unstabilized solution

For a final test, we consider the similar test with Chapter 4 but with even higher Rayleigh number, $Ra = 10^6$. Here, even with 40 modes, the POD is unable to give a good solution (see Figure 5.2), which is expected since Figure 4.1 shows a very slow decay of the eigenvalues of the snapshot matrix. As seen in the Figure 5.2, for $Ra = 10^6$, unstabilized POD did not matches with DNS solutions, but VMS-POD gave good qualitative results.

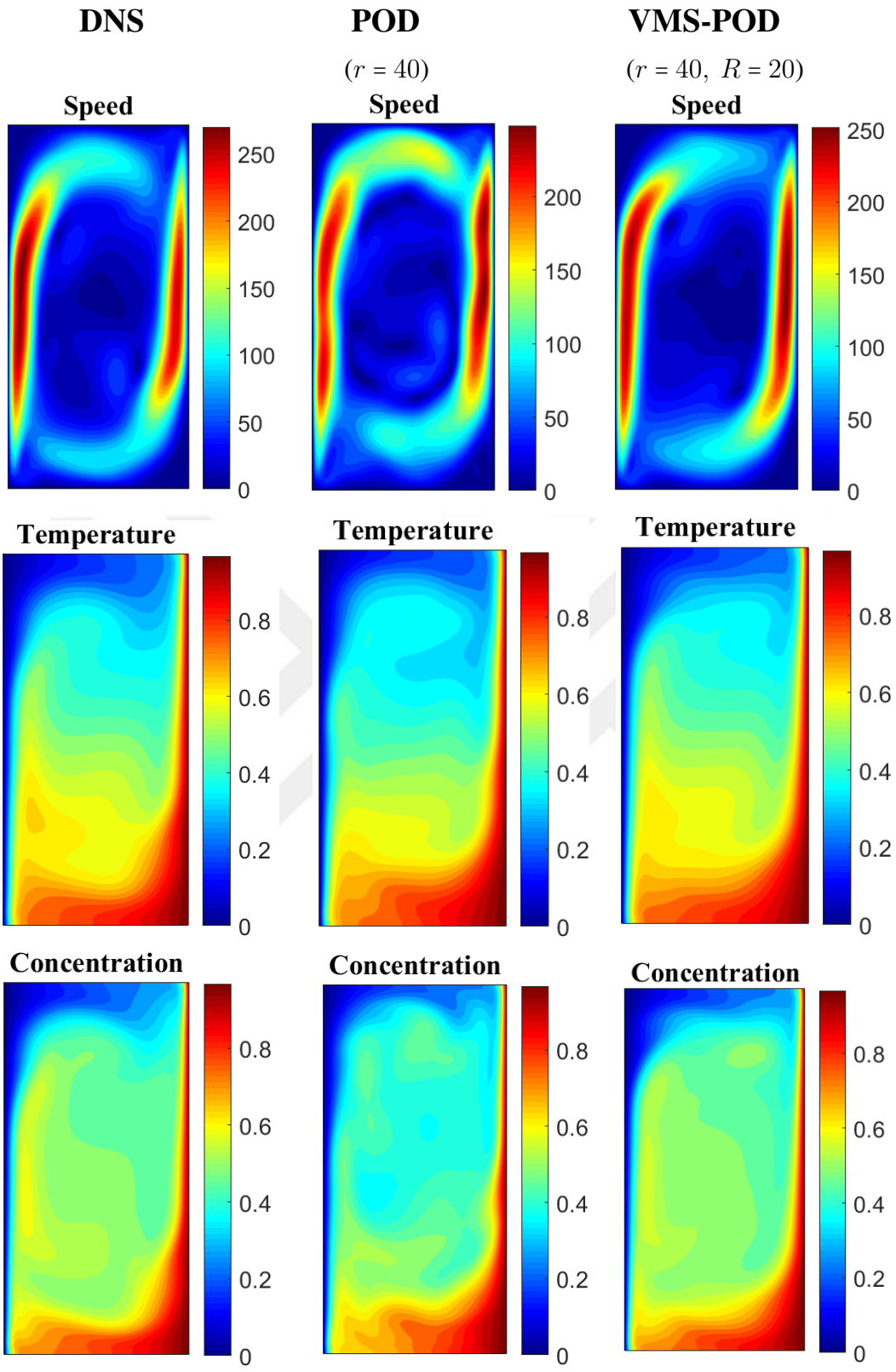

Figure 5.2: Shown above are $Ra = 10^6$ solution plots for the simulations using DNS, POD and VMS-POD using 40 modes at $t = 0.75$.

CHAPTER 6

CONCLUSIONS AND FUTURE WORKS

In the first part of the thesis, we proposed, analyzed and tested a VMS-POD method for incompressible NSE simulation, where the stabilization is completely decoupled into the second step of a two step implementation at each time step. Decoupling of the stabilization has the advantage of easily being incorporated into existing POD-G codes, and also that stabilization parameters can be adjusted only in the stabilization step (and not as part of the evolution equation). We rigorously prove an error estimate for the model, in terms of the number of POD modes r, the stabilization parameters R (number of modes not to add stabilization to) and ν_T, as well as the time step size Δt and the mesh width h of the underlying FEM simulation that produced the POD modes.

Results from several numerical experiments are provided that how effective the method can be. In particular, we show for 2D channel flow past a step, POD-G has an energy growth that causes poor lift and drag prediction, especially for longer times. The proposed VMS-POD is able to fix this by stabilizing so that the energy matches the DNS energy, which in turn leads to excellent lift and drag prediction, even up to $t = 10$ (and from the plots, it appear the accurate predictions can continue for even longer time).

In the second part of the thesis extended the POD-ROM methodology to the Darcy-Brinkman double diffusion system is presented. Under the usual assumptions, we proved stability and convergence results for the POD-ROM scheme, and gave results of several numerical tests. Our tests showed very good results for Rayleigh numbers $Ra = 10^4,\ 10^5$, which were accurately simulated with $r = 10$ and $r = 20$, respectively. For higher Ra, POD-ROM did not perform well without stabilization, but with a VMS-type stabilization developed in Chapter 3, the stabilized it gave good qualitative

results.

In the third part of the thesis, we presented the extrapolated Crank Nicholson VMS-POD method for Darcy Brinkman equations with double diffusive convection. We performed the stability and the error analyses for the proposed scheme. The approach uses reduce order modelling by POD approach and increases numerical stability by adding artificial diffusion term with a projection based VMS method. Numerical experiments verified the efficiency of the algorithm (5.1.2)-(5.1.4).

This research will include some inspiring future directions. One of the possible direction is to work on selection of eddy viscosity coefficient ν_T. We carry out our analysis in Chapter 3 and Chapter 5 for bounded, positive and element-wise constant ν_T. The nonlinear ν_T produces more complex mathematical theory due to the strong monotonicity. Hence, the nonconstant and the nonlinear case of ν_T should also be examined.

Another direction is the choice of optimal snapshots. It plays an important role in improving the performance of the POD method. One could increase the success of POD method by using the trust region philosophy in TRPOD method or creating a special Voronoi cluster of snapshots in CVT method.

The problems studied in this thesis are nonlinear. The POD method can not decrease the process time of the nonlinear equations sufficiently. Therefore, the efficiency of the POD method must be increased by using empirical methods like EIM and DEIM.

We showed that POD is an effective approach for simulating NSE and Darcy-Brinkman with double diffusive convection. Also, the POD ideas herein should be applied for other multiphysics problems. For turbulence case, the optimal stabilization strategies should be used. In such a case, the post-processing VMS method may be used to support the POD method similar to Chapter 3. The stabilization step could be implemented as coupled or decoupled.

REFERENCES

[1] V. R. Algazi and D. J. Sakrison. On the optimality of the Karhunen-Loève expansion. *IEEE Trans. Inform. Theory*, 15:319–321, 1969.

[2] C. A. Andrews, J. M. Davies, and G. R. Schwarz. Adaptive data compression. *Proc. IEEE*, 55:267–277, 1967.

[3] E. Arian, M. Fahl, and E. W. Sachs. Trust-region proper orthogonal decomposition for flow control. *ICASE report no. 2000-25, NASA Langley Research Center, Hampton, VA, USA.*, 2000.

[4] J. P. Songbe B. Goyeau and D. Gobin. Numerical study of double-diffusive natural convection in a porous cavity using the Darcy-Brinkman formulation. *Int. J. Heat. Mass Tran.*, 39(7):1363–1378, 1996.

[5] G. Baker. *Galerkin approximations for the Navier-Stokes equations.* Harvard University, 1976.

[6] B. S. Baldwin and H. Lomax. Thin layer approximation and algebraic model for separated turbulent flows. *AIAA 16th Aerospace Sciences Meeting, Huntsville, AL.*, pages 78–257, 1978.

[7] M. Barrault, Y. Maday, N. C. Nguyen, and A. T. Patera. An 'empirical interpolation' method: application to efficient reduced-basis discretization of partial differential equations. *C. R. Acad. Sci. Paris, Ser. I*, 339(9):667–672, 2004.

[8] M. Benosman, J. Borggaard, O. San, and B. Kramer. Learning-based robust stabilization for reduced-order models of 2D and 3D Boussinesq equations. *Appl. Math. Model.*, 49:162–181, 2017.

[9] L. Berselli, T. Illiescu, and W. Layton. *Mathematics of Large Eddy Simulation of Turbulent Flows*. Springer, 2005.

[10] J. Borggaard, A. Hay, and D. Pelletier. Interval-based reduced-order models for unsteady fluid flow. *Int. J. Numer. Anal. Model*, 4:353–367, 2007.

[11] D. Braess. *Finite Elements: Theory, fast solvers, and applications in elasticity theory*. Cambridge University Press, 2007.

[12] S. C. Brenner and L. R. Scott. *The Mathematical Theory of Finite Element Methods*. 3rd edn. Springer-Verlag, Newyork, 2008.

[13] J. Burkardt, M. Gunzburger, and H. C. Lee. POD and CVT-based reduced-order modeling of Navier-Stokes flows. *Comput. Methods Appl. Mech. Engrg.*, 196:337–355, 2006.

[14] A. Caiazzo, T. Iliescu, V. John, and S. Schyschlowa. A numerical investigation of velocity-pressure reduced order models for incompressible flows. *J. Comput. Phys.*, 259:598–616, 2014.

[15] Q. Cao, D. Y. H. Pui, and W. Lipiński. A concept of a novel solar-assisted large-scale cleaning system (SALSCS) for urban air remediation. *Aerosol Air Qual. Res.*, 15:1–10, 2015.

[16] S. Chaturantabut and D. C. Sorensen. Nonlinear model reduction via discrete empirical interpolation. *SIAM J. Sci. Comput.*, 32(5):2737–2764, 2010.

[17] S. Chen, C. Foias, D. D. Holm, E. Olson, E. S. Titi, and S. Wynne. A connection between the Camassa-Holm equations and turbulent flows in channels and pipes. *Phys Fluids*, 11:2343–2353, 1999.

[18] S. Chen, J. Tölke, and M. Krafczyk. Numerical investigation of double-diffusive (natural) convection in vertical annuluses with opposing temperature and concentration gradients. *Int. J. Heat Fluid Fl.*, 31(2):217–226, 2010.

[19] F. D. Deffenbaugh and F. J. Marshall. Time development of the flow about an impulsively started cylinder. *AIAA Journal*, 14(7):908–913, 1976.

[20] F. G. Eroglu and S. Kaya. *An extrapolated Crank Nicholson VMS-POD method for Darcy Brinkman Equations.* Applied Mathematics: Advanced Topics, Springer (submitted).

[21] F. G. Eroglu, S. Kaya, and L. Rebholz. A modular regularized variational multiscale proper orthogonal decomposition for incompressible flows. *Comput. Methods Appl. Mech. Engrg.*, 325:350–368, 2017.

[22] F. G. Eroglu, S. Kaya, and L. Rebholz. POD-ROM for the Darcy-Brinkman equations with double-diffusive convection. *J. Numer. Math., to be published*, 2018, doi:https://doi.org/10.1515/jnma-2017-0122.

[23] L. C. Evans. *Partial differential equations*. Graduate studies in mathematics, vol 19, 2nd edn. American Mathematical Society, Providence, RI, pp xxii+749, 2010.

[24] M. Fahl. *Trust-region methods for flow control based on reduced order modelling*. PhD thesis, Universitätsbibliothek, 2001.

[25] F. Fang, C. C. Pain, I. M. Navon, M.D. Piggott, G. J. Gorman, P. A. Allison, and A. J. H. Goddard. Reduced-order modelling of an adaptive mesh ocean model. *Int. J. Numer. Methods Fluids*, 59(8):827–851, 2009.

[26] K. Ghorayeb and A. Mojtabi. Double diffusive convection in a vertical rectangular cavity. *Phys. Fluids*, 9 (8):2339–2348, 1997.

[27] S. Giere. *Numerical and Analytical Aspects of POD-Based Reduced-Order Modeling in Computational Fluid Dynamics*. PhD thesis, Freie Universität, Berlin, 2016.

[28] V. Girault and P. A. Raviart. *Finite element approximation of the Navier-Stokes equations*. Lecture Notes in Math., Vol. 749, Springer-Verlag, Berlin, 1979.

[29] V. Girault and P. A. Raviart. *Finite element methods for Navier-Stokes equations: Theory and Algorithms*. Springer-Verlag, 1986.

[30] P.M. Gresho, R.L. Lee, S.T. Chan, and R.L. Sani. *Solution of the time-dependent incompressible Navier-Stokes and Boussinesq equations using the Galerkin finite element method. In: Approximation Methods for Navier-Stokes Problems., pp. 203–222*. Springer, Berlin, 1980.

[31] J. L. Guermond. Stabilization of Galerkin approximations of transport equations by subgrid modeling. *M2AN*, 33:1293 – 1316, 1999.

[32] M. Gunzburger. *Finite element methods for viscous incompressible flows: A guide to theory, practice, and algorithms*. Academic Press, Boston, 1989.

[33] K. Hasselmann. PIPs and POPs: The reduction of complex dynamical systems using principal interaction and oscillation patterns. *J. Geophys. Res. Atmos.*, 93:11015–11021, 1988.

[34] J. Heywood and R. Rannacher. Finite element approximation of the nonstationary Navier-Stokes equations, Part II: Stability of solutions and error estimates uniform in time. *SIAM J. Numer. Anal.*, 23:750–777, 1986.

[35] T. J. R. Hughes. Multiscale phenomena: Green's functions, the Dirichlet-to-Neumann formulation, subgrid-scale models bubbles and the origin of stabilized methods. *Comput. Methods Appl. Mech. Engrg.*, 127:387 – 401, 1995.

[36] T. Iliescu and Z. Wang. Variational multiscale proper orthogonal decomposition: convection-dominated convection-diffusion-reaction equations. *Math. Comput.*, 82(283):1357–1378, 2013.

[37] T. Iliescu and Z. Wang. Variational multiscale proper orthogonal decomposition: Navier-Stokes equations. *Numer. Meth. Partial. Diff. Eqs.*, 30(2):641–663, 2014.

[38] V. John. Reference values for drag and lift of a two-dimensional time-dependent flow around a cylinder. *Int. J. Numer. Meth. Fluids*, 44:777–788, 2004.

[39] V. John. *Finite Element Methods for Incompressible Flow Problems*. Springer Series in Computational Mathematics, 2016.

[40] V. John and S. Kaya. A finite element variational multiscale method for the Navier-Stokes equations. *SIAM J. Sci. Comput.*, 26:1485–1503, 2005.

[41] V. John and S. Kaya. Finite element error analysis of a variational multiscale method for the Navier-Stokes equations. *Adv. Comput. Math.*, 28:43–61, 2008.

[42] V. John, S. Kaya, and W. Layton. A two-level variational multiscale method for convection-dominated convection-diffusion equations. *Comput. Methods Appl. Mech. Engrg.*, 195:4594–4603, 2006.

[43] D. A Johnson. and L. S. King. A mathematically simple turbulence closure model for attached and separated turbulent boundary layers. *AIAA Journal*, 23(11):1684–1692, 1985.

[44] B. H. Jørgensen, J. N. Sørensen, and M. Brøns. Low-dimensional modeling of a driven cavity flow with two free parameters. *Theoretical and Computational Fluid Dynamics*, 16(4):299–317, 2003.

[45] A. Komiya K. Tsubaki, S. Maruyama and H. Mitsugashira. Continuous measurement of an artificial upwelling of deep sea water induced by the perpetual salt fountain. *Deep Sea Res. Part I Oceanogr. Res. Pap.*, 54:75–84, 2007.

[46] K. Karhunen. Zur spektraltheorie stochastischer prozesse. *Ann. Acad. Sci. Fennicae, Ser.*, A1:34, 1946.

[47] M. Karimi-Fard, M.C. Charrier-Mojtabi, and K. Vafai. Non-Darcian effects on double-diffusive convection within a porous medium. *Numer. Heat Transfer, Part A: Appl.*, 31 (8):837–852, 1997.

[48] J.P. Kelliher, R. Temam, and X. Wang. Boundary layer associated with the Darcy-Brinkman-Boussinesq model for convection in porous media. *Physica D.*, 240:619–628, 2011.

[49] D. D. Kosambi. Statistics in function space. *J. Indian Math. Soc.*, 7:76–88, 1943.

[50] J. Kramer, R. Jecl, and L. Škerget. Boundary domain integral method for double diffusive natural convection in porous media saturated with compressible fluid. *AIP Conference Proceedings*, 1048:332–335, 2008.

[51] J. Kramer, J. Ravnik, R. Jecl, and L. Škerget. Three-dimensional double-diffusive natural convection with opposing buoyancy effects in porous enclousure by boundary element method. *Int. J. Comp. Meth. and Exp. Meas.*, 1:103–115, 2013.

[52] T. Küçükseyhan. *Optimal control and reduced order modelling of FitzHugh-Nagumo equation*. PhD thesis, Middle East Technical University, 2017.

[53] K. Kunisch and S. Volkwein. Galerkin proper orthogonal decomposition methods for parabolic problems. *Numerische Mathematik*, 90(1):117–148, 2001.

[54] O. Ladyzhenskaya. *The Mathematical Theory of Viscous Incompressible Flow*. Gordon and Breach, New York, 1969.

[55] W. Layton. A connection between subgrid scale eddy viscosity and mixed methods. *Appl. Math. Comput.*, 133:147 – 157, 2002.

[56] W. Layton, L. Röhe, and H. Tran. Explicitly uncoupled VMS stabilization of fluid flow. *Comput. Methods Appl. Mech. Engrg.*, 200:3183–3199, 2011.

[57] S. Ling. *Numerical Investigations of Reduced Order Models for Convection-Diffusion Equations*. Master thesis, Freie Universität, Berlin, 2016.

[58] Y. Liu, L. Zhang, X. Wang, and W. K. Liu. Coupling of Navier–Stokes equations with protein molecular dynamics and its application to hemodynamics. *Int. J. Numer. Methods Fluids*, 46(12):1237–1252, 2004.

[59] M. Loéve. Functions aléatoire de second ordre. *Comptes Rendus Acad. Sci. Paris*, page 220, 1945.

[60] J. L. Lumley. The structure of inhomogeneous turbulence. *In A.M. Yaglom and V. I. Tatarski, editors, Atmospheric Turbulence and Wave Propagation*, 24:166–78. Nauka, Moscow, 1967.

[61] Z. Luo, J. Zhu, R. Wang, and I.M. Navon. Proper orthogonal decomposition approach and error estimation of mixed finite element methods for the tropical Pacific Ocean reduced gravity model. *Comput. Methods Appl. Mech. Engrg.*, 196:4184–4195, 2007.

[62] R. March, A.L.G.A. Coutinho, and R.N. Elias. Stabilized finite element simulation of double diffusive natural convection. *Mecanica Computacional*, XXIX:7985–8000, 2010.

[63] J. Marshall, A. Adcroft, C. Hill, L. Perelman, and C. Heisey. A finite-volume, incompressible navier–stokes model for studies of the ocean on parallel computers. *J. Geophys. Res.*, 102:5733–5752, 1997.

[64] M. A. Medebber and N. Retiel. Numerical study of double diffusive convection within the annular region of two concentric vertical cylinders. *In Defect and Diffusion Forum*, 374:1–17, 2017.

[65] H.G. Melhem. *Finite Element Approximation to Heat Transfer Through Combined Solid and Fluid Media.* PhD thesis, University of Pittsburgh, 1987.

[66] A. Mojtabi and M.C. Charrier-Mojtabi. *Double-diffusive convection in porous media, in: Handbook of Porous Media Part III*. Taylor and Francis, 2005.

[67] M. Müller, S. Schirm, and M. Teschner. Interactive blood simulation for virtual surgery based on smoothed particle hydrodynamics. *Technol. Health Care*, 12(1):25–31, 2004.

[68] C. L. M. H. Navier. Mémoire sur les lois du mouvement des fluides. *Mém. Acad. Royal Society*, 6:389–440, 1823.

[69] D.A. Nield and A. Bejan. *Convection in Porous Media*. Springer, Berlin, 1992.

[70] A. M. Obukhov. Statistical description of continuous fields. *Trudy Geophys. Int. Aked. Nauk. SSSR*, 24:3–42, 1954.

[71] T. N. Palmer. Towards the probabilistic earth-system simulator: a vision for the future of climate and weather prediction. *Q. J. Royal Meteorol. Soc.*, 138(665):841–861, 2012.

[72] A. Papoulis. *Probability, Random Variables, and Stochastic Processes.* New York: McGraw-Hill, 1965.

[73] R. G. Parr. and W. Yang. *Density-functional theory of atoms and molecules*. Oxford Univ. Press, New York, 1989.

[74] C. S. Peskin. Numerical analysis of blood flow in the heart. *J. Comput. Phys.*, 25(3):220–252, 1977.

[75] V. S. Pougachev. General theory of the correlations of random functions. *Izv. Akad. Nauk. SSSR. Math. Ser.*, 17:401–402, 1953.

[76] R. W. Preisendorfer and C. D. Mobley. *Principal component analysis in meteorology and oceanography.* Amsterdam: Elsevier, 1988.

[77] A. Quarteroni and A. Valli. *Numerical approximation of partial differential equations*. Springer Ser. Comput. Math., 1994.

[78] S. S. Ravindran. Real-time computational algorithm for optimal control of an MHD flow system. *SIAM J. Sci. Comput.*, 26:1369–1388, 2005.

[79] J. P. Roop. A proper-orthogonal decomposition variational multiscale approximation method for a generalized Oseen problem. *Advances in Numerical Analysis*, Volume 2013:1–8, 2013.

[80] A. Rosenfeld and A. C. Kak. *Digital Picture Processing.* New York: Academic, 1982.

[81] D. D. Holm E. Olson E. S. Titi S. Chen, C. Foias and S. Wynne. Camassa-Holm equations as a closure model for turbulent channel and pipe flow. *Phys. Rev. Lett.*, 81:5338–5341, 1998.

[82] D. D. Holm E. Olson E. S. Titi S. Chen, C. Foias and S. Wynne. The Camassa-Holm equations and turbulence. *Phys D*, 133:49–65, 1999a, Predictability: quantifying uncertainty in models of complex phenomena (Los Alamos, NM, 1998).

[83] O. San and J. Borggaard. Basis selection and closure for POD models of convection dominated Boussinesq flows. *Proceeding of the Twenty-first International Symposium on Mathematical Theory of Networks and Systems, Groningen, The Netherlands*, pages 132–139, 2014.

[84] O. San and J. Borggaard. Principal interval decomposition framework for POD reduced-order modeling of convective Boussinesq flows. *Int. J. Numer. Methods Fluids*, 78:37–62, 2015.

[85] A. Sartori, A. Cammi, L. Luzzi, and G. Rozza. A multi-physics reduced order model for the analysis of Lead Fast Reactor single channel. *Ann. Nucl. Energy*, 87:198–208, 2016.

[86] M. Schäfer and S. Turek. Benchmark computations of laminar flow around a cylinder. *Wiesbaden: Vieweg*, pages 547–566, 1996.

[87] L. Shan, W. Layton, and H. Zheng. Numerical analysis of modular VMS methods with nonlinear eddy viscosity for the Navier-Stokes equations. *Int. J. Numer. Anal. Model*, 10:943–971, 2013.

[88] A. Shapiro. The use of an exact solution of the Navier–Stokes equations in a validation test of a three-dimensional nonhydrostatic numerical model. *Mon. Wea. Rew.*, 121(8):2420–2425, 1993.

[89] L. Sirovich. Turbulence and the dynamics of coherent structures. parts I, II and III. *Quart. Appl. Math.*, 45:561–590, 1987.

[90] P. R. Spalart and S. R. Allmaras. A one-equation turbulence model for aerodynamic flows. *In Proceedings of the 30th Aerospace Sciences Meeting and Exhibit, Aerospace Sciences Meetings, Reno, NV, USA, 6–9 January*, 1992.

[91] M. E. Stern. The "salt-fountain" and thermohaline convection. *Tellus*, 12:172–175, 1960.

[92] G.G. Stokes. On the theories of the internal friction of fluids in motion and of the equilibrium and motion of elastic solids. *Trans. Cambridge Philos. Soc.*, 8:287–319, 1845.

[93] H. Stommel, A. B. Aarons, and D. Blanchard. An oceanographic curiosity: the perpetual salt fountain. *Deep-Sea Res.*, 3:152–153, 1956.

[94] Z. Wang. *Reduced-Order Modeling of Complex Engineering and Geophysical Flows: Analysis and Computations*. PhD thesis, Virginia Polytechnic Institute and State University, 2012.

[95] C. Winton, J. Pettway, C.T. Kelley, S. Howington, and O. J. Eslinger. Application of proper orthogonal decomposition (pod) to inverse problems in saturated groundwater flow. *Adv. Water Resour.*, 34:1519–1526, 2011.

[96] D. Xiao, F. Fang, A. G. Buchan, C. C. Pain, I. M. Navon, J. Du, and G. Hu. Non–linear model reduction for the Navier–Stokes equations using residual DEIM method. *J. Comput. Phys.*, 263:1–18, 2014.

[97] X. Xie, D. Wells, Z. Wang, and T. Iliescu. Numerical analysis of the Leray reduced order model. *J. Comput. Appl. Math.*, 328:12–29, 2018.

CURRICULUM VITAE

PERSONAL INFORMATION

Surname, Name: Güler Eroğlu, Fatma
Nationality: Turkish (TC)
Date and Place of Birth: 05.04.1991, Elmalı
Marital Status: Married
E-mail: fguler.eroglu@gmail.com

EDUCATION

Degree	Institution	Year of Graduation
B.S.	Süleyman Demirel Üniversitesi	2012
High School	Elmalı Anatolian High School	2008

COMPUTER SKILLS

Proficient in Matlab, LaTeX, Scientific Workplace, Microsoft Office Packages

PROFESSIONAL EXPERIENCE

Year	Place	Enrollment
2013-17	Middle East Technical University, Mathematics Departments	Research Assistant
2017-18	Bartın University, Mathematics Departments	Research Assistant

TEACHING AND TUTORING EXPERIENCE

Year	Semester	Course Code	Course Name
2013-17	Fall	MATH 119	Calculus with Analytic Geometry
2013-17	Spring	MATH 120	Calculus of Functions of Several Variables
2017-18	Fall	MATH 117	Calculus I
2017-18	Fall	MATH 219	Introduction to Differential Equations

PUBLICATIONS

- F. G. Eroglu, S. Kaya and L. Rebholz, "A Modular Regularized Variational Multiscale Proper Orthogonal Decomposition for Incompressible Flows", Computer Methods in Applied Mechanics and Engineering, 325, 350-368, 2017.

- F. G. Eroglu, S. Kaya, and L. Rebholz, “POD-ROM for the Darcy-Brinkman Equations with Double-Diffusive Convection”, 2019, to be published, doi:10.1515/jnma-2017-0122.

- F. G. Eroglu, S. Kaya, "An extrapolated Crank Nicholson VMS-POD method for Darcy Brinkman Equations", Applied Mathematics: Advanced Topics, Springer (submitted).

PROCEEDINGS

- Fatma G. Eroglu, Songul Kaya and Leo G. Rebholz, "Variational Multiscale Proper Orthogonal Decomposition with Modular Regularization", Proceedings of the 17th International Conference on Computational and Mathematical Methods in Science and Engineering, pp. 854-857, July 4-8, 2017, Cádiz, Spain.

- Fatma G. Eroglu, Songul Kaya and Leo G. Rebholz, "A Numerical Investigation of VMS-POD Model for Darcy-Brinkman Equations", Proceedings of the World Congress on Engineering, Vol I, pp. 7-11, July 4-6, 2018, London, U.K.

SCIENTIFIC MEETINGS

Presentations in International Scientific Meetings

Fatma G. Eroglu, Songul Kaya and Leo G. Rebholz, "Variational Multiscale Proper Orthogonal Decomposition with Modular Regularization" CMMSE Spain 2017, July 4-8, 2017, Costa Ballena, Rota, Cadiz, Spain.

Fatma G. Eroglu, Songul Kaya and Leo G. Rebholz, "A Numerical Investigation of VMS-POD Model for Darcy-Brinkman Equations", WCE 2018, July 4-6, 2018, London, U.K.

Presentations in National Scientific Meetings

Fatma G. Eroglu and Songul Kaya, "Numerical Aspects of POD-Based Reduced-Order Modeling for Darcy-Brinkman Equations" BEYOND: Workshop on Computational Science and Engineering, 20-21 October, 2018, METU, Ankara-Turkey.

Fatma G. Eroglu and Songul Kaya, "Sıkıştırılamaz akışlar için projeksiyona bağlı çok ölçekli varyasyonel uygun dik ayrıştırma metodu" AMG Turkey 2017, 12. Ankara Matematik Günleri, 25-26 Mayıs, 2017, Hacettepe University, Ankara, Turkey.

Fatma G. Eroglu and Songul Kaya, "Projeksiyona Bağlı Modüler Regülarizasyonlu ve Ortogonal Ayrıştırmalı Metodun Sayısal Analizi " AMG Turkey 2016, 11. Ankara Matematik Günleri, 26-27 Mayıs, 2016, Ankara University, Ankara, Turkey.

AWARDS AND SCHOLARSHIPS

11/2018	"Best Student Paper Award of The 2018 International Conference of Applied and Engineering Mathematics", The International Association of Engineers.
2013-2018	2211-Doctorate Scholarship Turkish Scientific and Technical Research Council (TÜBİTAK).
06/2012	Süleyman Demirel University Undergraduate Courses Performance Award (The most successful student in the Undergraduate Program of the Faculty of Arts and Science in 2011-2012 Academic Year).